Cortical PV and VIP Neurons are Necessary for Texture Discrimination Performance of Freely Behaving Mice

Dissertation

for the award of the degree

“Doctor rerum naturalium”

of the Georg-August-Universität Göttingen

within the doctoral program *Sensory and Motor Neuroscience*

of the Georg-August University School of Science (GAUSS)

submitted by

Aybeniz Ece ÇETİN

from Malkara, Turkey

Göttingen 2025

Thesis advisory committee

Prof. Dr. Jochen Staiger

Institute for Neuroanatomy, University Medical Center (UMG), Göttingen

Prof. Dr. Hansjörg Scherberger

Neurobiology Laboratory, German Primate Center (DPZ), Göttingen

Prof. Dr. Hannelore Ehrenreich

Experimental Medicine, Central Institute of Mental Health (CIMH), Mannheim

Members of the examination board

Referee: Prof. Dr. Jochen Staiger

Institute for Neuroanatomy, University Medical Center (UMG), Göttingen

2nd Referee: Prof. Dr. Hansjörg Scherberger

Neurobiology Laboratory, German Primate Center (DPZ), Göttingen

Other members of the examination board

Prof. Dr. Hannelore Ehrenreich

Experimental Medicine, Central Institute of Mental Health (CIMH), Mannheim

Prof. Dr. Oliver Wirths

Division of Molecular Psychiatry, Department of Psychiatry, UMG, Göttingen

Prof. Dr. Tim Gollisch

Sensory Processing in Retina, Department of Opthalmology, UMG, Göttingen

Prof. Dr. Thomas Dresbach

Institute for Anatomy and Cell Biology, UMG, Göttingen

Day of the oral examination: 20th of March 2025

Table of Contents

ABSTRACT

Rodents gather information about their surroundings through their whiskers, enabling them to differentiate textures, recognize objects, and navigate. Each whisker is represented in the barrel cortex (S1BF) by a single cortical column in an isomorphic manner. The microcircuits within each barrel-related column comprise both excitatory and inhibitory neurons. Extensive literature exists on genetically defined GABAergic neurons—parvalbumin (PV), vasoactive intestinal polypeptide (VIP), and somatostatin (SST)—and their involvement in tactile perception through whisking, including both passive stimulation of the whiskers and active touch. S1BF is well established as the core node for whisker-based texture discrimination. However, how PV, VIP, and SST interneurons contribute to the behavioral outcome of information processing during tactile perception in texture discrimination remains unclear.

This study aims to further investigate the role of PV and VIP neurons in S1BF through chemogenetic activation in awake, freely behaving mice trained in a texture discrimination task. For this purpose, a novel whisker-based texture discrimination paradigm, the textured T-maze (TT), was developed, allowing mice to explore the maze freely while being trained on texture discrimination. PV-cre and VIP-cre mice exhibited comparable baseline performance. An activating Cre-dependent chemogenetic virus was bilaterally injected into the S1BF of PV-cre and VIP-cre mice to express “activating” DREADDs, enabling selective manipulation of PV and VIP cells via intraperitoneal administration of clozapine-N-oxide (CNO). Chemogenetic activation of either PV or VIP neurons impaired texture discrimination, reducing performance to chance level. Whole-cell patch-clamp experiments demonstrated that the intrinsic properties of transfected cells were comparable to those of non-transfected counterparts. The depolarizing effect of CNO on transfected cells was tested via bath application. Recordings confirmed that PV cells exhibited depolarization as expected from the viral construct, whereas VIP cells underwent depolarization block.

In conclusion, although the chemogenetic virus did not produce equivalent depolarization effects in PV and VIP cells, the activation of PV cells or the putative deactivation of VIP cells in S1BF disrupted perceptual discrimination in freely behaving mice during the texture discrimination task.

INTRODUCTION

Galileo Galilei (1564-1642), a great astronomer and physicist, is also considered as the pioneer of modern sensory neuroscience. He was the first one who defined and connected what is physical and what is perceptual or, in other words, what is external stimuli and what is internal experience in the 17th century (Piccolino & Wade, 2008). He set the stage for the scientific exploration of senses by attempting to quantify perception, and many scientists following his legacy studied and still are studying perception and sensory pathways.

Being an attraction center for many scientists over the centuries, the perception of the outer world still keeps its charm to be fully discovered. Today, with the help of many advanced techniques like chemogenetics and model organisms like transgenic mice, we can extract more precise information on not only perception but also circuitries and cellular processes behind it. As we deepen our understanding of the cellular and circuit-level mechanisms maintaining perception, we move closer to answering age-old questions.

Having the enthusiasm to contribute to our knowledge in this field, I focused on the primary somatosensory barrel field (S1BF), the cortical area of whisker-based tactile perception and I wanted to explore the contributions of different kinds of inhibitory neurons (in the scope of this thesis: parvalbumin (PV)- and vasoactive intestinal polypeptide (VIP)-expressing neurons) on whisker-based texture discrimination of mice by recruiting the chemogenetics method. The well-defined somatotopy of S1BF and well-studied characteristics of pathways and circuitries, which will be elaborated on in the next sections, made working on whisker-based perception appealing, despite its laborious nature.

1. Contact with the environment for a mouse

Before going into the neuroanatomical properties of S1BF, one should first have an understanding of rodents', as many other mammalian species (Woolsey et al., 1975), way of using their whiskers (i.e. facial vibrissae) playing an integral role in their perception of the outer world. In the literature, whiskers were compared to human fingertips due to their feature selectivity in perception, and whisking is accepted as a complex behavior since it is a controlled set of movements (i.e. active sensing) requiring attention to a better quality of perception (Grant et al., 2023).

Rodents use their whiskers to navigate, recognize borders and gaps on the way, socialize, hunt, and characterize objects (by location, shape, and size) and textures by actively whisking (Diamond et al., 2008). All these functions are explored with behaviorally two main types of experiments. The first version is done on freely behaving animals, which allowed the subject to move freely in an experimental arena (e.g., T-maze, open field) with a variety of different behavioral batteries (e.g., 2-alternative forced-choice -2AFC- tasks, gap crossing, object exploration, see below) and without the presence of any external apparatus like headsets or probes which makes it possible to generalize/compare findings with the natural behavior of mice or rats. A lot of behavioral batteries are also possible to adapt to the second type, which is head-fixed experiments. In these types of experiments, the subject's head is fixed to a frame usually for the sake of photostimulation, imaging, or electrophysiological recordings (Schwarz et al., 2010). The literature is greatly missing studies executed on freely moving animals, especially for more complex tasks (e.g. whisker-based texture discrimination). However, I will try to summarize whisking behavior, mostly based on the non-head-fixed experiments.

The very first behavioral study highlighting the importance of whiskers, compared rats' reliance on different senses, and showed that whisker clipping causes a behavioral change during maze navigation (Vincent, 1912). The rats slowed down and showed an increased tendency to make navigational errors in the maze compared to vision-deprived conditions. Another study showed that when whiskers were removed unilaterally, animals relied on the side which whiskers were intact and moved in the maze by turning this side to the walls for thigmotactic scanning (Milani et al., 1989).

Not only for navigation but also to perceive the distance between two objects (Krupa et al., 2001) or the tunnel width is perceived by whisking. Whiskers supply rodents with good guidance for locomotion also when it comes to recognizing the depths, both mice (Voigts et al., 2015) and rats (Carvell & Simons, 1990; Jenkinson & Glickstein, 2000) can detect gaps before they initiate the next step which also signals their ability to locate objects. Even in the absence of all whiskers but a single one, rodents manage to learn gap-crossing tasks and successfully detect the gap although the learning phase is slower compared to learning with the complete set of whiskers (Harris et al., 1999; Celikel & Sakmann, 2007).

Whiskers are also actively used for social interactions. Besides sniffing, rats are intensely whisking in different ways in social conditions. They are observed to make whisker-to-whisker contact with their conspecifics (Lenschow & Brecht, 2015). More specifically, they protract their whiskers more, and whisking amplitude is increased during an aggressive interaction. In contrast, smaller whisking amplitudes were observed in female rats while interacting with male (Blanco-Hernández et al., 2024).

Similar to other detection tasks, rodents can find objects in an empty arena and detect their shapes. When rats were searching for cookies in an empty arena, their whisking increased and regardless of their visual capability (e.g. blind or normal vision) they discriminated the shape and size of the cookies by whisker-based tactile cues (Brecht et al., 1997). Another example of shape detection is head-fixed mice, which discriminate concave and convex shapes by comparing the number of contacts coming from multiple whiskers (Rodgers et al., 2021).

Whisker-based perception is also fine-tuned to detect and discriminate textures. In texture discrimination experiments, two different discriminanda are usually used. Discrimination of varying coarseness of sandpaper (SP) is widely used as a mode of perceptual learning. Another emerging option for texture discrimination paradigms is using identical 3D-printed objects with different amount or different angles of slits carved on them (e.g. more frequently placed slits on a surface/object being similar to coarse sandpaper) can be discriminated by rodents. Both mice (Lipp & Van der Loos, 1991; Wu et al., 2013) and rats (Bourgeon et al., 2004; Montuori & Honey, 2016) can discriminate textures through their whiskers.

In one of the experiments by Pacchiarini et al. (2020), 2 sawdust-filled bowls were presented to food-restricted mice. One of the 3D-printed bowls had a buried food reward: either the one with a grooved or smooth surface. Mice successfully found the food reward depending on no other cues but tactile information from intact whiskers (Pacchiarini et al., 2020). This experiment was modified from another study showing that rats can find the food reward in the bowls covered with 2 different types of SP (Birrell & Brown, 2000), which indicates both mice and rats can learn to discriminate textures through their whiskers regardless of the discriminanda. Another example of whisker-based texture discrimination of freely moving mice is shown by a quite recently established 2AFC task. In this self-

initiated task, mice first learned to do a nose-poke to reach the discriminanda, and then they were exposed to a pair of SP with two different grit sizes and if they were successful in detecting coarse SP (e.g. P120) they received a water reward. Mice were not only successful in discriminating P120 against P400 SP but also were able to discriminate SP with lower contrasts (e.g. P280 and P180; Qi et al., 2022). These findings indicate that not only the absence/presence of the texture, but also similar textures coming with slight differences (e.g. P120 vs P180) can be perceived through whiskers.

To sum up, the whiskers for rodents are essential for contact with their outer world in a multitude of different aspects: social interactions, navigation, detection of gaps, object detection/localization, and most importantly the size, shape, and texture of the objects. When one considers how precise the perception through whiskers, it makes more sense that the abovementioned scientists compared mouse whiskers to human fingertips. Other than whiskers playing an integral role in tactile perception for mice, the ability to detect/discriminate textures through them are exciting and a mind-blowing skill of rodents. When one wants to understand more about this sensory system, ends up with the barrel cortex, the station behind all these percepts. Given that it all starts with whisking, the whisker-to-barrel pathway and its well-defined but complex structure (Staiger & Petersen, 2021) paved the way for this very project's aim.

2. An exquisite journey of signal: from whiskers to barrels (and further on)

As the many examples above illustrate, mice use their whiskers to perceive their surroundings in multiple ways. A core node in the circuits for all mentioned percepts is the barrel cortex, which will be explained under this subtitle. Interestingly, the discovery of the barrel cortex's relation to whiskers was much later than the discovery of both whiskers' sensory roles and the cluster of neurons in Layer (L) 4 (Erzurumlu & Gaspar, 2020). The scope of this thesis majorly focuses on mice, yet when it is necessary, findings from other rodents (e.g. rats) are also used.

Before going into barrels and barrel cortex, one should remember the layered structure of the cortex. Although the function of the layers is still an ongoing debate (Guy & Staiger, 2017; Adesnik & Naka, 2018; Staiger & Petersen, 2021), there is a consensus in

the literature on the subdivision of the neocortex into 6 Ls due to observed differences in cell type morphology, developmental origin, gene expression patterns, and most importantly their connectivity (Feldmeyer, 2012; Staiger et al., 2015). The cortical lamination is essential to understanding other organized structures within the cortex, such as barrel columns in the primary somatosensory cortex (S1) and canonical circuitry within these columns.

In a way supporting the functional relevance of the cortical layers, barrels were recognized in L4. The term “barrel” for the unusual cluster of cells in L4 of the S1 was coined by Woolsey & Van der Loos (1970), who also recognized for the first time mouse whiskers have an organized representation in S1 (Woolsey, 1967). Later on, the barrel cortex became an attractive research field with its cellular patterning (Erzurumlu & Gaspar, 2020), and it is expanding until today because it feeds our understanding of somatotopy, morphology, and perception.

Let’s begin with the initial tactile interaction with the environment, which starts with the whiskers. The whisker array on the snout carries whiskers in an organized manner. The “coordinates” of whisker placement at each side of the snout have arcs from 1 to 5, and rows labeled from A to E (Brecht et al., 1997; Fig. 1). Since each large mystacial whisker is placed in a whisker follicle individually, this label system promotes the naming of the other whisker-related structures (e.g. barrel columns, see below) and provides a common language among barrel cortex researchers. Whiskers are thicker in the whisker follicle and get thinner towards the outer end which touches the surroundings (Williams & Kramer, 2010; Belli et al., 2017). This tapered shape of vibrissae makes it possible to be more flexible and perceive the texture of the contacted object (Williams & Kramer, 2010; Hires et al., 2013). The flexibility itself comes with two different modes of movement regarding texture perception: stick (e.g. being shortly stopped because of a curvature) and slip (e.g. being released and springing after the obstacle). A strong hypothesis (i.e. kinetic signature hypothesis; Arabzadeh et al., 2005) about whisker motion on texture is that perception of texture does not depend on how much whiskers vibrate/resonate during interaction with the texture yet the temporal encoding of the slip amplitude and velocity of whiskers (Wolfe et al., 2008).

Of course, the signal coming from these stick and slip events has a long way to go before turning into a percept. For example, a mouse gets the initial information from a walnut through whisking on it and this information goes to barrelettes of the brainstem (formed in the trigeminal nuclei), then barreloids of the thalamus (ventral posteromedial

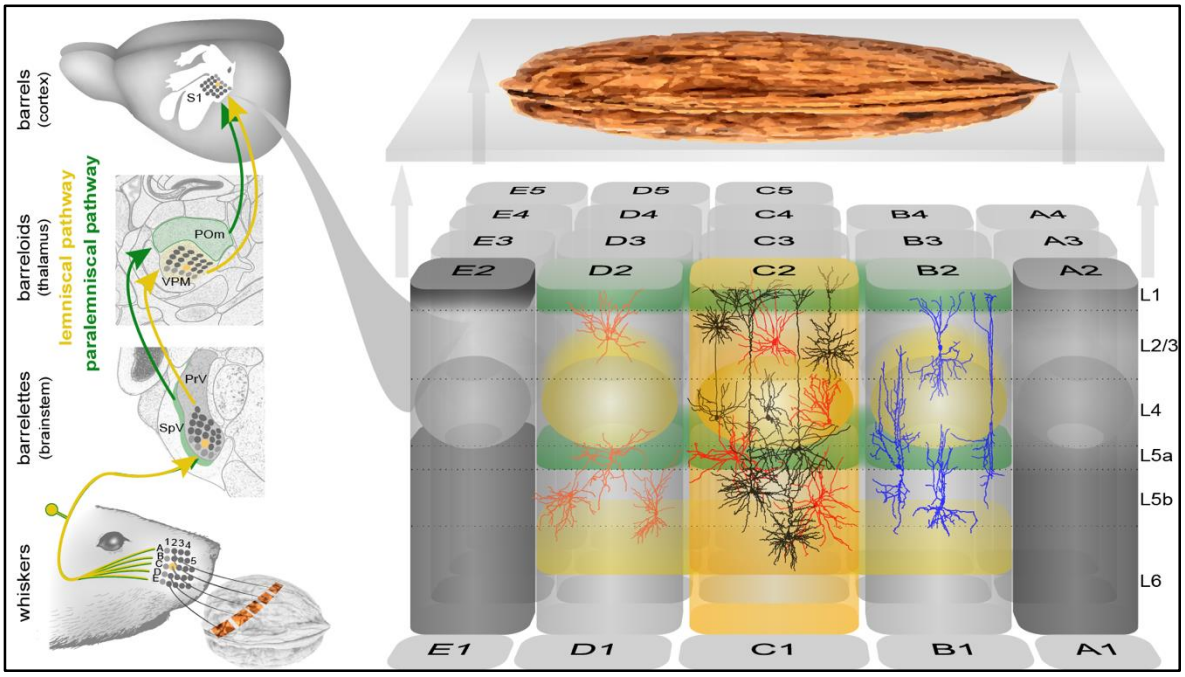

Figure 1. Whisker-to-barrel pathway. On the left, the path of the whisking signal is depicted. After whisking of a texture, the signal from the whisker follicles goes to trigeminal nuclei, then barrelettes of the brainstem, following two different pathways (i.e. lemniscal in yellow and paralemniscal in green) it arrives at barreloids of the thalamus, and then finally arrives at the barrels in the cortex. These pathways convey the signal in a complementary way to different layers of the S1BF. On the right, barrel-related columns in the primary somatosensory cortex are shown. Please pay attention that these columns are represented with the same numbers as each whisker was in the mouse figure's snout on the left side. This isomorphic representation is a result of the fact that each column receives input largely from an individual principal whisker (e.g. D1 whisker is represented in D1 barrel-related column). Also, on the right side, samples from different inhibitory cell types and excitatory neurons are exhibited. In the D2 column, somatostatin-expressing neurons, in the B2 column VIP neurons, in the C2 column PV (red) and principal neurons (black) are shown (figure is taken from Staiger & Petersen, 2021).

nucleus), and finally reaches the barrels of the neocortex (explained in detail below); each station housing an isomorphic representation of the whiskers on the animal's snout (Fig. 1). Even when described in these vague terms, the whisker-to-barrel pathway reveals its well-organized somatotopic structure. However, we need to dig deeper to understand what actually is going on when an animal whisks to gather information from the outer world.

The thicker end of the whiskers that is placed at the whisker pad of mice is housed within a whisker follicle. Each follicle has a multitude of nerve endings, which either run along the follicle vertically or circularly wrap the follicle (Rice et al., 1986; Ebara et al., 2002). According to Lee and Woolsey (1975), these nerve terminals originate from trigeminal ganglion neurons, with each follicle being invaded by up to 200 axons forming very different

types of mechanoreceptors. Trigeminal ganglion neurons then project to the trigeminal nuclei in the brainstem, where the first synapse en route to the cortex is established (Staiger & Petersen, 2021). In the trigeminal nuclei, individual whiskers are represented as dense clusters of cells (i.e. barrelettes) aligned somatotopically in the same fashion as whisker follicles (Belford & Killackey, 1979; Ma & Woolsey, 1984), especially in the principal sensory nuclei (PrV) and to some extent in the spinal nuclei (SpV). From there, these neurons project to the thalamus (Van der Loos, 1976): PrV neurons project to the contralateral ventral posteromedial nucleus (VPM), via the lemniscal pathway, and VPM has the organized clusters of cells (i.e. barreloids) represent whiskers. Also, SpV neurons project to the posterior medial thalamic nucleus (POm) via the paralemniscal pathway which does not show a detailed somatotopy (Deschenes & Urbain, 2009; El-Boustani et al., 2020).

Finally, the signal from VPM and POm reaches the S1BF barrel-related columns through the lemniscal and paralemniscal pathways, respectively. These two pathways innervate the barrel field in a complementary fashion (Staiger & Petersen, 2021). The axons coming from VPM target predominantly the barrels in L4 (also referred as the main input layer; Agmon & Connors, 1991; Diamond et al., 1992), partially to L2/3, and border of L5B-L6 (Haidarliu et al., 2008). However, POm projects to L1 and L5A (Wimmer et al., 2010; Jouhanneau et al., 2014). Not only the source and their target/termination layers in the S1BF, but also the transferred information by these two pathways differ. While the lemniscal pathway carries the spatial (i.e., whisker position) signal from the whiskers, the paralemniscal path is shown to be processing the temporal cues (Ahissar et al., 2000).

The S1BF is also characterized by barrel(-related) columns which radially span all layers and have a barrel's width (Fig. 1). Each barrel-related column represents a single principal whisker in a somatotopically organized manner, as barrels in L4, barreloids of VPM, or barrelettes of PrV (e.g., the C2 whisker corresponds to the C2 barrel column, Fig. 1). While the majority of input to a barrel column comes from its principal whisker, there is also a smaller input from neighboring whiskers, allowing for the integration of tactile signal gathered across the whisker pad (Zhu & Connors, 1999; Brecht & Sakmann, 2002; Staiger & Petersen, 2021).

The transition of processed signal in L4 continues preferentially within the barrel column, goes to L2/3 (Varani et al., 2022), and then to L5 before it’s distributed to other

cortices and a variety of subcortical structures (Lübke & Feldmeyer, 2007; Lefort et al., 2009). This pathway formed by excitatory neurons (also called the canonical microcircuitry; Douglas & Martin, 1991, 2004, 2007; Feldmeyer et al., 2013; Staiger & Petersen, 2021), is controlled and orchestrated by different kinds of inhibitory neurons. However, plenty of non-canonical circuits are formed, as well (Schubert et al., 2007; Lefort et al., 2009; Constantinople & Bruno, 2013; Feldmeyer et al., 2013).

3. Cortical neurons and excitation-inhibition balance

The canonical circuitry is a set of circuit motifs made of mainly 2 different types of neurons. These two major classes are excitatory (i.e. glutamatergic) and inhibitory (i.e. GABAergic) cells, which execute the abovementioned functions of the whisker-to-barrel pathway. Excitatory neurons make up ~80% of the neuronal population and are known for their long-range projections other than local connections (Fishell & Rudy, 2011; Harris & Mrsic-Flogel, 2013). Even though excitatory cells outnumber the inhibitory cells, excitatory and inhibitory inputs are shown to match in total activity (Cafaro & Rieke, 2010; Graupner & Reyes, 2013) which points to a functionally important balancing of cortical activity, termed excitation-inhibition balance (Isaacson & Scanziani, 2011).

Although there is a consensus in the literature for excitatory cells, the classification of GABAergic (γ-Aminobutyric acid) neurons, which make up 15 to 20% of all cortical neurons (Meyer et al., 2011; Staiger et al., 2015), is still a matter of debate due to the heterogeneity in target specification on the subcellular level, distribution of dendrites and axons within the cortex, circuit motifs, and molecular marker expression (Ascoli et al., 2008; DeFelipe et al., 2013; Harris & Shepherd, 2015; Tremblay et al., 2016; Staiger & Petersen, 2021). However, when cell types were taken into account with respect to their expressed molecular marker, achievement of 4 non-overlapping classes is possible: PV, somatostatin (SST), VIP, and other (i.e. Lamp5/Scng) neurons (Mao & Staiger, 2024). The interplay among 3 of these 4 cell groups and excitatory cells (shown in Fig. 2), and together with mainly Lamp5-expressing neurogliaform cells, enables harmony of the network activity in the cortex.

PV-expressing neurons are the most populated GABAergic cell class, covering around 40% of all inhibitory cells (Tremblay et al., 2016). They are present in all layers but

L1. They preferentially target excitatory cells and modulate their activity (Tremblay et al., 2016; Mao & Staiger, 2024), and also a proportion of SST cells (Walker et al., 2016). They receive input from excitatory cells (90%) and GABAergic cells (including other PV cells; Kameda et al., 2012). For example, L2/3 PV cells in S1BF are targeted mainly by L4 excitatory cells other than some minor projections from other cortices (Druga et al., 2023). Known for their fast-spiking properties and strong synaptic output, PV cells are often considered the main mediators of cortical inhibition. Although excitatory cells outnumber PV cells, the target rates also enable PV cells to have control over excitatory output since each PV cell is estimated to target around a thousand excitatory cells (Packer & Yuste, 2011). They provide rapid and precise feedforward and feedback inhibition, essential for sharpening sensory responses, ensuring temporal fidelity/tuning of neuronal firing, and maintaining excitatory-inhibitory balance within local circuits (Rupert & Shea, 2022). They also take an integral part in many perceptual functions in the cortex like auditory associative fear conditioning (Letzkus et al., 2011) or gain control of visual stimuli (Atallah et al., 2012). One of the good examples of their nature as main inhibitors is that, when optogenetically stimulated, they cause a significant drop in the mice's discrimination performance compared to two different contrasts of the visual stimulus (Cone et al., 2019) which means increased inhibition disrupts the perceptual processing in the cortex.

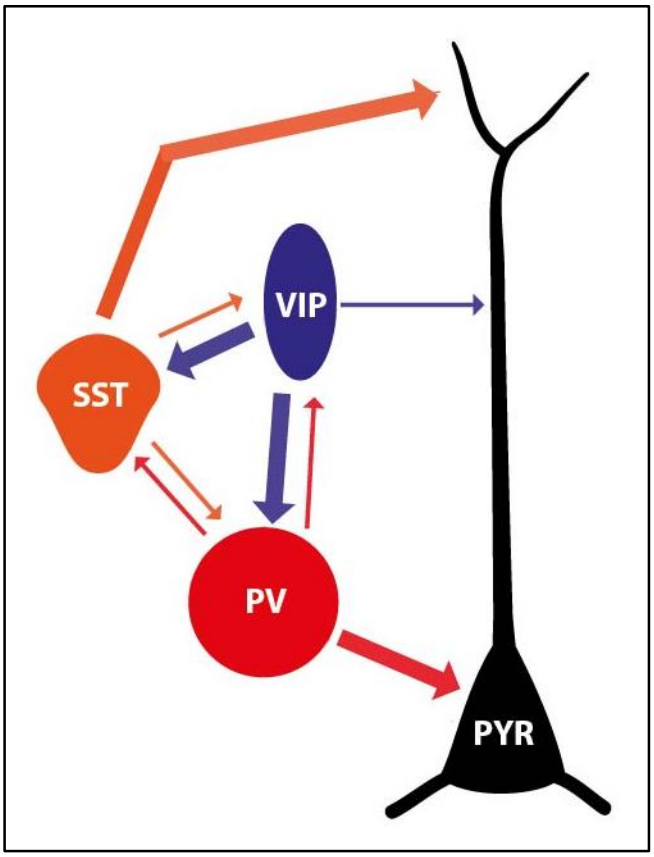

Figure 10. Harmony of the network activity. There are 3 non-overlapping groups of GABAergic neurons: PV- (in red), VIP- (in dark blue), and SST-expressing (in orange). All these cells target both excitatory/pyramidal cells (in black) and each other. IN the figure a microcircutry motif is presented. The arrows between cells shows the connections. Thickness of the arrows displays the main roles of these cells. For example, VIP cells target other inhibitory cells more than they target excitatory cells. They are known as disinhibitors since they inhibit the inhibition on the excitatory cells. PV and SST cells mostly target excitatory cells. However, the arrows here do not represent the connectivity strength. For example, excitatory cells receive input most strongly from the PV cells. For this reason, PV cells are known as the main inhibitors. The figure is adapted from Staiger & Petersen (2021).

SST cells represent 30% of the GABAergic cells (Rudy et al., 2011) and they also mainly take part in the inhibition of excitatory cells (Silberberg & Markram, 2007; Xu et al., 2013; Naka et al., 2019) although some proportion of them target PV cells (Hioki et al., 2013; Xu et al., 2013; Walker et al., 2016) or VIP cells (Walker et al., 2016; Rachel, 2022; Preuß, 2023). They are shown to regulate independently top-down and bottom-up input by different types of SST subtypes inhibiting specific layers (e.g. Martinotti cells in L2/3&5, while nonMartinotti cells in L4; Naka et al., 2019).

The story turns interesting regarding VIP-expressing neurons, 13% of all cortical GABAergic cells. VIP cells, mostly found in L2/3, exhibit distinct properties in terms of electrophysiological and morphological characteristics (Prönneke, 2017). Their role in the excitation-inhibition balance is also different compared to PV and SST cells. Although they are prominently known for inhibiting SST cells (Lee et al., 2013), they constitute 60% of the GABAergic inputs to PV cell bodies (Dávid et al., 2007; Druga et al., 2023). They inhibit other GABAergic cells rather than inhibiting excitatory neurons (Zhou et al., 2017; Yu et al., 2019), which results in the inhibition of the inhibition of excitatory cells (Staiger et al., 2004; Pfeffer et al., 2013; Pi et al., 2013; Karnani et al., 2016). It is also known that stimulation of VIP cells, increases spiking of excitatory cells (Pi et al., 2013). In other words, they disinhibit the excitatory cells (i.e. they release excitatory cells from inhibition), thereby amplifying cortical output. In this aspect, opposite to PV cells, VIP cells are known for being the main disinhibitors, although the other interneurons (INs) also target INs to some extent (see above).

This disinhibition is crucial in sensory processing, particularly during attention or active whisking. For instance, VIP cells are activated during rewarded auditory cues or changing visual stimuli, selectively suppressing SST-mediated inhibition on pyramidal neurons. (Pi et al., 2013; Karnani et al., 2016). Another good example of their responsiveness to sensory stimuli in S1BF is that they exhibit similar characteristics to excitatory cells during bottom-up processing (Ramamurthy et al., 2023). Also, Guy et al. (2023) showed that during passive whisker stimulation at different angles, VIP cells in S1BF are endowed with direction-specific tuning similar to excitatory cells. In another study, optogenetic stimulation of VIP cells in the visual cortex increased contrast discrimination performance of the mice, contrary to stimulation of PV cells (Cone et al., 2019).

Overall, the harmony of excitation-inhibition and the balance between inhibition and disinhibition are key in sensory processing and a product of the collaboration of different properties of inhibitory cells. Through the above-summarized complementary roles, inhibitory cells orchestrate a fine balance between inhibition and disinhibition, shape the excitatory output in barrel cortex activity, and enable precise sensory processing. In the scope of this project, PV- and VIP-expressing cells were selected as the main targets due to their opposing functions, as main inhibitors and main disinhibitors respectively, in S1BF.

4. To be inhibited, or not to be inhibited, that is the question

To explore the roles of PV and VIP neurons in the mouse neocortex, especially in the S1BF, is essential for understanding how sensory information is processed and especially how they contribute to tactile perception. Would the tactile percept still be precise enough to discriminate between different tactile stimuli if the activity of one of these cell groups is increased? Would this change find a way to reach the equilibrium of the balance of inhibition and disinhibition? Does increased inhibition cause a sort of numbness in terms of perceiving different textures? Or does the increased activity of main disinhibitors create a chance of perceiving the textures better?

None of these questions have been so far answered clearly in the literature. Given that we still have a minimal idea of the roles of INs in tactile perception, especially in the whisker-based texture discrimination ability of mice in a non-head-fixed setting, I started to design this project, in which the main research questions are:

- Can mice still perceive textures in case of increased inhibition?
- Is it possible for mice to increase their discrimination performance in case of increased disinhibition?

For these aims, first I needed to establish a novel texture discrimination test for freely behaving mice due to the small number of behavioral batteries described in the literature. The test enabled measuring of the animals' success rates in different experimental conditions in a non-head-fixed setup. In the continuing pages, I explain the details of the “textured T-maze”, which lets the subjects learn discrimination between two types of sandpapers having different coarseness.

Later, with the help of the chemogenetic method and IN-specific Cre-driver lines (in this project PV-Cre and VIP-Cre lines), I managed to manipulate different types of INs. Chemogenetics is a method that enables to possibility of expressing designer receptors exclusively activated by designer drugs (DREADDs) on the targeted cell population in the targeted field via cranial injection of a certain type of virus (see “Methods and Analyses” section for a detailed explanation). The activation of DREADDs needs a specific ligand (in this project it is clozapine-N-oxide; CNO) to be delivered mostly via intraperitoneal injection. For this reason, it was the perfect tool to use: It resolves the problem of light fibers that comes with the optogenetic method, which is a disadvantage when experiments are done in freely behaving animals across multiple days, even weeks. The DREADDs might have activating (increasing the firing of the targeted cell group by depolarizing it) or deactivating properties. In this project, I had the chance to test the mentioned research questions via expression of the activating type of DREADDs, with the virus injection in S1BF, in either VIP or PV cells.

The main hypothesis of this project was that chemogenetic activation of PV or VIP cells would cause distinct effects on texture discrimination performance of well-trained mice:

- Since they are the main inhibitors of the cortex, when PV cells are activated, a decrease in performance in texture discrimination due to the over-inhibited excitatory signal in the S1BF is hypothesized.
- However, an increase in texture discrimination rates of the animals when VIP cells are activated was expected, due to the reason that they are main disinhibitors and activation of VIP cells will release inhibition from excitatory cells to some extent.

The findings of this project indicated that S1BF PV and VIP neurons has a crucial role in whisker-based texture discrimination. Chemogenetic activation of both PV and VIP cells resulted in impaired texture discrimination ability.

METHODS & MATERIALS

Animals: For this project VIPcre+ (further referred to VIP or VIPcre; Strain: Vip$^{tm1(cre)Zjh}$/J, JAX Stock #010908, RRID: IMSR_JAX:010908; Taniguchi et al., 2011) and PVcre+ (further referred to PV or PVcre; Strain: B6;129P2-*Pvalb*$^{tm1(cre)Arbr}$/J, JAX Stock #008069, RRID: IMSR_JAX:008069; Hippenmeyer et al., 2005) mice were recruited. These lines are designed to have the endogenous vasoactive intestinal polypeptide (VIP; in VIPcre+ line) and parvalbumin (PV; in PVcre+ line) promoter/enhancer elements providing Cre recombinase expression to VIP- (in VIPcre+ line) and PV-expressing cells (in PVcre+ line).

Subjects: In total 25 mice, 16 VIPcre (6 females & 10 males, M±SD$_{age}$ = 14.3±1.2 weeks) and 9 PVcre (4 females & 5 males, M±SD$_{age}$ = 13.3±1.5 weeks) were used in the project. All animals were group-housed (2 or 3 animals/cage) in regular cages with *ad libitum* water (also food during the recovery period). All cages were kept in the same facility room with a 12:12 L:D cycle, ~20°C ambient temperature, and ~50% humidity. The cages were enriched only with nesting material, a wooden gnawing stick (100 x 20 x 20 mm), the handling tube (internal diameter = 50 mm, length = 100mm), and a glass Petri dish to serve food daily after the sessions (except during the recovery period).

Experimental timeline: All animals first went under stereotactic surgery for adeno-associated virus (AAV; see "Cehmogenetics" section) injection (Day 0). Then on Day 8, they started with the behavioral test. After they were trained on texture discrimination, animals were tested under the clozapine-N-oxide (CNO condition) and then they were sacrificed approximately at the end of a month either for verification of correct virus expression (stainings and imaging) or for verification of proper virus functioning (in vitro whole-cell patch-clamp experiments; Fig. 3).

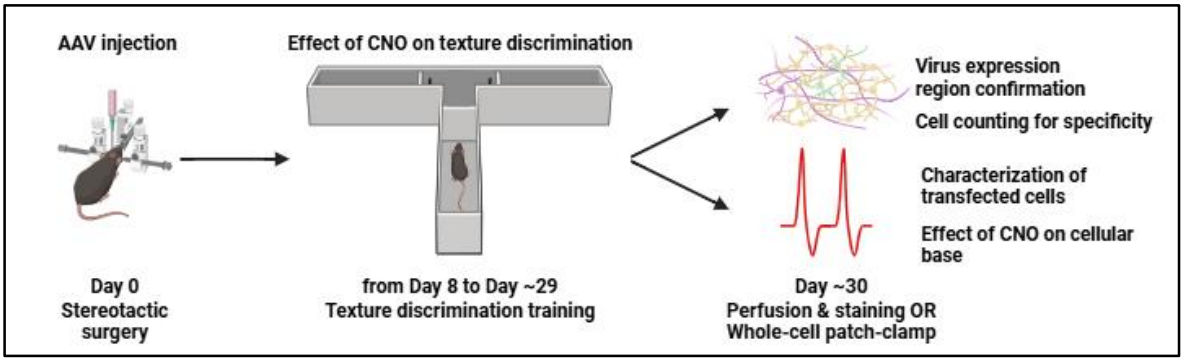

Figure 19. Experimental timeline. All animals initially went under stereotactic surgery for intracranial injection of AAV. After a week of recovery period, animals started their training in TT. At the end of maximum of 21 days in TT, animals were sacrificed either for staining or for electrophysiological experiments. The figure is created in BioRender.com

The protocols of each step will be elaborated under corresponding subtitles. All experiments were conducted following German law on animal research and under the permission of the Lower Saxony State Office for Consumer Protection and Food Safety (LAVES; AZ: 33-19-42502-04-19/3157).

1. Textured T-maze (TT) and food restriction

Unlike the abovementioned head-fixed experiments, a setting where animals can move freely might allow the experimenter to observe more natural behavior in active sensing conditions (Qi et al., 2022). Also, it frees up the time for the animal to be habituated to the head-fix apparatus and maintains a more comfortable time in their home cage. That is to say, a non-head-fixed battery might be more beneficial than it seems to supply data as close as possible to an animal's inherent behavior. For these reasons, a new behavioral essay was established, and we named it the textured T-maze (TT) which was custom-made and semi-automated (Fig. 4). It was a T-shaped maze with one start arm and 2 identical taget (goal) arms with food plates at the end. All arms were 10 cm wide and 30 cm long with 20 cm high walls. Each arm had a remotely controlled guillotine door opening to the center of the maze. By adding 2 cylindric blocks covered with different grit sizes (i.e. the size of the abrasive material on the sandpaper with the bigger the number, the softer the sandpaper texture) of SP, this maze was used as a texture discrimination battery. During the task, animals were food-restricted to increase their motivation for food-seeking as they were going to receive food reward (i.e. oat flakes) when the correct choices were made during the task. Special attention was paid to keeping their weight around 90% of their initial weight.

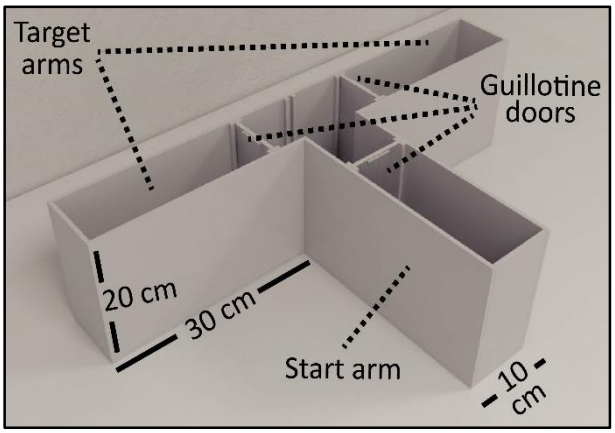

Figure 28. Textured T-maze (TT) basic structure. TT is a modified version of a regular T-maze. The T-maze has 2 target arms opposed to each other, and one start arm connecting these two arms perpendicularly in the middle. All arms are closed with a guillotine door, which the experimenter remotely controlled in these experiments. To turn it into a TT, 1 sandpaper-covered block (e.g. 50 ml falcons for this set of experiments) was placed in front of each target arm. These two sandpapers were in different grit numbers, and mice were trained to find the coarser texture. Both arms were opened at the end of an exploration period (e.g. 10-15 secs) and mice showed their decision by entering one of the target arms. The unchosen arms were immediately closed after one of the target arms was chosen. If the choice was correct (i.e. the animal found the coarse texture), they found oat flakes at the end of the arm.

Texture-covered blocks and discriminanda: In total 12 Falcon tubes (50 ml, Sigma Aldrich) covered with SP (6 of them with P120 and 6 of them with P1500, in total 6 pairs of coarse versus soft textures) were used during the experiments as texture blocks. After they were wrapped around the falcon tube and secured with two-sided tape, the lids of the tubes were also screwed because animals tended to bite the corners of the SP. The lid supplied protection since it is harder to bite for a mouse and also whenever there was a bite mark on the lids, it was easier to change just the lid rather than covering a new tube. SPs were odor-masked with 80% EtOH by repeatedly spraying before the first use and every session they were freshly sprayed again. The texture blocks were fixed in the maze, right in front of the target doors, with double-sided tape, and the texture block pair was replaced with an unused pair in each trial.

A session in the TT: The animals were transferred individually from their home cage to the carrying cage with the handling tube. The mouse was examined quickly for any wound and it was made sure that their whiskers were intact. The cage was secured with the cage grit and then the subject animal was taken to the observation room (i.e. the room separated by a sliding door with the test room having a monitor connected to the TT (please see “Measurements and Analyses” section for details). The animal was weighed and then left in the dark test room (infrared lights on) inside the carrying cage for pretest habituation (i.e. 20 mins for the very first session and later on 15 mins for all sessions). At the end of the habituation period, the soft alarm sound of the stopwatch went on. The experimenter entered the test room, turned the dim red light on, and introduced the animal to the start arm of the TT with the handling tube. Then the dim light went off, and the start arm opened remotely from the observation room, after the exploration period (cued to the animal with a stopwatch alarm) both target doors opened. The unchosen arm's door was closed after the subject’s 4 paws entered one of the target arms. In the case of a correct choice (i.e. hit) the animal was allowed to eat and finish the food reward (e.g. oat flakes), and in the case of an incorrect choice (i.e. miss) the animal was waited until they reached the empty food plate. Afterward, the experimenter entered the test room, turned the dim light on again, and returned the mouse to the carrying cage. The stimuli and the food reward were refreshed/relocated, and feces or urine were quickly cleaned with a dry paper towel. Then the maze was ready for the next trial. This was repeated mostly 12 times (e.g. mostly 12

trials per session, but sometimes 18 or 24 trials per session, too), and after the last trial, the animal was taken back to the home cage and fed within approximately 1 hour with the daily amount of food necessary to maintain max 10% (of the initial weight) weight loss. The carrying cage was kept the same until the last day of experiments, and the same one was used for the cage mates which made mice more comfortable during the experiment due to the constant familiar smell.

Food restriction: Food restriction was applied as an incentive of mice in TT to learn texture discrimination. Stemming from the restricted food rather than *ad libitum* reach, animals were motivated to seek food reward in the maze.

All animals were weighed on the first day of TT, and this weight was taken as the reference for each mouse's weight loss. To keep close track of the weight loss curve, animals were weighed every day before the experiments started. The cage mates were being tested right after each other, and only after the last animal was tested they were given their daily amount of food (e.g. usually around 3 grams of regular facility food per animal). The actual weights taken into consideration, small changes were made in the amount of total food they were fed. Animals were usually group-fed but only in very few cases, they needed to be fed separately to get rid of the unbalanced weight(loss) among cage mates.

Protocol: TT protocol consisted of 3 slightly different, gradually changing designs to prepare animal for the actual texture discrimination task, and 4 phases as follows (see Fig. 5 for a summary):

I. *T-maze Habituation:* Since animals needed to get habituated to a new environment (i.e. T-maze) and also the reward food (i.e. oat flakes), they were taken to the maze for 6 habituation sessions (2 sessions/day) with gradually changing conditions. Intersession duration for each animal was 2 to 3 hours, one being before noon and the latter being in the afternoon.

a. Habituation Session 1, 2, & 3: When the animals were first introduced to the maze, all guillotine doors were closed. Animals were free to move in the empty maze for 10 minutes, after opening all of the guillotine doors in 15 seconds. These sessions were for the animals to get used to the transport cage, behavioral room, the maze environment, and the movement of the doors.

b. Habituation Session 4: This session was almost identical to the prior habituation sessions except for one novelty. In this session, animals met the food reward for the first time. 200 mg of oat flakes were shared to 2 goal arms equally and randomly spread, and animals were allowed to eat and move in the maze as much as they liked for 10 minutes.
c. Habitation Session 5: The only difference in this session compared to Habituation Session 4 was the location of the reward food. Rather than being spread randomly within the goal arms, most of the oat flakes were in the food plates located at the end of each goal arm. In this way, animals were able to see for the first time that they needed to move towards the endpoint of the goal arms to get a food reward.
d. Habituation Session 6: This session was just a small training of the actual task with 6 trials only. For the first time, a texture-covered block was placed pseudo-randomly in front of one of the target doors to cue the food reward (e.g. usually 3 oat flakes/trial). Animals were introduced to the maze in the start arm. They had 15 seconds (later this period will be called the "exploration window") from the opening of the start door to the opening of both target doors. After they entered an arm, the unentered arm's door was closed. If animals made a correct choice, the trial was finished after they finished eating and they were put back in the carrying cage until the next trial. If it was the incorrect choice, they were shown the correct arm and again let to eat the reward. Performances in these sessions were not scored since the only aim here was to habituate animals to repetitive trials.

II. *Training for 2AFC task:* In this phase, there was only one texture block (coarse) cueing the food reward pseudo-randomly in one of the target arms. This means that while one of the target doors was pointed with the texture block, the other one did not have any object/texture. To randomize the order of the baited arms, predetermined 20 sequences (each consisted 6 left and 6 right, in total 12, locations for the bait) for 2-choice discrimination tasks were used (Fellows, 1967).

To make learning the discrimination task easier, animals were first trained to choose the target arm with a texture block in front of it. This step was not evaluated with regard to

animals' ability to discriminate any texture but was only a pre-training for the nature of 2AFC tasks. Animals were first carried to the test room with a carrying cage (identical to their home cages) and left under infrared lights for 15 minutes for habituation with the handling tube inside the cage. The flow for a trial was as follows: Animals were moved inside the start arm with the transport tube under red lights. Seconds later, the red lights went off and the start door opened. Animals went to the exploration zone and 15 seconds later both target doors opened. Animals made a choice and entered one of the target arms. When all 4 paws were inside one of the target arms, the unchosen arm's door closed. After the animals reached the food plate at the end of the goal arm, the red light went on and the transport tube was placed in the start arm for the animal to return. Animals learned to return inside the tube themselves with the exception of the initial sessions where they were gently (mostly with no touch) directed in there and put back in the carrying cage until the next trial. After the animals were secured in the carrying cage, the maze was prepared for the next trial: removal of any feces/urine, changing the side of the texture block (if required by Fellow's (1967) abovementioned sequences), and refreshing the food reward.

III. *Discrimination training:* After animals met the success criteria (see below) in the last phase, they switched to the discrimination task. This phase being quite similar to the former phase, was to determine animals' ability to discriminate 2 textures (soft versus coarse). This means that there were 2 texture blocks introduced in the maze each being in front of one of the target arms (e.g., the coarse SP was in front of the left target arm and the soft SP was in front of the right one). Always the coarser SP was used to cue the food reward. Randomization of the texture blocks and the success criteria was identical to the former training phase.

IV. *Testing:* After animals reached the "learner" stage (serving also as one of the control conditions) in the discrimination training phase, the 4th phase started. This phase, being similar to phase 3, was called "testing" because mice were injected with either clozapine-N-oxide (CNO; 3 mg/kg in 100 µl sterile 0.9% NaCl/saline; see the section below for details) or saline intraperitoneally, 1h before they were carried to the experimental room (e.g. 75 mins before they start the task).

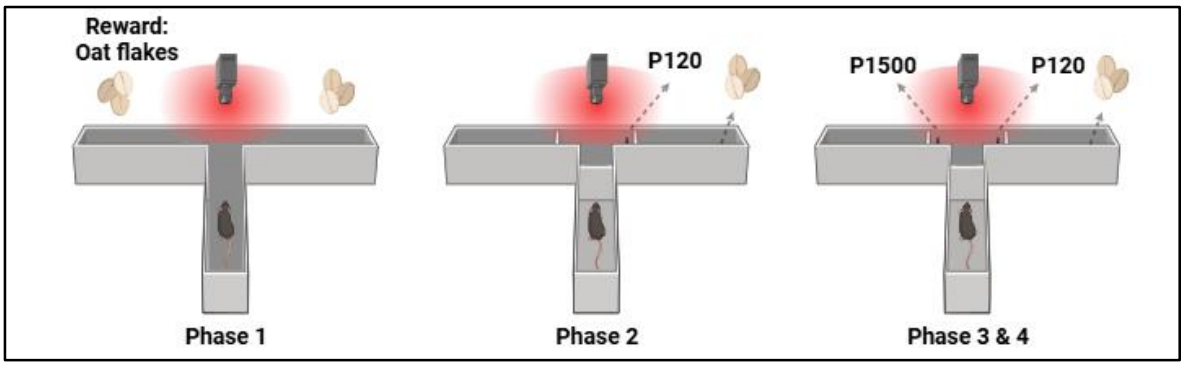

Figure 37. TT protocol. Protocol of TT had slight differences for different phases of the task. Initial phase (e.g. habituation, Phase 1) was not goal-oriented but for the sake of animals' habituation to the experimental environment. In the 2nd phase (e.g. 2AFC training), animal was just supposed to learn that the texture block was cueing the reward. The 3rd and the 4th phase (e.g. texture discrimination training and the test respectively) was in principle identical; animals were supposed to find the food reward by discriminating coarser SP. However, during phase 3 there were no manipulation and so it gave the chance for taking final session(s) as the baseline performance of the animals. In phase 4, animals were injected with both CNO and saline (on different sessions) to test the effect of the activation of DREADDs via IP injection of CNO.

Success criteria: Animals had 2 phases to show that they are learners to start with the testing phase. For this reason, learner's criteria needed to be set. In principle, if they are performing over chance level continuously, this should already be an indicator of a trained choice, yet to make it statistically clear, initially the binomial probability of a successful session was calculated (calculations made with inert scripts of MATLAB v.2020a, The MathWorks Inc., USA):

Initially, the minimum number of hits was determined for different sets of trials, for above chance level thresholds. For a binomial distribution, the mean (μ) and standard deviation (σ) were calculated:

$$\mu = n * p$$

$$\sigma = \sqrt{n * p * (1 - p)}$$

Than threshold of number of successes indicating above chance level was calculated (always rounded up, *z* implies corresponding z-score):

$$Threshold = \mu + z * \sigma$$

Due to the slightly changing performances over the sessions, an animal was expected to score above the chance level at least 2 and at most 3 sessions to count as a learner. For this reason, thresholds for 24 and 36 trials were calculated and taken as a joint value for these sessions:

$$Threshold\ (24\ trials) = (24 * 0.5) + 1.654 * \sqrt{(24)(0.5)(0.5)} \approx 17$$

and following the same route, Threshold(36 trials) ≈ 23 was found (See Fig. 6 for a summary graph for all determined thresholds between 12 and 48 trials).

Since between 5 to 7 hits were taken as chance level (random choice), animals were expected to score minimum 8 hits per 12 trials. Together with calculated thresholds, animals were supposed to score minimum 8/12 (67%) and 9/12 (75%) for 2 consecutive sessions (e.g. in total 17/24 hits, meets the joint threshold for 24 trials, see calculation of "learner score" under Measurements and Analyses section).

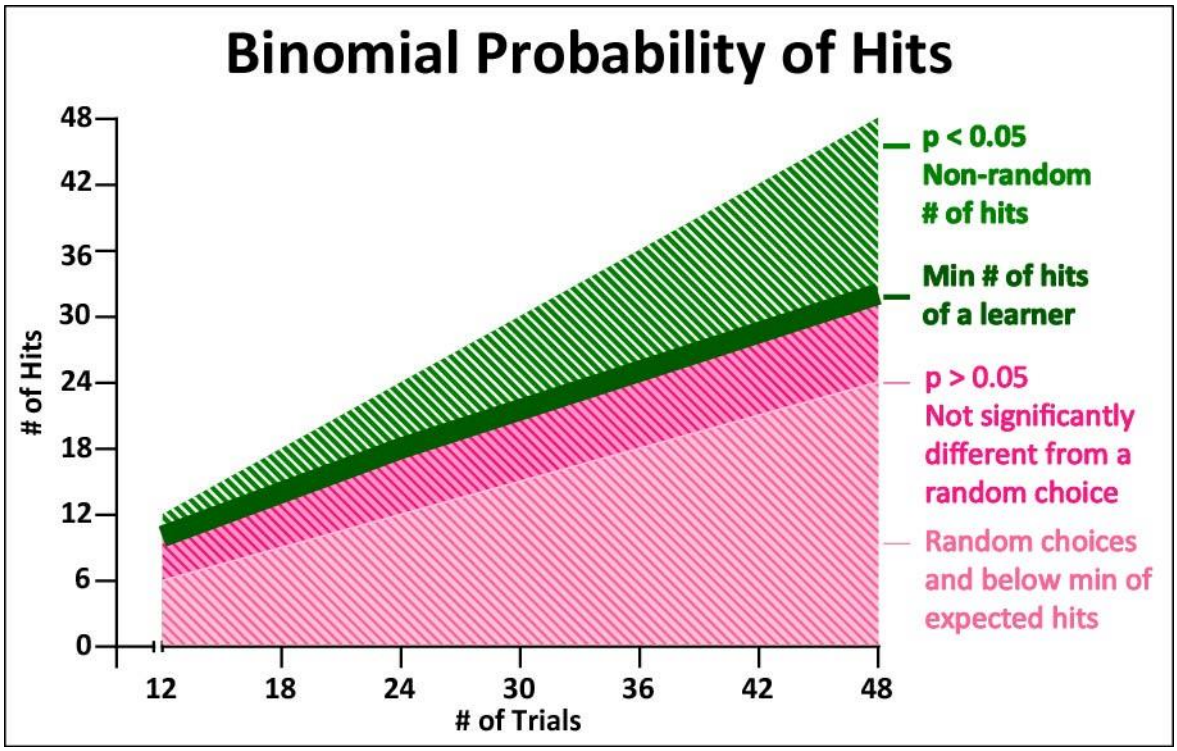

Figure 46. Calculation of learner's criteria. The table was generated to follow up during the experiments. The dark green line denotes the threshold for each possible set of trials. Mostly criteria for 24 and 36 trials were used with a joint threshold. For each possible score above the chance level, a p value was calculated. Animals were accepted as learners, only when they scored the success levels statistically above random-choice (chance) levels.

Secondly, probability of scoring the threshold was calculated. Where, x = # of successes, p = probability of success in one trial, n = total # of trials:

$$\mathrm{P(x: n, p)} = \binom{n}{x} p^x (1-p)^{(n-x)}$$

$$P(x) = \frac{n!}{x!\,(n-x)!} p^x (1-p)^{n-x}$$

For example, binomial probability of scoring 17/24 hits was calculated as:

$$\mathrm{P(17: 24\,, 0.5)} = \binom{24}{17} (0.5)^{17} (0.5)^7 \approx 0.00000206$$

which proved statistically significant thresholds for TT.

Intraperitoneal injection: Previously prepared frozen aliquots of 20 µl diluted CNO (see Chemogenetics section for details) or saline was left at room temperature (RT) for at least 90 mins prior to injection and drawn into a syringe just before the injection time. The mouse subjected to injection was restrained carefully and the needle was inserted in lower left or right quadrant of the abdomen. After the injection, the injection area was shortly observed to make sure there is no backflow (e.g. due to subcutaneous injection). Then the animal was released in the home cage until the habituation period.

Most of the mice received saline 24h later and were tested again in TT. If animals performed 67% and above under saline condition, they received in the next session, 24h later, CNO again. If performance was below 67%, they received saline up to 2 more days until they perform conveniently with a learner performance. Later with the observation of the regular learner behavior, the mice were injected CNO again. In other words, animals were injected at least 1 (CNO only) and maximum 5 (CNO-3 times saline-CNO again) times as the legal permission allowed.

Saline injection in this phase was needed to create a control condition for the effect of the injection protocol. Retesting animals under CNO condition was for clarifying if the effect of CNO was reproducible. Due to the restriction with allowed number of days for the experimental period, it was not possible to test a small portion of mice under more than 1 injection condition (see “Results” section).

2. Chemogenetics - DREADDs

To make it possible to control the activity of certain cell populations (in this project PV and VIP cells in the S1BF) remotely and in a reversible way, the chemogenetic method was employed. Being coined initially more than 3 decades ago (Forkmann & Dangelmayr, 1980), today it is being used as an umbrella term for processes of engineered macromolecules’ interaction with small molecules (Urban & Roth, 2015). For this project’s sake, designer receptors activated by designer drugs (DREADDs) were used. Simply put, cre-dependent AAV vector was injected bilaterally to express DREADDs in the target cell population (VIP cells in VIPcre and PV cells in PVcre animals) in S1BF and later these populations were aimed to be activated with intraperitoneal injection of the inert ligand (i.e. CNO). This method was advantageous for various reasons: high spatial accuracy, being

remote (e.g. no probes, cables, headsets required) and so being comfortable for freely moving animals in the textured T-maze, and having a reversible effect on transduced cells which made it possible to retest the same subjects.

As the method requires, to express the designer receptors (i.e. modified human muscarinic acetylcholine receptor 3 which couples to Gq-type G proteins; hM_3D-Gq; Armbruster et al., 2007) in S1BF, all animals first underwent stereotactic surgery and later were administered the designer drug (i.e. CNO as the synthetic ligand) to observe the effect of activation of the specific cell population (i.e. either PV or VIP cells) on texture discrimination performance.

Stereotactic surgery (SS): All instruments and surgery area were sterilized with 75% EtOH. All animals were first weighed and then injected with Buprenorphine (0.1 mg/kg, Buprenovet, Bayer) intraperitoneally (IP), 30 minutes before surgery for pain relief. Meanwhile, a Nanoject Glass Capillary (Drummond Scientific Company, USA) which was pulled with P-97 Flaming/Brown Puller (Sutter Instruments, USA) and the tip diameter manually cut to 20±2 µm was backfilled with mineral oil (Sigma-Aldrich), and placed into the Nanoject II Nanoliter Injector (Drummond Sci. Co., USA) which was controlled by Micro4 Microsyringe Controller (World Precision Instruments, USA). Later the pipette was front-filled with viral vector (the cre-dependent chemogenetic viral vector, AAV5: pAAV-hSyn-DIO-hM3D(Gq)-mCherry, which was a gift from Bryan Roth, Addgene viral prep # 44361-AAV5; RRID: Addgene_44361, Krashes et al., 2011).

Later the mice were taken to the anesthesia box and deeply anesthetized (3-4% isoflurane in 1.5 L/minute oxygen). Then they were immediately taken to the stereotactic frame (World Precision Instruments, USA) where anesthesia (1.5-2.5% isoflurane) was maintained with a snout mask attached to the mouth fix of the frame and ears were also fixed tightly while the body temperature was secured with a heating pad. The eyes were covered with an eye ointment (Bepanthen Eye and Nose Ointment, Bayer Vital GmbH) and it was refreshed in case of need. The incision area was cleaned with 75% EtOH. A local anesthetic, Lidocaine (100-200 µl, Lidocainhydrochlorid 2%, bela-pharm GmbH & Co.), was injected subcutaneously at the incision site and the fur was trimmed with the help of scissors to make the incision area clean enough. An incision was made with the help of a

freshly opened sterile scalpel, and the detached skin was gently pushed to the sides of the head and kept with custom-made sterile weights.

Using coordinates from the mouse brain atlas (Paxinos & Franklin, 2019), one cranial window per hemisphere was opened with a dental drill (OS-40, Osada Electric Company, Japan), and two injections per cranial window, each 250-300 nl of AAV were made (relative to the bregma: at -1.4 and -1.6 mm anteroposterior, +/- 3 mm mediolateral). Each was dispensed in two depths (600 µm and 400 µm below pia, respectively).

The virus was injected at an optimum speed (100 nl/min; Lerchner et al., 2014), and no backflow was observed. After all of the 4 injections were completed, the skin was released to get ready for suturing. After suturing, an eye ointment (Vitagel, Bausch + Lomb Inc.) spread on the wound for a faster recovery process.

Afterward, animals were kept in pre-warmed cages until they were awake and ambulant again. They were supplied with mashed food containing oat flakes and regular mouse food pellets. They were administered Carprofen (5 mg/kg, Pfizer) at the end of the surgery, 24 and 48 hours after the surgery to extend the pain relief. Animals were checked daily for 7 postoperative days for general health (e.g. wound recovery, breathing, behavior, movement, and so on) and weight control. In case their weight dropped by 5% they were supplied with the mashed food again.

The area of virus expression was confirmed with mCherry signal, and immunohistochemistry (IHC) and fluorescent in situ hybridization (FISH) analysis of PV and VIP expression (see below). Transduced cells were thus analyzed for their specificity to exclude leak expression of the viral construct (see below).

CNO preparation: Bilateral expression of cre-dependent AAV enables the opportunity to manipulate different types of INs. As described above, because this virus transduces target cells to express DREADDs, animals were supposed to be given CNO to see the effect of the activation (in electrophysiological terms: depolarization of the transduced cells) in behavior or at the electrophysiological level. For this sake, it was used at 2 timepoints as follows:

i. CNO was used after animals were proficient in texture discrimination, they were administered CNO (3 mg/kg in 100 µl saline, CNO dihydrochloride, HelloBio)

intraperitoneally ~75 mins before the session in the TT started. CNO was dissolved in saline and kept in a -20°C freezer in aliquots. The necessary number of aliquots was taken out of the freezer and kept at RT for 90 minutes. Later on, the stock in the aliquots was diluted with sterile 0.9% NaCl (RT) to the final dosage of 3 mg/kg and the final ready-to-inject amount of 100 µl.

ii. The same stock was also used in electrophysiology experiments for bath application, with each bath solution having a final concentration of 4 µM CNO when in 50 ml artificial cerebrospinal fluid (ACSF; for the application in these experiments, please see the "CNO bath application" section below).

3. *In vitro* electrophysiology

Subjects: Thalamocortical slices of 5 VIPcre (M_{age} = 18.9 weeks, on average 6 weeks after SS, n = 7 labeled and n = 2 unlabeled cells) and 3 PVcre (M_{age} = 18.3 weeks, on average 5.7 weeks after SS, n = 5 labeled cells) AAV-injected mice were used for whole-cell patch-clamp recordings.

Slice preparation: Mice were deeply anesthetized with isoflurane and decapitated. Brains were removed to freshly prepared, carbogenated (infused with 95% O_2 and 5% CO_2), ice-cold cutting solution (pH: 7.4, prepared with (in mM): 87 NaCl, 1.25 NaH_2PO_4, 2.5 KCl, 10 glucose, 75 sucrose, 0.5 $CaCl_2$, 7 $MgCl_2$, 26 $NaHCO_3$). Two hemispheres were separately glued on the microtome stage (Leica VT1200 S, Germany) after the correct angles for S1BF were arranged following Porter et al.'s (2001) modifications. With a speed of 0.12 mm/s, 300 µm thick slices were obtained from S1BF, and in total 12 slices from both hemispheres were collected. Slices were incubated ~1h at 34°C in freshly prepared and carbogenated ACSF (pH: 7.4, prepared with (in mM): 125 NaCl, 1.25 NaH_2PO_4, 2.5 KCl, 25 glucose, 2 $CaCl_2$, 1 $MgCl_2$, 26 $NaHCO_3$). Once the incubation was finished, the heater was turned off and the incubation chamber was left at RT. Until the end of the experiment, the slices in the incubation chamber were kept carbogenated.

Whole-cell patch-clamp and electrophysiological characterization of neurons: A fixed-stage upright microscope with a recording chamber (Axio Examiner A1, Zeiss, Germany) was used for electrophysiological recordings. Slices were placed in the recording chamber (i.e. bath) with a constant flow of carbogenated ACSF (2 ml/min) and kept at 32°C

in the bath. S1BF was first targeted with 2.5x magnification and later transduced PV or VIP cells were identified by mCherry fluorescence under a 40x water immersion objective (Olympus, Germany).

Borosilicate glass capillaries with filament (GB150F-8P, Science Products, Germany) were pulled by a pipette puller (P-1000, Sutter Instruments, USA) for patch electrodes and later they were filled with intracellular solution (pH: 7.4, osmolarity: 290 mOsm, prepared with (in mM): 13d5 K-gluconate, 5 KCl, 10 HEPES, 0.5 EGTA, 4 Mg-ATP, 0.3 Na-GTP, 10 Na-P-creatine and later added 0.3-0.5% biocytin). The patch electrode was directed to the target cell by micromanipulators (Luigs & Neumann GmbH, Germany). Access resistance (R_{acc})was monitored. All recordings (except access resistance) were done in current clamp configuration, and no holding current was applied (recordings at resting membrane potential). After the whole-cell configuration was obtained, the passive and active properties of the cells were characterized.

CNO bath application: Previously prepared aliquots of CNO were left in RT for at least 90 minutes. For the bath application, a 50 ml syringe was filled with ACSF, and CNO stock was added to a final concentration of 4 µM added into this extracellular solution and connected to the inflow of the recording chamber with a separate switch. After the initial cell characterization was completed, the ACSF supply was switched to ACSF with CNO. Bath application (i.e. wash-in) was monitored by recording in current clamp mode for 10 minutes to observe the changes in membrane potential and monitor input resistance by applying -10 pA pulses lasting 200 ms every 6 seconds.

In the end, CNO was tried to be washed out by switching back to regular ACSF circulation (for 40 mins to 1.5h), yet no change was observed in the membrane potential of the patched cells within this lengthy period.

4. Transcardial perfusion, IHC, FISH, and imaging

After being deeply anesthetized with a ketamine (150 mg/kg; CP-Pharma) and xylazine (10 mg/kg; Ecuphar GmbH) mixture, mice were fixed in the Styrofoam surgical station by fixing the paws. Diaphragm was pierced open following thoracotomy. The rib cage was cut through both sides, and pinning the sternum to the surgical station over the head of the animal allowed for the exposure of the heart, the liver, and the lungs. The perfusion

needle was inserted and secured in the left ventricle during the very slow flow of the rinsing solution (e.g. saline or 10% sucrose solution) and a small incision was made on the right atrium to get rid of the blood and excess liquid once the perfusion started. Initially, the blood was flushed by sterile 0.9% NaCl (for PVcre mice, see below) or 10% sucrose solution (for VIPcre mice, see below) for ~2 mins. After the paling of the liver, 4% paraformaldehyde (PFA; Sigma Aldrich) in 0.1 M phosphate buffered saline (PBS) started to be perfused for ~18 mins.

When the fixation was over, the brain was dissected and put into the 4% PFA solution for post-fixation of 2-4h. Then 2 different procedures were followed for PVcre and VIPcre animals:

i. IHC for PVcre mouse brains: Barrel cortex area was sectioned 40 µm thick via VT 1200 S vibratome (Leica, Germany) and slices were collected in PBS and rinsed for 15 mins. Later, sections were rinsed in order of 3x15 mins phosphate-buffer (PB), TRIS buffer (TB) 2x15 min, TRIS-buffered saline (TBS) 2x15 min, and TBS + 0.5% Triton X-100 (TBST) 2x15 min (all except PB at pH: 7.6). For blocking, sections were incubated 90 mins at RT in 0.25% bovine serum albumin (BSA) and 10% normal goat serum in TBST (Jackson ImmunoResearch). For primary antibody labeling, sections were incubated 60-72h at 4°C with mouse anti-PV (Swant; Cat#235, RRID:AB_10000343; diluted 1:5000) and rabbit anti-RFP (Rockland; Cat# 600-401-379, RRID:AB_2209751; diluted 1:500) to amplify mCherry signal. On the second day of IHC, after sections were rinsed 4x15 min with TBST, they were incubated overnight at RT (in a dark room) with Alexa Fluor 488-conjugated goat anti-mouse IgG1 (Molecular Probes/Thermo Fisher Scientific; Cat# A-21121, RRID:AB_2535764; diluted 1:500) and Alexa Fluor 568-conjugated goat anti-rabbit (Molecular Probes/Thermo Fisher Scientific; Cat# A-11037, RRID:AB_2534095; diluted 1:500) in TBST for secondary antibody labeling. After being washed with TBST 1x5 mins, sections were rinsed with 2x15 mins TBST and 1x15 TBS. Later, sections were stained with 4',6-diamidino-2-phenylindole (DAPI; diluted 1:5000 in TBS). Lastly, they were rinsed with 1x15 mins TBS and 2x15 mins TB.

ii. FISH for VIPcre mouse brains: When post-fixation was finished, brains were stored overnight at 4°C in 20% sucrose solution in 0.1 M PBS (treated with diethyl

pyrocarbonate (DEPC)). Later it was pre-frozen in isopenthane at -40°C and then stored at -80°C. Using the CM3050S cryostat microtome (Leica, Germany), 40 µm thick sections were cut in coronal plane in the area of the barrel cortex at -20°C. The coronal sections containing the target area were selected based on the mouse brain atlas (Paxinos & Franklin, 2019). Sections were collected in well plates in 0.1 M PBS. The brain sections were then rinsed in PBS for 3x15 mins. Afterwards, Prönneke et al.'s protocol (2015) was followed, only serums being supplied from a different company (Jackson ImmunoResearch). For staining VIP cells, RNA probes against VIP (367 BP, forward primer: CTGTTCTCTCAGTCGTCGGC, reverse primer: GCTTTCTGAGGCGGGTGTAG) and Streptavidin-Alexa Fluor® 488 conjugate (2mg/ml; for GFP fluorescence; Molecular Probes) was used.

Last step - Imaging and cell counting: After both IHC and FISH, sections mounted on microscope slides were covered with Aqua-Poly-Mount (Polysciences) and coverslips, and kept at 4°C until they were processed for imaging. For cell counting 1 random slice per group were chosen and scanned with an inverted confocal (LSM 880, Zeiss, Germany) or epifluorescence microscope (Axio Observer, Zeiss, Germany) using a 25x water-immersion objective.

5. Measurements and analyses

I. Stainings and imaging

For cell counting (somas expressing only mCherry: off-target expression, expressing only GFP: non-transduced target cell, and expressing both mCherry and GFP: targeted expression) was done manually with Neurolucida software (MBF Bioscience, USA) in the S1BF.

A 3D representation is created on Blender software (Blender Online Community, version 4.2.4, Netherlands) to show the succeeded expression of DREADDs in S1BF (Lein et al., 2007; Bakker et al., 2015).

For the animals who did not perform as expected in TT after CNO injection (N = 4; see "blind controls" under Results section), only one slice was chosen to be shown from the 10x scans obtained via epifluorescence microscope (Axio Observer, Zeiss, Germany).

II. TT performance analyses

Analyses of learning curves: Animals' scores per session were the rates of the hits (Hits/Total # of trials). Mann-Whitney U tests were conducted to detect session-by-session differences, and subjective last 3 sessions of performances as their most advancedly trained days (with two-stage step-up correction; Benjamini et al., 2006). A Mann-Whitney U test was also run to compare the total number of sessions that need a mouse to be counted as a learner.

Analyses of weight loss: A mixed-effects analysis (Animal type X Time) was made on both raw weights and fraction of weights (compared to baseline weight measured on the first day of the behavioral experiments). Later, percentages of weights were also compared for the day before CNO injection and CNO injection day.

Analyses of texture exploration duration and forepaw touch in TT: Mice performing in TT were recorded with a camera above the maze and later recorded videos were manually scored in EthoVision XT 14.0 (2019, Noldus Information Technology, Netherlands), for the measurement of their total exploration duration, and exploration per texture (in secs). Animals' forepaw touch to texture blocks were counted individually and averaged per trial.

Analyses of experimental conditions: A learner score (LS) was calculated for all animals and this score was used to compare saline injection and CNO injection sessions. For this score, animals' final sessions achieving above mentioned learning criteria (see above) were used:

$$Learner\ Score\ (LS) = \frac{Total\ \#\ of\ Hits}{Total\ \ \#\ of\ Trials}$$

As an example, when a mouse made 8/12 and 9/12 in the last two days, criteria was fulfilled to count this animal as a learner (please see "Success criteria" subtitle under TT section). This animal's LS was calculated as follows:

$$LS = \frac{8+9}{12+12} = \frac{17}{24} = 0.71$$

For saline injection condition (SI), while some animals took only one session (N = 4), some took 2 (N = 7) or 3 (N = 4). When animals had multiple sessions after saline injections, only

the performance of the last session was taken into analyses. Similarly, while some animals were tested with CNO injection in two different sessions (N = 11), some were tested only once (N = 5). Performances in the CNO-injected sessions were analyzed both separately (CNO1 & CNO2, for animals took 2 sessions) and also by a calculated score (CNO-S), with the same logic of LS:

$$CNO - S = \frac{Total\ \#\ of\ hits\ under\ the\ effect\ of\ CNO}{Total\ \#\ of\ trials}$$

Wilcoxon matched-pairs signed-rank tests were run to compare LS vs SI, and CNO1 vs CNO2 scores. The same test was applied also to LS vs CNO-S to compare fairly adjusted scores in control and CNO conditions.

All graphs to visualize data were generated on GraphPad Prism (v. 10.0.0. for Windows, GraphPad Software, USA) and later organized and modified with Adobe InDesign CS6 (Adobe Inc., USA).

III. Whole-cell patch-clamp recordings analyses

Resting membrane potential (RMP) was noted and observed during the recordings after the whole-cell patch-clamp configuration was obtained. When the initially measured RMP was above -55 mV, no measurements were made. Other than RMPs, input resistance at highest voltage deflection ($R_{i(hd)}$), input resistance at steady state ($R_{i(ss)}$), sag index, membrane time constant (τ), rheobase, AP firing threshold (AP-FT), AP amplitude (AP-A), AP time to peak, AP width (AP-W), and AP slope (AP-S) were measured/calculated, as well. Measurements for $R_{i(hd)}$, $R_{i(ss)}$, and τ were made from the average of responses to -10 pA currents each lasting 1 s. $R_{i(hd)}$ and $R_{i(ss)}$ were calculated with Ohm's Law (i.e. V = I*R). For measuring $R_{i(hd)}$ the formula was:

$$Ri\ (M\Omega) = \frac{20\ ms\ average\ of\ max\ amplitude\ of\ the\ membrane\ potential\ response\ (mV)}{amplitude\ of\ the\ injected\ current\ (pA)}$$

and calculated at steady state 20 ms current onset ending 10 ms before the current offset as follows:

$$Ri\ (M\Omega) = \frac{20\ ms\ average\ of\ the\ membrane\ potential\ \ (mV)}{amplitude\ of\ the\ injected\ current\ (pA)}$$

Sag index being an indicator of inward rectification was calculated with $R_{i(hd)}$ and $R_{i(ss)}$ values:

$$sag\ index = \left(1 - \frac{Ri(ss)}{Ri(hd)}\right) * 100$$

τ being the index of how fast the membrane potential reaches 63% of its final value was measured (in ms) and later τ fit was calculated as the exponential fit where a_0 = amplitude (mV), a_1 = τ (s), a_2 = offset (mV):

$$f(x) = a0 * e^{-x/a1} + a2$$

Recorded cells were stimulated with increasingly suprathreshold current applications (1 sec duration, 10 pA increment) to cover the full range of firing patterns, from just suprathreshold responses to maximal firing. In these recordings the instantaneous firing frequency of each inter-spike interval was measured. Dynamic frequency ranges (DFR) were analyzed after instantaneous frequencies of individual cells were binned in 10 Hz intervals, and the two groups were then compared in cumulative percentages. To refrain from false discovery rate, two-stage step-up correction was made on p values (Benjamini et al., 2006). Also, the frequency bins which shows (at least) 50% of all instantaneous frequencies were depicted for each group.

All data were collected via custom-made configurations, and recordings were analyzed via custom-written scripts by Dr. Martin Möck in Signal 5 software (CED Ltd., UK). Statistical tests and data graphs were made on SigmaPlot 14.0 and GraphPad Prism (v. 10.0.0. for Windows, GraphPad Software, USA). Figures exhibiting firing patterns and membrane potentials were created in Signal 5. All figures are organized and adjusted for optimal presentation in Adobe InDesign CS6 (Adobe Inc., USA).

IV. Statistical analyses

In the Results section, results are reported as follows: means are represented with *M*, standard deviations with *SD*, standard error of the means with *SEM*, medians with *Mdn*, and significance value with *p*.

Whenever data were not normally distributed, a Mann-Whitney-U test was used to compare multiple groups. For the comparison of 2 unpaired groups of data, the t-test was used but when the normality assumption was not validated a Wilcoxon Signed-Rank test is

used. If paired groups are compared in the absence of normal distribution of the data, the Wilcoxon matched-pair signed-rank test is used. In all statistical analyses significance value was set as $p = 0.05$.

RESULTS

All animals consecutively went through (i) stereotactic surgery, (ii) texture discrimination experiments (TT), and in the end they were sacrificed either for (iii) stainings or for whole-cell patch-clamp experiments. Although the main hypotheses were based on performance in texture discrimination, stainings and electrophysiological experiments were as important. Stainings were important to ensure the DREADD expression area and target specificity of the virus. Patch-clamp recordings served the electrophysiological validation of expected effect on the targeted cell types and offered the opportunity to precisely observe the effect of CNO on the cellular level.

I will start with the results of DREADD localization verifications, continue with the behavioral results and finally report the results of the electrophysiology experiments as "post-hoc controls".

1. DREADD expression in S1BF and targeting specificity

In all surgeries, S1BF was targeted bilaterally. AAV was injected at 2 injection sites per hemisphere each, at two different depths to cover the targeted area homogenously via targeting as many PV cells in the PVcre line, and VIP cells in the VIPcre line as possible.

Initially, the target specificity of the cre-dependent virus was checked via manual cell counting. The specificity of the DREADD expression is quantified via counting cells in different channels. Cells carrying DREADDs were visualized in red, according to their mCherry signal. For PV cells, IHC was used to stain PV-expressing cells and due to Alexa Fluor 488 coupled to the secondary antibody, these cells were visible in the green channel. When these two channels were merged together, colocalized signal was detected as yellow fluorescent.

A random 40 µm-thick section located within S1BF was chosen to count cells for (i) only PV, (ii) only DREADD, and (iii) colocalization of both. The tissue was imaged with z-stacks to enable cell counting through z-plate (depth). Out of in total 505 cells counted, 440 of them carried both signals (87% colocalization, Fig. 7B"), 22 cells were not transduced and showed only green fluorescence (4.4%), and 43 cells expressed only mCherry (8.5%) as putative off-target expression. An example section chosen for cell counting is exhibited in

Fig. 7A as maximum intensity projection and color density is balanced to maintain better visibility in the figure. The blue signal (DAPI) on the left side, is to show all layers were included for cell counting. It is also visible that there is no somatic signal in L1, and the distribution of PV cells are almost balanced, other than increased signal in L4 and L5b

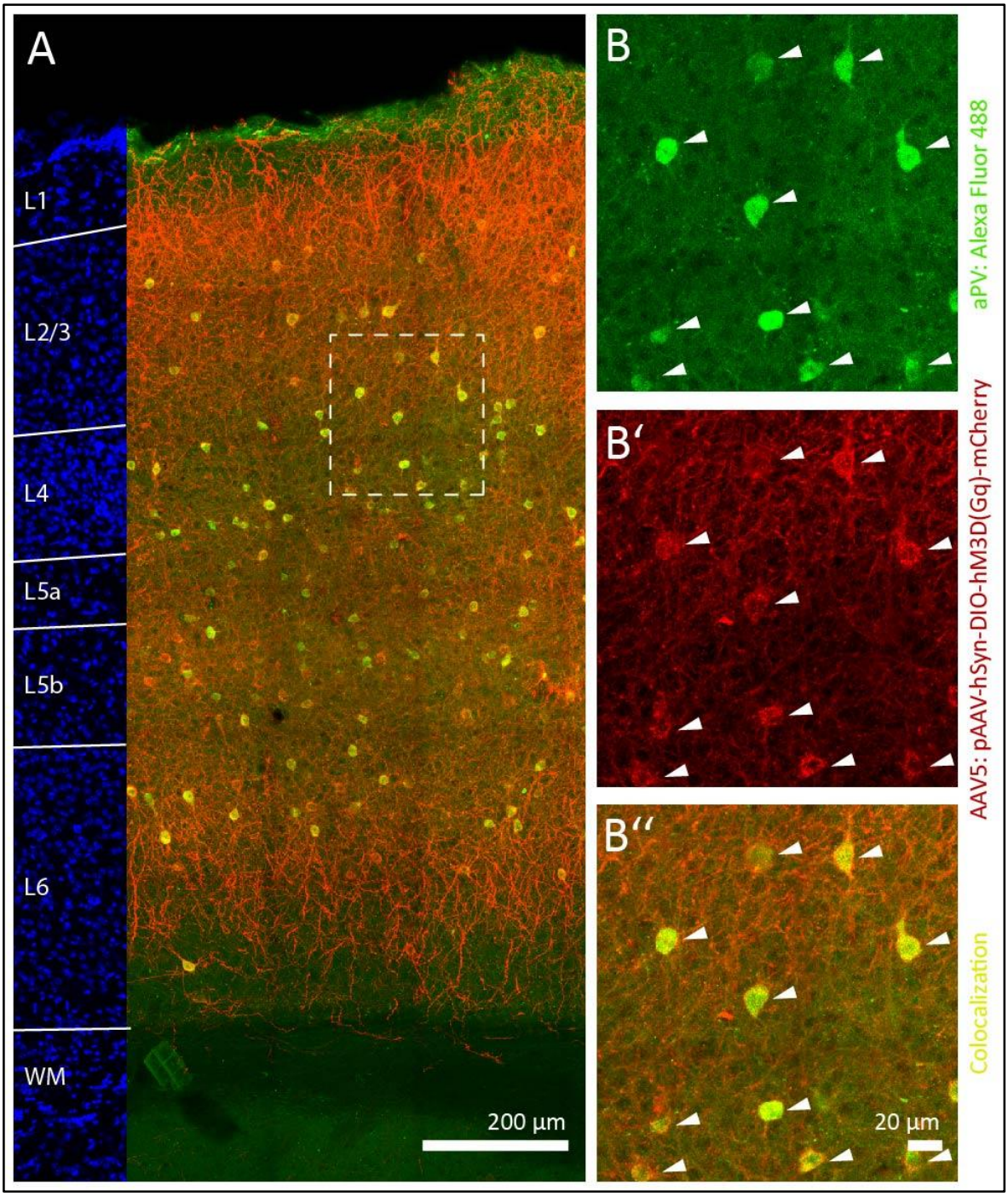

Figure 55. Colocalization of DREADD expression and aPV staining. **A)** One of the randomly chosen slices was scanned with a confocal inverted microscope to visualize the injection site in S1BF. In total 505 cells were counted in this image. **B)** PV cells were visible in the green channel. The cells showing only green fluorescent constituted 4.4% of all counted PV cells. The soma of the cells looks quite crisp although some of them show lower levels of fluorescent. **B')** The transduced cells were visible in the red channel and only 8.5% of the transduced cells were not labeled as a PV cell by aPV. **B'')** Most importantly 87% colocalization of mCherry and aPV signal showed high specificity and sensitivity of the virus in the PVcre line.

(Almási et al., 2019). In Fig. 7-B, B', and B", a small fraction of the tissue displayed by dotted square in Fig. 7A, is exhibited as visible in the green (Fig. 7B) and red (7B') channel separately. Fig. 7B" shows the colocalization of the signals in Fig. 7B and 7B' by merging both channels.

Cell counting for the VIP line was done with a similar logic except that this time RNA probes against VIP were conjugated with Streptavidin-Alexa Fluor 488. In the randomly chosen slice for the VIP line (Fig. 8), in total 109 cell were counted. In this slice, 100 cells

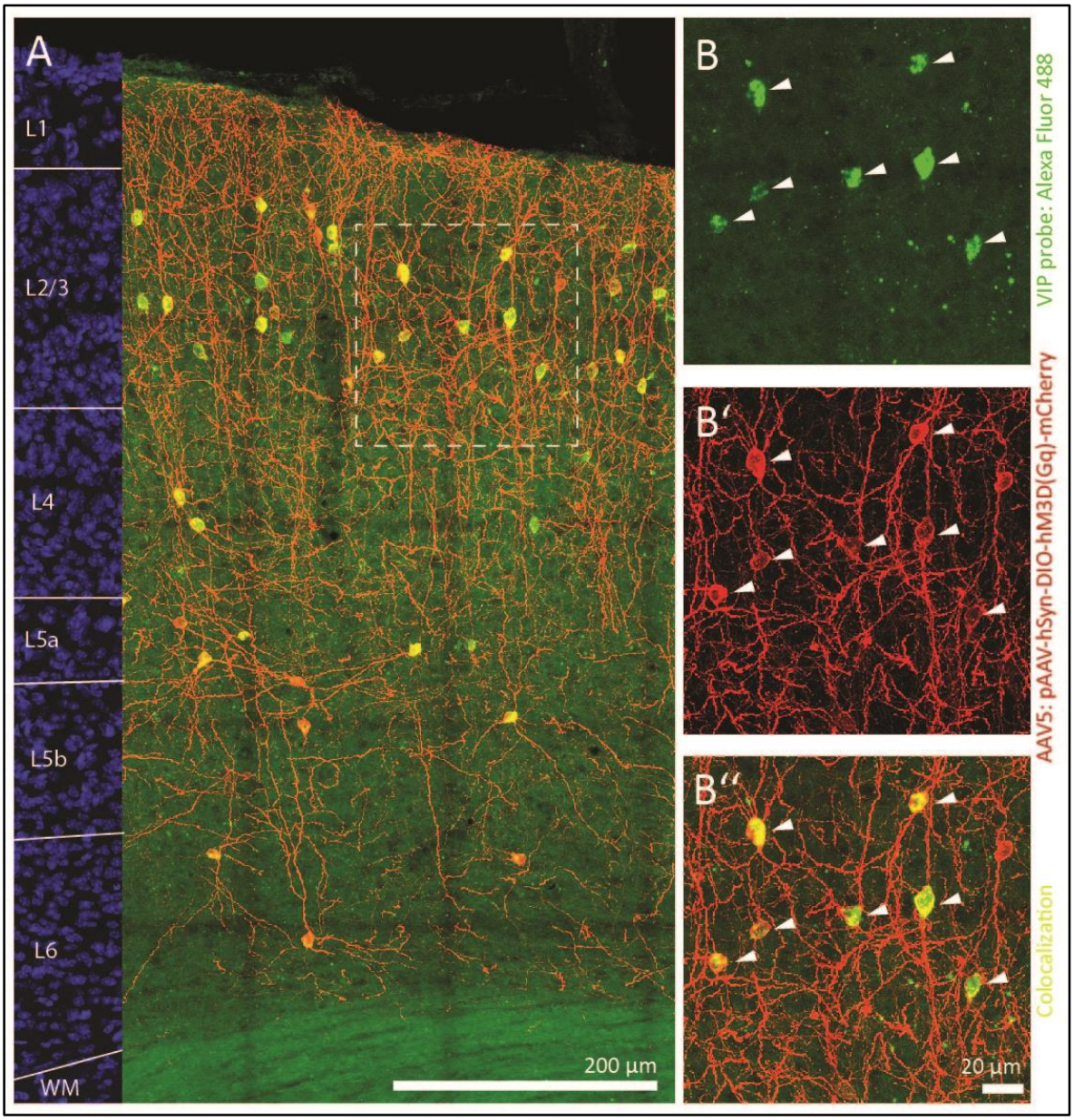

Figure 64. Colocalization of DREADD expression and the VIP probe. **A)** One of the randomly chosen slices was scanned with a confocal inverted microscope to visualize the injection site in S1BF. In total 109 cells were counted in this image. **B)** VIP cells were visible in the green channel. The cells showing only green fluorescent constituted 2.8% of all counted VIP cells. The soma of the cells looks a little different than PV cells due to different methods of staining. B') The transduced cells were visible in the red channel and only 5.5% of the transduced cells were not labeled as VIP cells by the VIP probe. **B'')** Most importantly 92% colocalization of mCherry and Alexa Fluor 488 signal showed high specificity of the virus in the VIP line.

expressed both fluorescent signals (92% colocalization), and there were 3 cells only visible in the green channel (2.8%) while 6 cells showed putative off-target expression (5.5%). This high percentage of colocalization ensures that the virus was target-specific and allows to claim that IP injection of CNO will enable the activation of the targeted cell groups.

In Fig. 8A, the chosen section is shown. VIP cells were mostly present in L2/3, as expected (Prönneke et al., 2015; Almási et al., 2019). Fig. 8B" exhibits the colocalized green and red signals in Fig. 8B and 8B'. Important to note that, the number of counted VIP cells is less than PV due to the fact that PV makes up to 40% of all cortical GABAergic cells while VIP only amounts to 13%. PV and VIP cells exhibited green signal but the shapes and the background signal were different due to different methods of staining. Overall, the cell counting showed the DREADD expression was visible in all layers and covered most of the targeted cells with only a small percentage of putative off-target expression.

Later, the consecutive slices were checked if the coordinates of the AAV injection provided DREADD expression restricted to S1BF. The injection site and diffusion of the viral construct was confirmed by analyzing the mCherry signal carried by DREADDs. In total stainings from 6 VIPcre and 5 PVcre animals confirmed that coordinates used for injection successfully covered the majority of the S1BF area. In Fig. 9, consecutive sections of one PV brain are shown as an example of specific S1BF coverage. The hippocampus was taken as a guide to choosing the sections to present. On the right hemispheres, the alignment of the transduced areas is stressed. On the left, the secondary somatosensory area (S2), lateral ventricle, and hippocampus are labeled according to the mouse brain atlas (Paxinos & Franklin, 2019). In all sections, the area corresponding to S1BF was mostly covered with the mCherry signal. This meant, that not only expression specificity but also injection area served the purpose of the experiments successfully.

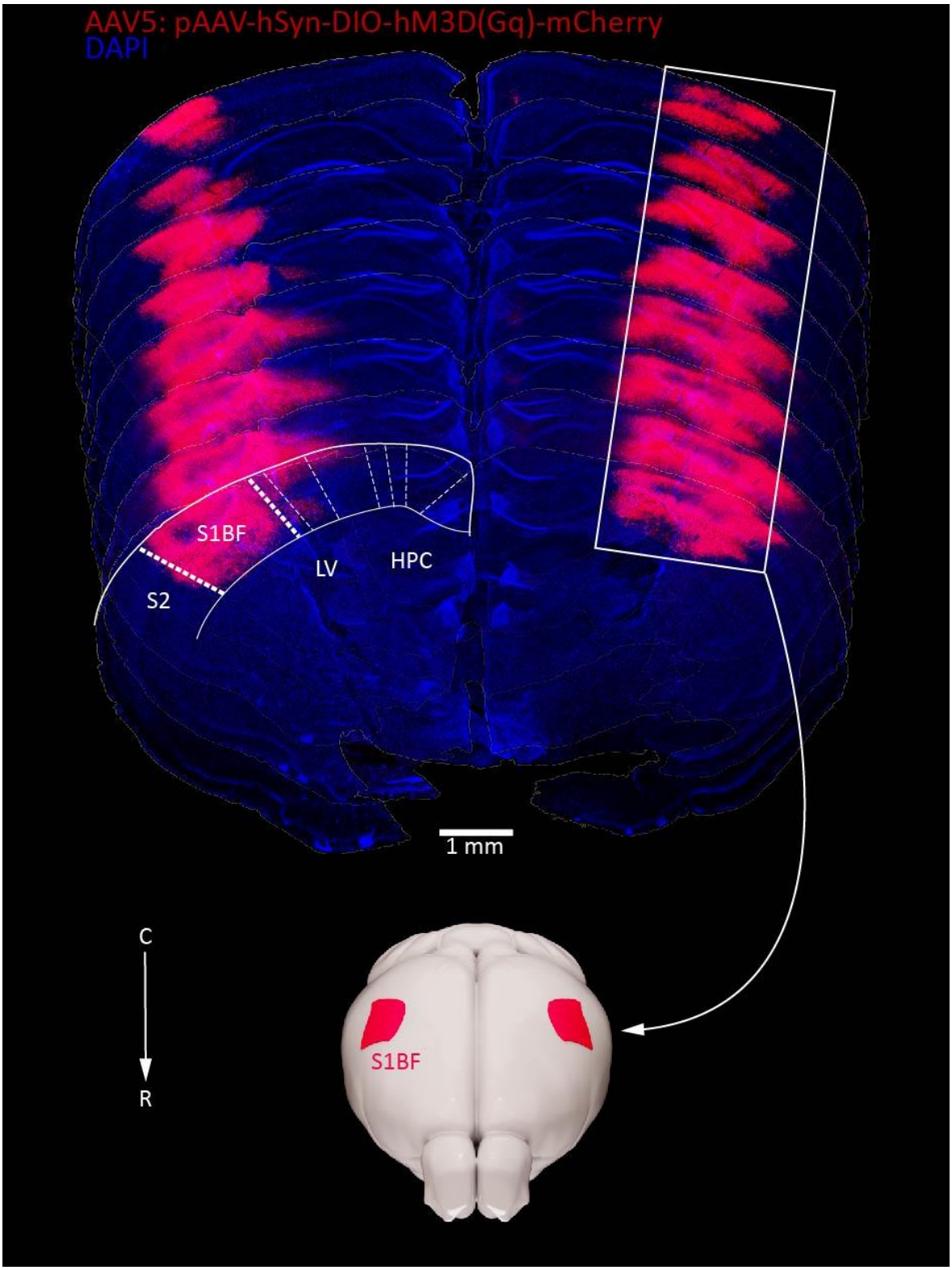

Figure 73. Specific transduction of S1BF. In this figure, consecutive slices from a PVcre animal's S1BF are represented as an example for area-specific transduction of DREADDs. Slices are ordered from caudal to rostral, from top to bottom. Red channel is amplified to maintain a better representation. Deficits due to staining are deleted during the image generation. The slices were chosen from S1BF, which is represented on the brain figure in red due to the fact that cells expressed DREADDs showed mCherry signal. On the left, a section from the mouse atlas (Paxinos & Franklin, 2019) is modified and merged with the first slice to show transduced area specificity. Other than S1BF, S2 (secondary somatosensory cortex), LV (lateral ventricle), and HPC (hippocampus) are shown as they were represented in the atlas.

2. TT and effect of CNO on texture discrimination

All animals started with food restriction and TT and completed in 21 days. Not all animals were able to learn the task, and for the analyses of TT only the learners' performance was taken into account. In total 12 VIPcre+ (75% of all VIPcre+, 5F & 7M, M_{age} = 15.3 weeks) and 7 PVcre+ (78% of all PVcre+, 4F & 3M, M_{age} = 14.5 weeks) mice were able to complete all steps in TT. There were 2 animals per group who did not show a behavioral change after CNO injection (please see the "blind controls" section below). For the TT analyses, data from the animals who showed a behavioral change after CNO injection (N= 10 VIP + 5 PV animals) were used.

CNO effect: The hypotheses in this project predicted a performance change in TT. Activation of DREADDs via CNO injection was expected to cause a difference between trained PV and VIP animals, and PV animals were expected to perform lower compared to VIP animals in the texture discrimination task. A two-tailed Mann-Whitney U test showed that VIP and PV mice were showing similar performance in CNO conditions (p = 0.77; Fig. 10), and both groups exhibited a decrease in their performance to chance level in texture discrimination (Mdn_{VIP} = 0.52 and Mdn_{PV} = 0.5). This meant that while the hypothesis about the chemogenetic activation of the PV cells was proved, the hypothesis about the chemogenetic activation of the VIP cells failed to be confirmed at this level (Fig. 10).

Due to the restricted number of experimental days not all but only some animals (N_{VIP} = 8, N_{PV} = 3) were also tested again with an IP saline injection to see if the effect of CNO was reproducable. The animals that were tested in 2 or 3 more sessions (1 session/day) with saline injection, showed similar performance to final sessions of training period (i.e. last 3 sessions of training, no injection condition; NI) which was before CNO injection. Once their performance was above baseline, they received CNO once more (CNO2), and again a performance drop to chance level was observed. (Fig. 10). Although there are small differences exhibited between the two groups, a mixed-effect analysis (Experimental Sessions x Animal Type) revealed that these performance differences between PV and VIP were not significant ($F_{animal\ type}(1, 9) = 1.389$, p = 0.27), neither was the interaction between experimental sessions and animal type (F(2.62, 1.13) = 0.63, p = 0.68). There was only a significant main effect of the experimental session on the texture discrimination performance. The pairwise comparisons also showed that, performance in the CNO1 versus

CNO2 sessions did not differ significantly for either of the groups ($p_{VIP} = 0.068$, $p_{PV} > 0.99$). This pointed to the consistent but not permanent effect of DREADD activation via CNO injection. The performance decrease to chance levels in both groups meant that manipulation of PV or VIP cells via "activating DREADDs" caused an impairment in texture discrimination ability.

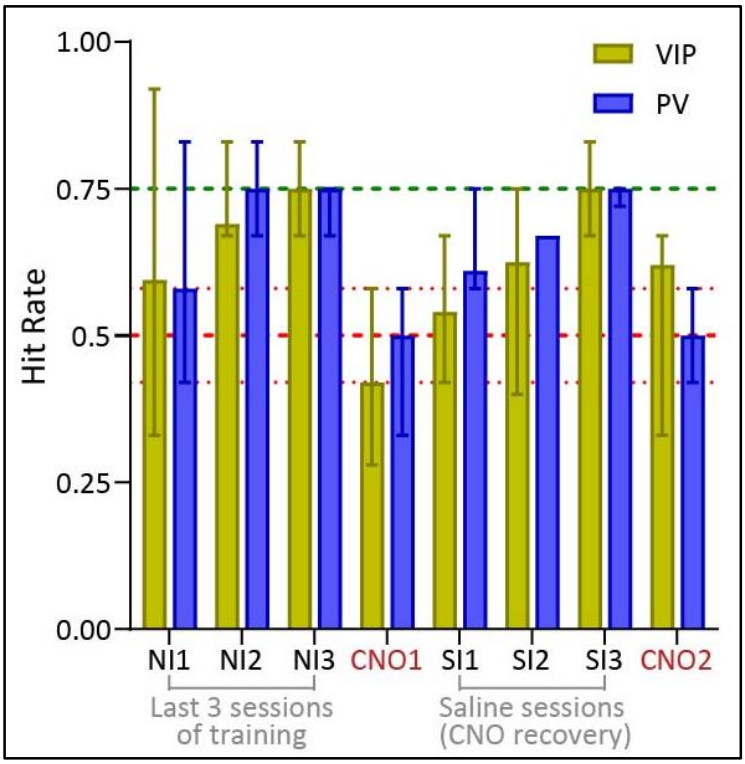

Figure 82. DREADD activation impaired texture discrimination performance in both groups. The figure displays the comparative hit rates of the VIP (in green) and PV (in blue) animals in 3 NI sessions, 2 CNO, and 3 SI sessions. It shows the last 3 days of the training phase, which were also used as a control of the injection so named NI (no injection). CNO1 shows the first and CNO2 shows the second session done after CNO injection. SI, is the saline injection sessions. The histogram represents the median, and the bars show min and max values. Both groups reach 75% percent success rate at the end of the training session and the performance of both groups exhibits a drop in both CNO1 and CNO2 sessions. In between these 2 CNO sessions, animals were tested after saline injection, and both groups showed similar recovery in their hit rates. There were statistically no significant differences between VIP and PV animals in either of the sessions.

Further analyses on hit rates were conducted to understand how robust CNO's effect was and compare other experimental conditions. For this, on the last 3 days of training, learning scores (LS), performances on the last day of saline injection (SI), and averaged CNO scores (CNO-S) were compared. The comparison of the last 3 training sessions revealed the fact that the animals were performing similarly in the last session before the CNO injection (NI3, $p = 0.89$), the session before the last session (NI2, $p = 0.19$), and two sessions before the last one (NI1, $p = 0.68$; Fig. 10). Also, their LS were similar, too ($Mdn_{VIP} = 0.71$, $Mdn_{PV} = 0.73$, $p = 0.57$; Fig. 11, left).

PV and VIP groups did not differ significantly in their SI performance either according to a two-tailed Mann-Whitney U test ($Mdn_{VIP} = 0.75$, $Mdn_{PV} = 0.74$, $p = 0.32$; Fig. 11, left). This meant, also the CNO2 session was undertaken under similar baseline conditions, or in other words, the effect of CNO was temporary in both groups and there was no carry-over effect of the initial CNO injection. However, it is visible in the Fig. 11 (the graph on the left)

while the distribution of data in LS and SI conditions are not variable, VIP mice's CNO-S scores showed a larger variability compared to PV animals. This difference might be stemming from the smaller sample size of the PV group, yet it is important to note that activation of DREADDs via CNO injection in VIP cells, might have variable effect on the behavior.

Since the VIP and PV group did not differ significantly in LS, SI and CNO conditions, the data was pooled together and analyzed further together to reveal the effect of CNO. A Friedman's test comparing LS, SI and CNO-S revealed the significant differences between LS and CNO-S ($p = 0.004$) and SI and CNO-S ($p = 0.0004$), and no significant difference between LS and SI ($p > 0.99$). Which meant, the animals' scores for no injection and saline injection sessions were comparable while CNO injection session scores were significantly lower (Fig. 11, right), in other words, mice performed poorly only on the CNO sessions. In Fig. 11 (the graph on the right) exhibits the similar variability observed in the group-based analyses: this time LS and SI shows quite similar distributions, while CNO-S varies around the chance level, from minimum 0.38 to 0.63.

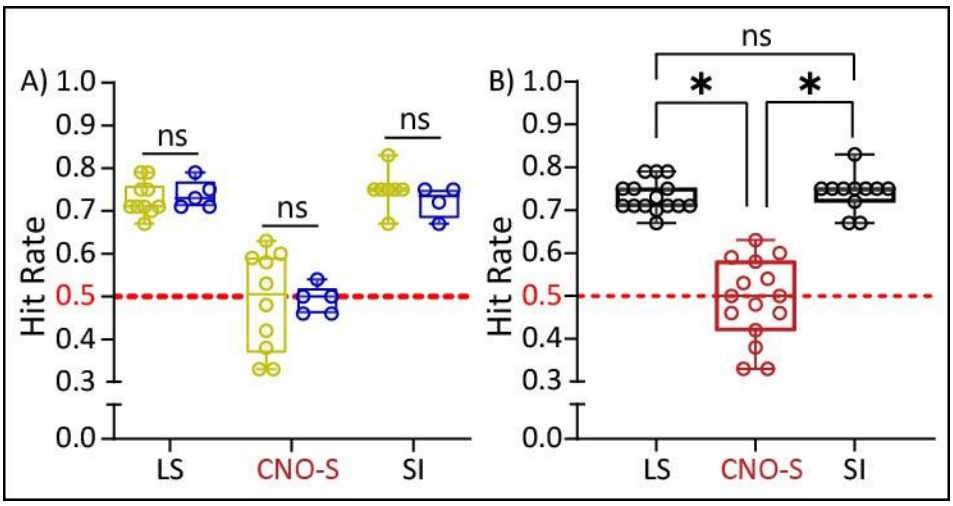

Figure 91. Comparison of experimental conditions. VIPcre mice are represented in light green and PVcre mice in dark blue **(A)**. Chance level hit rate is exhibited with the dotted red line at 0.5 in both graphs. **Graph A** exhibits comparisons between VIP and PV groups in LS, CNO-S, and SI. The mice did not differ in neither of the conditions so later on their scores pooled together, and another analysis was made to reveal the differences among these 3 conditions. **Graph B** shows the statistically significant difference between LS & CNO-S, and SI & CNO-S. There was no significant difference between LS and SI hit rates.

Although there was no significant difference in LS, SI and CNO performances of VIP and PV groups, to make sure the difference in CNO condition was not caused by other factors, further analyses were done in the two groups' learning parameters, weight loss curves, and other behaviors in TT.

Learning curves: For all animals, a learning curve (Fig. 12A&B) was created with their hit rates over the sessions. These curves were maintained by sorting the data from the TT Day 1 to Day 9, since in both groups there were animals who passed the criteria to be counted as a learner took 9 days. Although only learners were taken into account, to make sure there was no difference in their learning process, the two groups' performances were also compared over the course of the texture discrimination training. VIP and PV mice did not differ in their average success rates throughout the texture discrimination training period (Fig. 12 A&B). This meant there was no significant difference in their learning processes. Also, the total number of sessions taken to pass the criteria to be counted as a learner was the same (Min-Max: 3-9, Mdn_{VIP} = 5.5, Mdn_{PV} = 5 days, Fig. 12C). This meant their learning pace was also comparable and ensured a comparable baseline for TT performance. In both Fig. 12 A and B, all learners were plotted with dotted lines. As it is

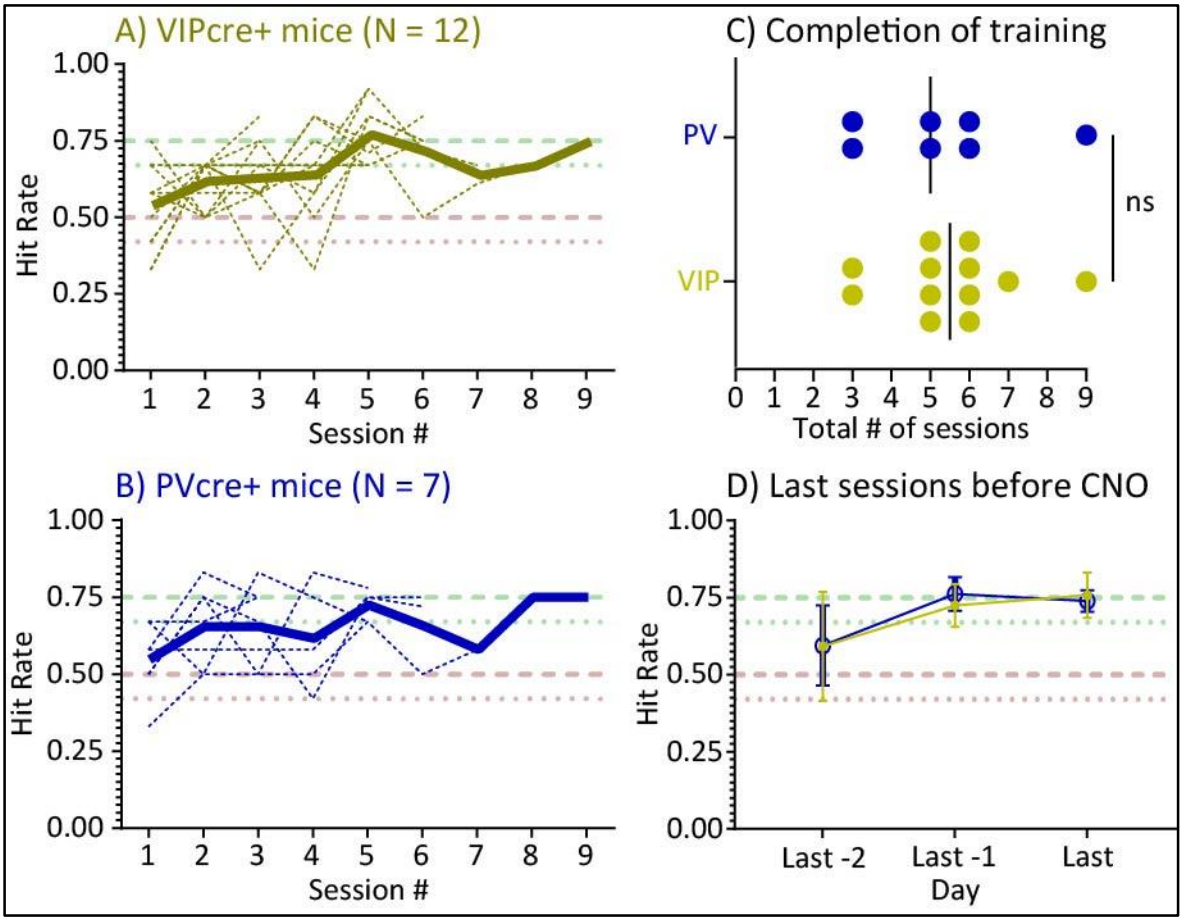

Figure 100. Analyses of hit rates of learners in TT. VIP mice represented in light green and PV mice in dark blue. On graph **A)** and **B)**, performance of all animals (VIP and PV respectively) is shown by dotted lines and the thick line denotes the mean of the all performances. While 1 is the maximum possible score in texture discrimination task, the performances around 0.5 (from 0.42 to 0.58) was taken as the lowest possible scores (due to the nature of 2AFC tasks, chance level can be the lowest). There was no significant difference between two groups in terms of their learning progress. **C)** shows the number of total training sessions per animal and the median values. There was no significant difference between groups, and please note the median values being around 5 sessions. In **D),** LS for final 3 sessions of the animals are shown. There was no significant difference in VIP and PV group's performances before CNO administration.

clear that in both groups animals rather start with a random hit rate, their averages are at the chance level (signified by transparent dotted red lines). It seems that the average performance peaked in session 5, dropped again in the following session, and showed a second peak in session 9. This pattern, being almost identical for both groups, stems from the fact that most of the animals finished the training period around 5 days (Fig. 12C) and once they finished training, there were only slower learners who completed the training later than them. In other words, the drop in the average performance caused by a plotting choice to show overall learning periods for the whole groups, and does not point out directly to their subjective last days. One should also recognize that the variability on the very first session is greatly decreased by the end of the training period for both groups.

Weight-loss curves: All animals were subjected to food restriction and fed only once daily with a limited amount of food. Food restriction was needed to increase the motivation to seek food in TT (Herrnstein & Loveland, 1974; Raynor & Epstein, 2003). Since they had to associate the food reward with the correct texture, food restriction indirectly motivated animals to learn the task. A comparison of weights through all TT experimental days revealed that VIP and PV mice differed significantly ($M_{VIP} = 22.8$, $M_{PV} = 27.2$, $p < 0.0001$; Fig. 13, left). This difference might be due to the different genetic backgrounds since they already differ on Day 1, in their baseline weights. However, the more crucial aspect of the food restriction was the percentage of weight loss compared to their initial weight. They

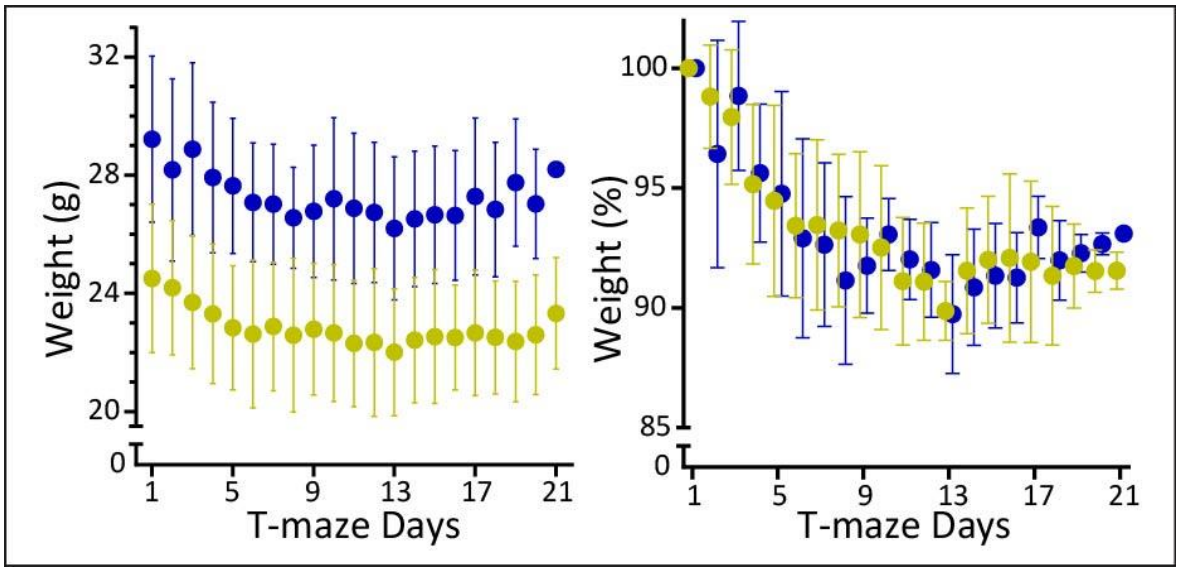

Figure 109. Comparison of weight loss curves. Light green represents VIPcre animals, and dark blue represents PVcre. Filled circles shows the means and whiskers denotes SD. VIP and PV mice differed significantly in their weight throughout the experiments (left) yet their weight loss graph does not constitute a difference (right). The graph on the right shows the measured weights compared to the weight on Day 1 meaning all animals started with 100% and then drop to around 90% of their initial weight.

did not show a difference in their fraction of weight loss compared to the baseline weight (M_{VIP} = 93.22%, M_{PV} = 93.28%, p = 0.94; Fig. 13, right). Even though there was a difference in the baseline weights, their weight loss trends and weight loss conditions in TT training had a comparable trend.

Since the weight loss percentage could be a confounding factor for mice's performance in the texture discrimination task, the last session before the CNO injection and the initial session with CNO injection were also compared. Because the two groups did not differ in weight loss percentages, the fractions of weights of VIP and PV animals were pooled together. A two-tailed Mann-Whitney U test showed that there was no significant difference (Mdn_{VIP} = 93.22%, Mdn_{PV} = 93.28%, p = 0.94; Fig. 14) and eliminated the potential confounding factor coming from weight differences.

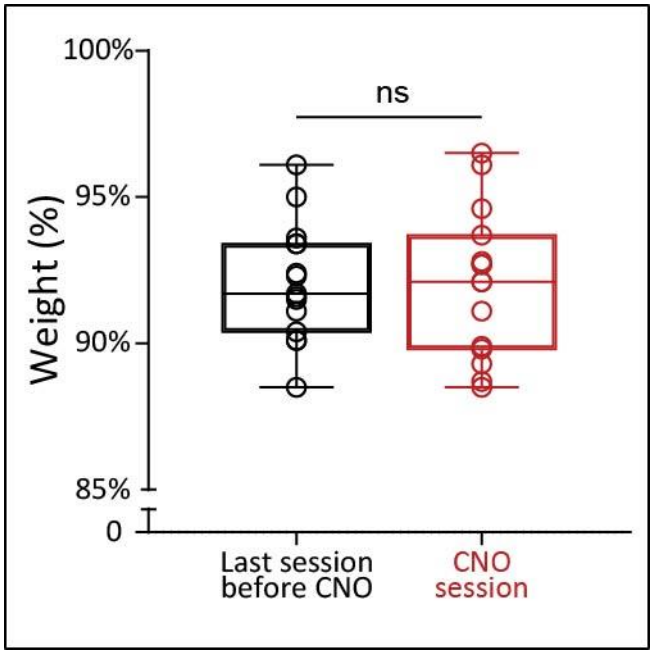

Figure 118. Control for the potential effect of weight on CNO session performance. Since all animals have a subjective day to receive CNO, other than comparison of all experimental days, their relative weight was compared separately for the CNO injected session (red) and the session before (i.e. control; black). These two sessions showed no significant difference.

TT-related parameters: Not only weight loss and learning curves but also animals' diverse behaviors during the task were evaluated. For this purpose, 4 learners per group were randomly selected to complete video analyses. The first parameter to analyze was forepaw touch to the textured object. During the experiments, it was recognized that animals occasionally touched the texture block with their paws to support themselves to stand on their hind paws. During this behavior, active whisking was continued. Although it is known that paws are not the major organs to sense texture (Wu et al., 2013), to test whether the forepaw touch assisted mice in finding the coarser texture, the number of contacts to correct and wrong textures per mouse on the last day before CNO injection was compared. A paired t-test revealed there was no significant difference in the frequency of paw touches made to correct versus wrong texture ($M\pm SD_{correct}$ = 5.11±5.01, $M\pm SD_{wrong}$ = 4.11±2.32, p = 0.31). For this reason, as long as the whisking continued, when the animals'

snout was directed towards one of the texture blocks, the time spent was measured as exploration duration.

Exploration duration was important to reveal since it shows an animal's motivation to solve the task. For this reason, mice's exploration duration in the first CNO session and the session before (the last training session, no injection) needed to be compared. To test whether a difference in the exploration duration caused the performance drop during CNO sessions, the total exploration duration for both textures is measured and averaged by dividing by the number of trials taken. A two-tailed Mann-Whitney-U test revealed that there was no significant difference between the CNO session (Mdn = 2.98 secs) and the session before (no injection; Mdn = 2.55 secs, p = 0.42, Fig. 15, top). Also, the total number of touches to either block, in the CNO session and the session before was compared to understand if forepaw touch was used as an alternative to whisker-based tactile perception. An average touch frequency per trial is calculated per animal for the CNO session and the session before and a Mann-Whitney-U test revealed two conditions did not differ, either ($Mdn_{no\ injection}$ = 0.77, Mdn_{CNO} = 0.39, p = 0.27, Fig. 15, bottom). These results together indicated that forepaw touch was not used as an assistive behavior to perceive texture nor as a placeholder of the whiskers during CNO sessions. Also, the performance drops in the CNO session did not depend on the exploration duration of the animals.

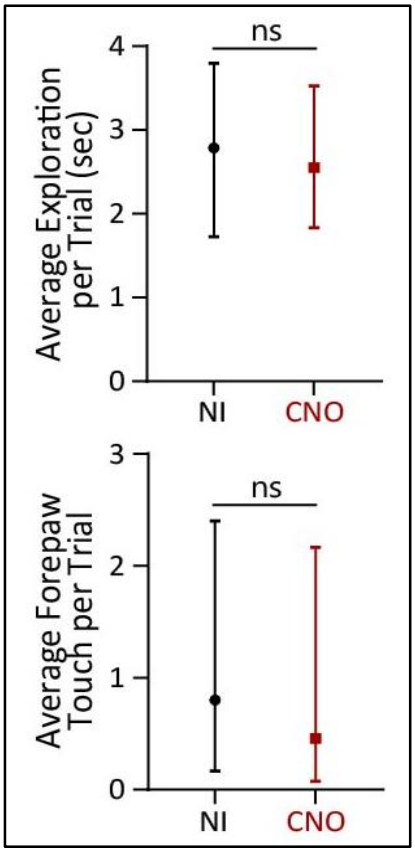

Figure 127. Comparison of video-based data. Animals' CNO session (red) and the session before (NI, black) was compared for two parameters. Neither their average exploration duration nor the number of average forepaw touches per trial changed significantly in the CNO session.

Blind controls: 2 animals per group did not show a decrease in their performance after CNO administration. These animals were perfused and the brain slices were scanned to determine the cause for this. The scans showed that the expression of AAV was not in the desired way. This means that the expression of DREADDs was either too low (Fig. 16A), limited to one hemisphere (Fig. 16B), or was not limited to S1BF (Fig. 16 C&D). These animals, serving as blind controls, proved that CNO does not have an adverse effect on

behavior by itself, and suggest that the expression of the DREADDs needs to be in S1BF, and only in S1BF, to cause a deficit in texture discrimination ability.

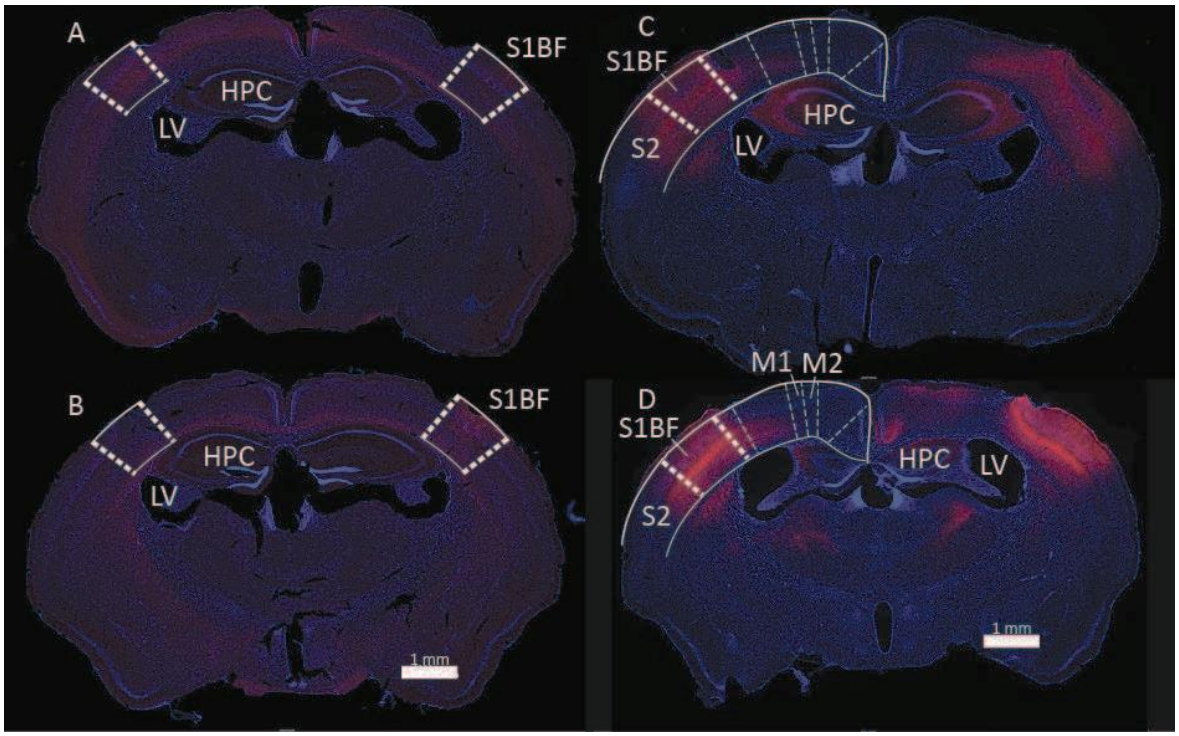

Figure 134. Animals with the stable performance in CNO condition did not have proper DREADD expression. In the figure one section per animal is presented to show the unsuccessful expression of DREADDs. Blue is DAPI and red is mCherry signal. S1BF, HPC (hippocampus), LV (lateral ventricle), S2 (secondary somatosensory cortex), M1 (primary motor cortex), and M2 (secondary motor cortex) are shown. Both sections in **A** and **B** belong to VIP mice. In **A**, other than the background, there seem only a few cells in both hemispheres. In **B**, transduced cells are only visible on the right hemisphere, so transduction was only successful unilaterally. Sections **C** & **D** belong to PV mice. In both of the sections, the mCherry signal is quite strong, yet in 15C the DREADDs were expressed in also S2 and hippocampus, and in D it is even more spread in the cortex. Also, in section **C** the mCherry signal is not visible in certain spots (e.g. S1BF L2/3).

3. Electrophysiological analyses

Behavioral results showed that both PV and VIP groups showed impaired performance during the CNO sessions. The staining results confirmed that virus specificity and sensitivity was high and that S1BF transduction is essential to see the effect of CNO on the behavioral level. However, to investigate the electrophysiological properties of the transduced cell types and the effect of DREADD activation on them, whole-cell patch-clamp experiments were conducted. All recorded cells showed expected cell type-specific electrophysiological characteristics. In Fig. 17, one VIP and one PV cell's spike patterns are shown as examples. On the left, a transduced cell from a VIPcre mouse is exhibited and this

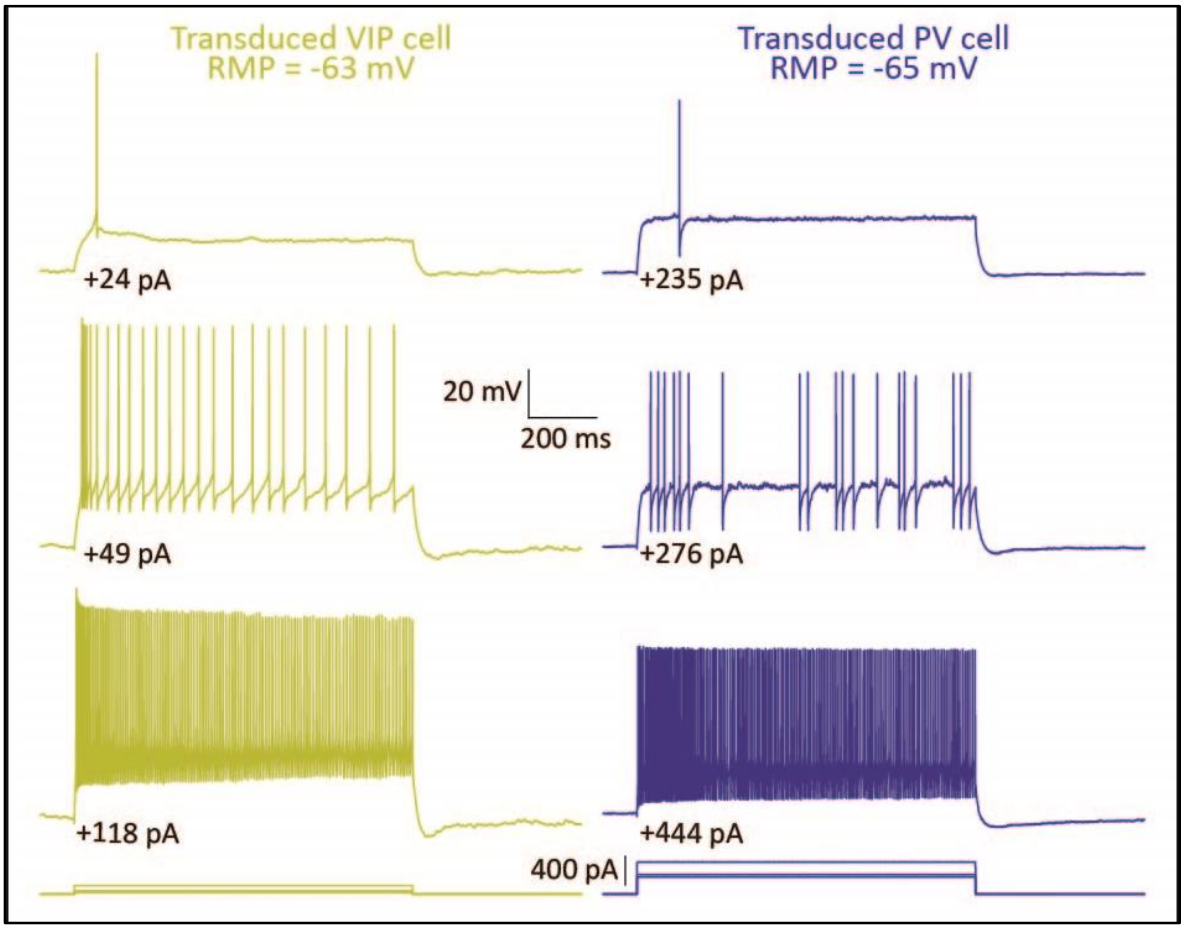

Figure 138. Firing patterns of transfected cells. To approve a healthy physiology of the transduced cell types, cells expressing red florescence (due to mCherry protein in AAV) in both VIP- and PVcre mice were patched. There is an example from each group in the figure (VIP on the left and PV cell on the right hand side). The traces in the first three rows were recorded from an individual neuron (the light green from a transfected VIP cell from a VIPcre animal, and the dark blue traces are recorded from a transfected PV cell from a PVcre mouse) and in the bottom current stimuli are represented (1 s long). Both cells were from the S1BF area of the neocortex. The top traces show the responses at rheobase, on the third row responses to the maximum stimulus strength are exhibited. The traces on the second row show the firing pattern more comprehensively as a response to a current stimulus between rheobase and the maximum stimulus. Next to each response trace, stimulus strength is noted. The transfected cell from the VIPcre mouse had characteristics of a continuously adapting VIP cell. Meanwhile the transduced cell from the PVcre animal was characterized as a fast-spiker (being stuttering at intermediate stimulus strength), which can be expected from a PV cell. Not only the example traces in the figure but also 10 more cells recorded, confirmed electrophysiologically that the transfected cells were on target, and showed formerly defined characteristics of the VIP cells in VIPcre, and PV cells in PVcre animals.

cell showed characteristics of a non-burster VIP cell of the barrel cortex, with an adaptive firing pattern as response to rectangular depolarizing current injections. On the right, a transduced cell from a PVcre mouse S1BF is presented. This cell shows the well-known characteristic of the PV cells with its fast-spiking action potential firing pattern (Fig. 17, right column) These recordings confirmed the transduced cell types and showed that under regular conditions, they show usual firing patterns, in agreement with the maintanence of a healthy physiology. Not only the firing patterns but also the intrinsic properties were analyzed to control the viability of the cells and quantify the initial observation about the cell types.

Intrinsic electrophysiological properties of 7 VIP and 5 transduced PV neurons were characterized to confirm cell type-specific properties. Initially, the following passive properties (please see Table 1 for the descriptives, and Fig. 18 for comparisons) were characterized: (i) resting membrane potential (V_M), (ii) input resistance ($R_{i(hd)}$), (iii) input resistance at steady-state ($R_{i(ss)}$), (iv) sag index, (v) τ, and (vi) membrane capacitance. A one-tailed unpaired t-test revealed that VIP cells showed a significantly more depolarized V_M compared to PV cells ($t = 2.79$, $p = 0.0096$). The two groups also significantly differed in τ ($t = 2.93$, $p = 0.011$), with VIP cells responding slower to current inputs. Mann-Whitney U tests showed that VIP cells have significantly higher $R_{i(hd)}$ ($p = 0.0013$), $R_{i(ss)}$ ($p = 0.0013$), and lower membrane capacitance ($Mdn_{VIP} = 20.95$ pF, $Mdn_{PV} = 34.11$, $p = 0.048$) while no significant difference was detected in sag index ($p = 0.185$).

	V_M (mV) Mean±SD Min/Max	$R_{i(hd)}$ (MΩ) Mean±SD Min/Max	$R_{i(ss)}$ (MΩ) Mean±SD Min/Max	Sag index (%) Mean±SD Min/Max	τ (ms) Mean±SD Min/Max
PV	-60.7±4.3	121.9±23.9	112.4±22.3	7.8±4.7	10±2.9
	-65.26/-55.72	83.5/142.5	73.6/125.8	0.8/12.4	6.2/12.8
VIP	-66.2±2.6	490.5±165.7	438.7±164.1	11.4±8.6	23.1±11.4
	-71.84/-64.33	300.4/776	247.3/688.4	3.3/24.5	10.8/41.5

Table 7. Passive Properties of PV and VIP Cells. *Passive were recorded from the transfected cells in current clamp mode with -10 mV current injection. The table shows descriptive measurements for means, SDs, minimum and maximum values.*

Secondly, AP properties (please see Table 2 for the descriptives and Fig. 19 for comparisons) were characterized by: (i) rheobase, (ii) AP firing threshold (AP-FT), (iii) AP amplitude (AP-A), (iv) AP time to peak, (v) AP width (AP-W), and (vi) AP slope (AP-S). One of the PV cells was excluded from the analyses due to depolarized RMP (above -55 mV) during the recordings. Comparison of VIP and PV cells revealed significant differences in multiple active properties, as well. VIP cells were observed with significantly smaller rheobase ($t = 12.5$, $p = 0.0004$), and APs of VIP cells having significantly bigger amplitudes

(t = 3.5, p = 0.01), significantly longer time to peak (t = 3.56, p = 0.0031), and significantly larger widths (p = 0.003). However, there was no significant difference between VIP and PV cells in their thresholds (p = 0.69).

Table 15. Active properties of PV and VIP cells. *The transfected cells were recorded at rheobase, and only the first spike was evaluated in case of multiple spike sweeps. By averaging these values, numbers are obtained as a single measurement. The values in the table are gathered over these numbers.*

	Rheo (pA) Mean±SEM Min/Max	AP-FT (mV) Mean±SEM Min/Max	AP-A (mV) Mean±SEM Min/Max	AP-t to peak (ms) Mean±SEM Min/Max	AP-W (ms) Mean±SEM Min/Max
PV	208±14.4 170.6/236	-33.6±6.4 1.610656	38.2±12.9 20.2/48.1	0.33±0.04 0.28/0.38	0.29±0.04 0.25/0.33
VIP	29.2±7.6 15.5/37	-35±1.9 1.157407	63.6±38.2 54/75.1	0.43±0.05 0.38/0.52	0.53±0.09 0.4/0.67

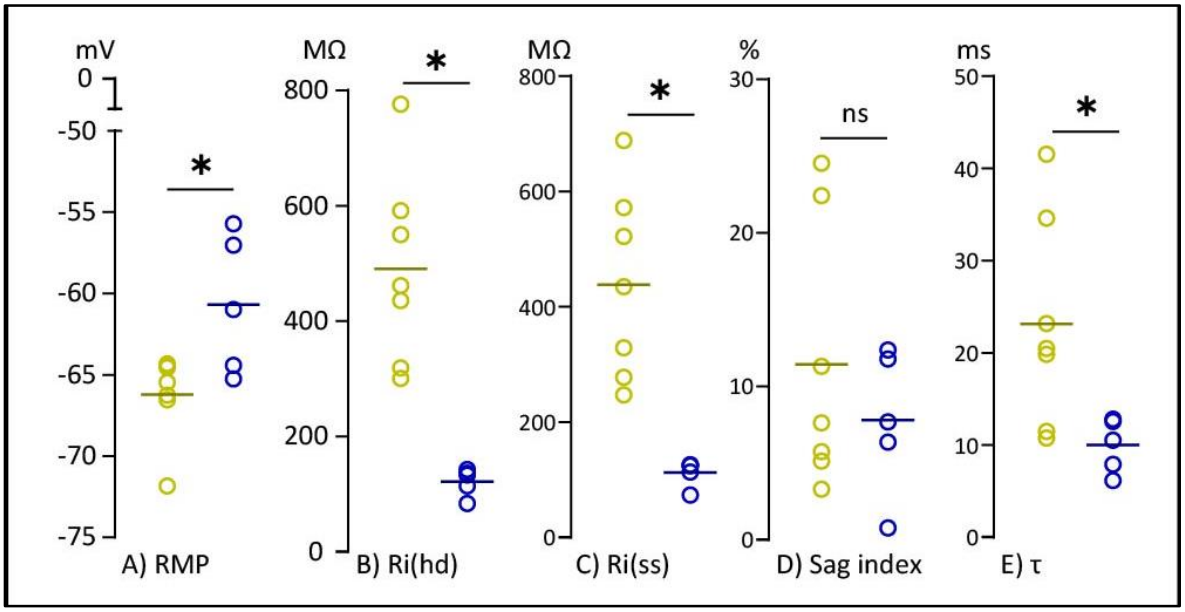

Figure 157. Comparison of passive properties of transduced VIP and PV cells. Green circles signify individual VIP cells and PV cells are shown in dark blue. The lines among the data points denote the mean values of the represented group. There was a significant difference between VIP and PV cells in RMP, $R_{i(hd)}$, $R_{i(ss)}$, and τ. No significant difference detected in sag index.

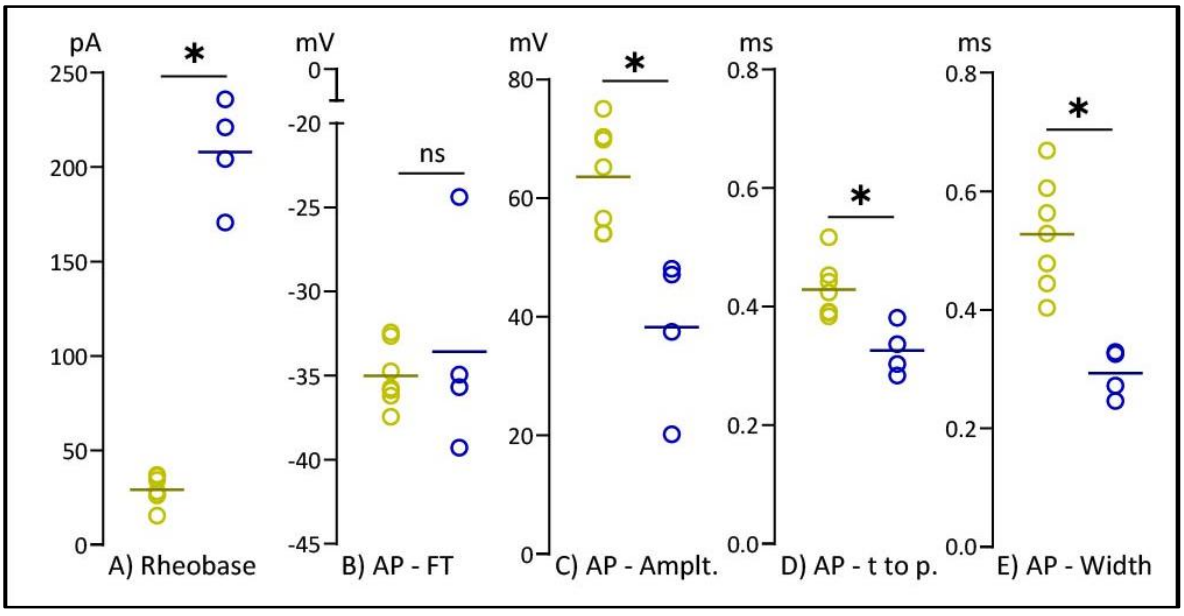

Figure 148. Comparison of active properties of transduced VIP and PV cells. Green circles signify individual VIP cells and PV cells are shown in dark blue. The lines among the data points denote the mean values of the represented group. While they did not differ in AP firing threshold, there was a significant difference between VIP and PV cells in rheobase, AP amplitude, AP time to peak, and AP *width.*

There were also differences between the two cell groups in their afterhyperpolarization (AHP) characteristics (Fig. 20). All PV cells showed a fast AHP (fAHP; peak M±SEM = -51.8±6.3 mV, amplitude M±SEM = -19.9±3.4 mV, time to peak M±SEM = 0.55±0.21 ms) but no medium AHP (mAHP) was exhibited during rheobase recordings. Similarly, all VIP cells showed a fast AHP (fAHP; peak M±SEM = -46±5.2 mV, amplitude M±SEM = -12.1±3.8 mV, time to peak M±SEM = 1.12±0.87 ms) yet 5 of them also showed medium AHP (mAHP; peak M±SEM = -49.1±2.7 mV, amplitude M±SEM = -14.1±1.7 mV, time to peak M±SEM = 42.4±11.4 ms) during rheobase recordings. One-tailed Welch's t-test revealed that VIP cells had significantly smaller fAHP amplitudes compared to PV cells ($t = 3.19$, $p = 0.0089$). There was no statistically meaningful difference in fAHP peak and time to peak.

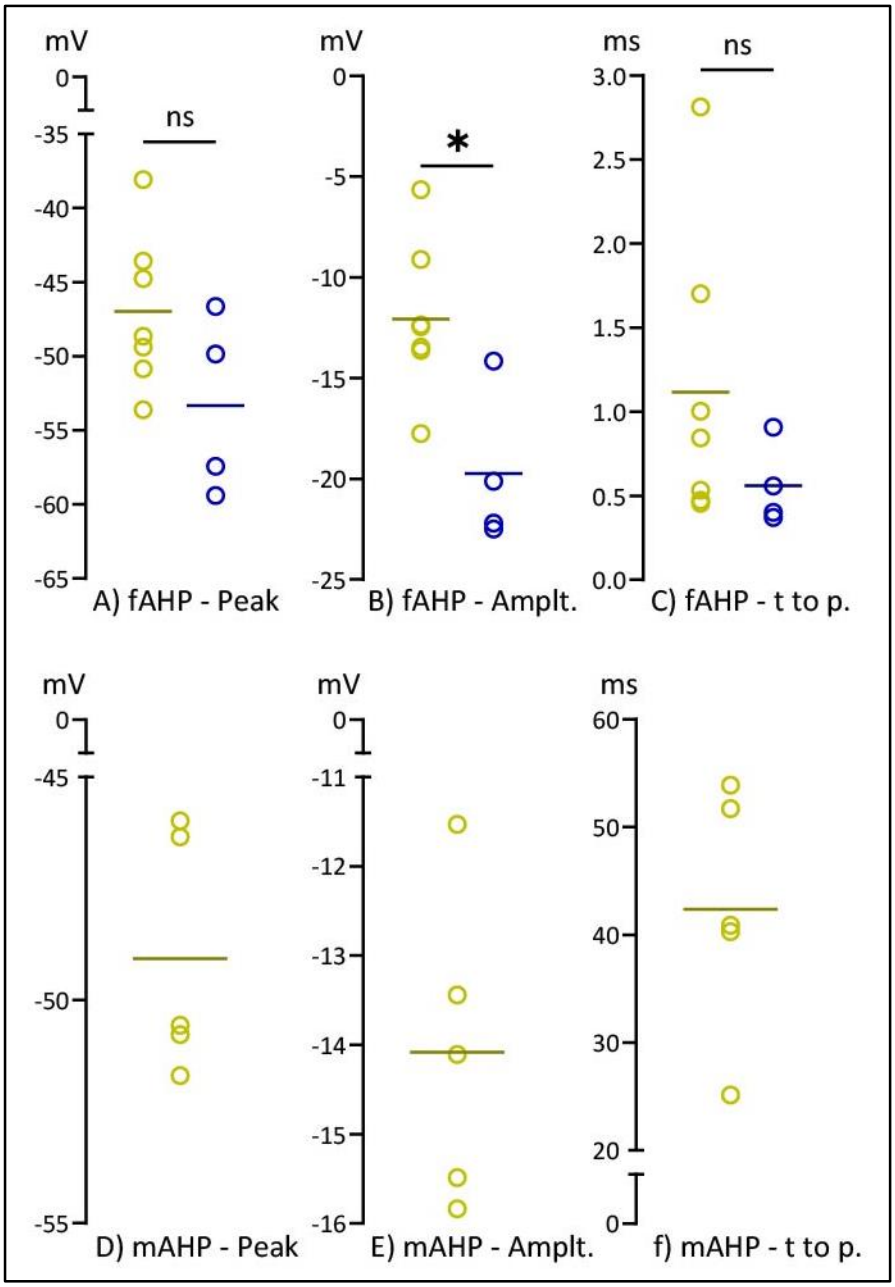

Figure 166. AHP characteristics of transduced VIP and PV cells. Green circles show individual VIP cells and PV cells are shown in dark blue. The lines among the data points denote the mean values of the represented group. Only VIP cells exhibited mAHPs. In terms of fAHPs, two groups differed significantly only in fAHP amplitude.

The frequency of APs was also distinct feature in firing patterns of VIP and PV cells. The instantaneous firing frequency patterns were compared in cumulative percentiles from 10 Hz to 400 Hz. The two groups differed significantly from 6th to 11th bin (i.e. from 60 to 110 Hz; $p < 0.05$; Fig. 21) which revealed a different dynamic frequency range (DFR) of the two groups. VIP cells had a narrower DFR compared to PV cells. Also, VIP cells reached 50% in the lower frequency bins (50 Hz) compared to PV cells (150 Hz).

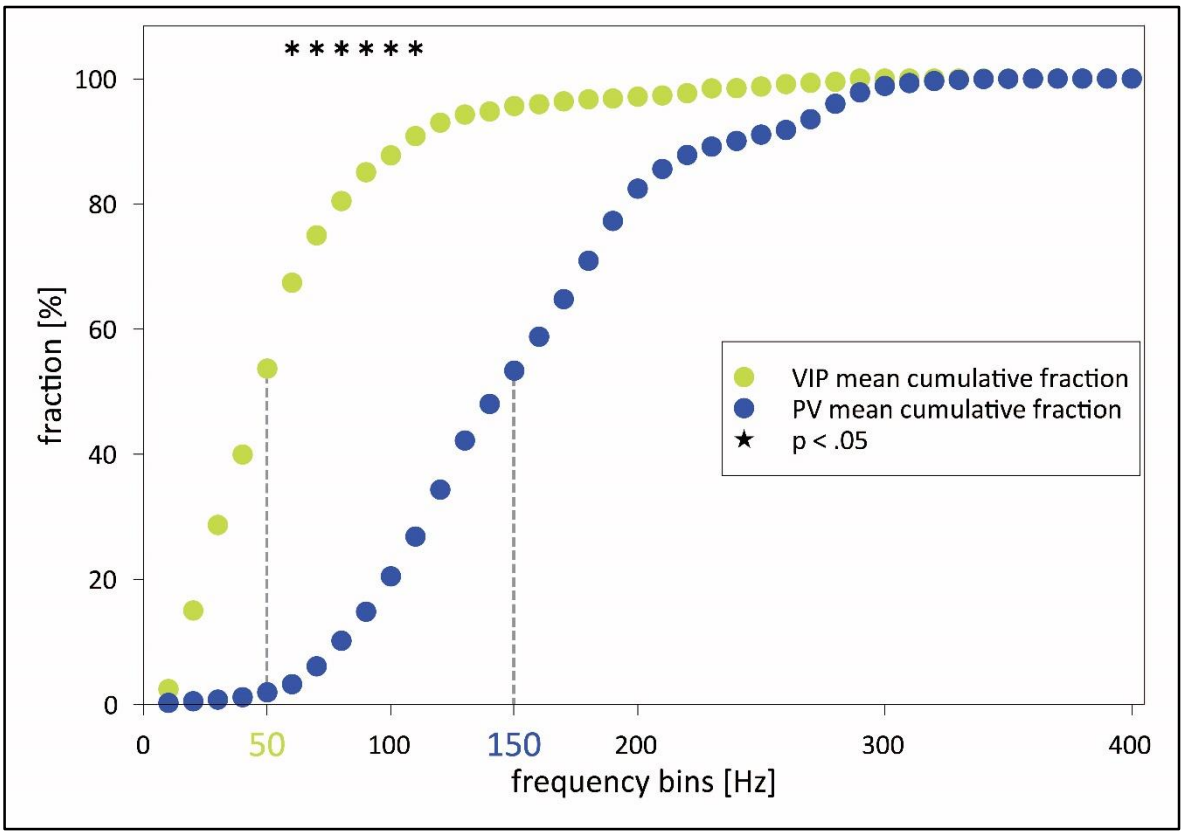

Figure 175. Dynamic frequency ranges of transduced cells. Cumulative fraction of instantaneous frequencies are shown in 10 Hz bins (VIP cells in light green and PV cells in dark blue) from 10 to 400 Hz. Vertical dotted lines points the bin in which 50% was exceeded for each group. Instantaneous firing rates were signficantly different form 60 to 110 Hz, denoted by black stars. VIP cells crossed 50% at 50 Hz, while PV cells reached it at 150 Hz.

Overall both transduced VIP cells and transduced PV cells exhibited intrinsic properties as their non-transduced versions reported in the literature (Hu et al., 2014; Prönneke, 2017; X. Mao & Staiger, 2024). This meant that expressing DREADDs did not change the intrinsic properties of these cells, and they were functioning properly in the absence of CNO.

CNO bath application: After the basic characterizations of transduced neurons, there was one question to answer: What effect does CNO administration cause in these neurons? To study this, CNO was bath-applied to patched cells and meanwhile the cells were recorded in current clamp mode to observe RMP change. Transduced cells were

depolarized as the nature of the viral vector would have let us to anticipate, yet its effect was different for VIP and PV cells.

Three PV cells were recorded before and during the bath application of 4 µM CNO. There initial V_M was -62.27 mV. As shown by an example in Fig. 22C around 3 minutes after starting CNO application, the membrane potential started to depolarize slowly and reached a steady state value at the end of the 10-minute recording. The average V_M of the 3 PV cells at steady-state was -48.87 ± 2.34 mV. Importantly, the steady state depolarization was clearly below the firing threshold (M_{FT} = -32.87 mV). While spontaneous APs were never observed in control recordings, PV cell occasionally fired APs during CNO-mediated depolarization. Notably, these APs were not correlated in time with the hyperpolarizing current pulses

In the VIP group, CNO was bath applied to 7 transduced cells ($M_{initial\ Vm}$ = -61.46 mV, M_{FT} = -35.01 mV). Two cells were exposed to only 4 µM CNO, two others were first exposed to 2 µM CNO followed by 4 µM, and three cells were exposed to 0.5 µM CNO followed by 4 µM. The bath application of 4 µM CNO caused depolarization of on average 29.22 mV. This

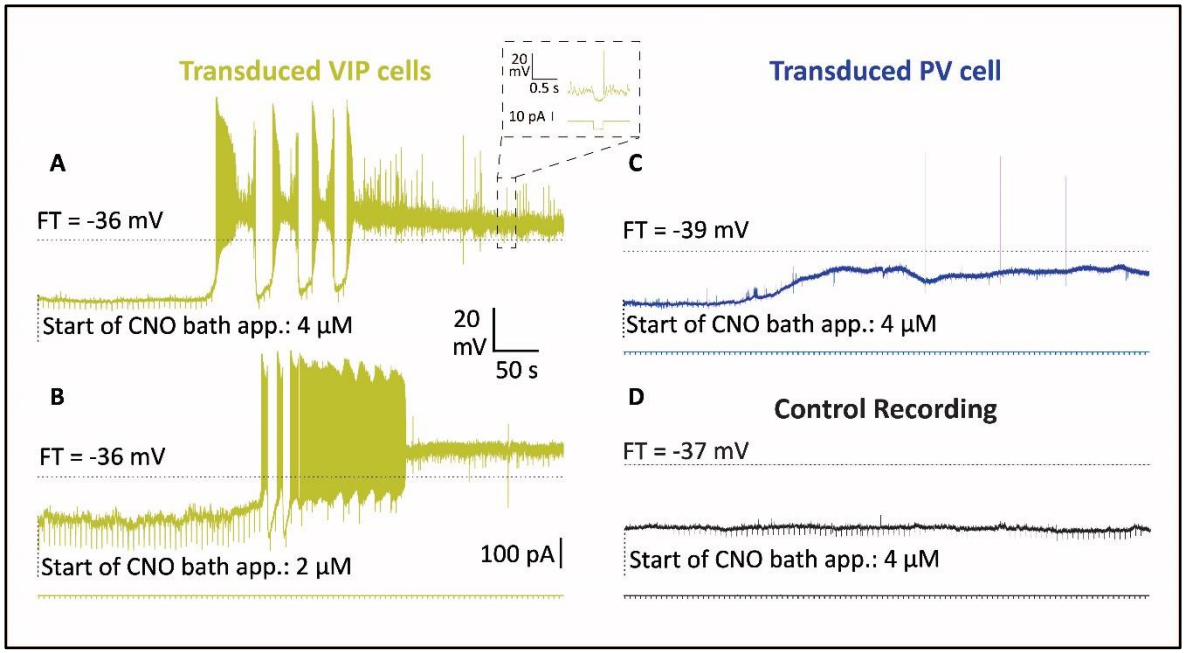

Figure 182. Effect of CNO on RMP of transduced cells. There are 4 responses from individual cells (**A**&**B**: 2 VIP in light green, **C**: 1 PV in dark blue, and **D**: a non-transduced cell in black) represented in the figure. The trace in **A** as well as the top traces in **B**, **C**, and **D** represent current clamp recordings of the RMP of individual cells during 10 min CNO bath application. The bottom traces in **B**, **C**, and **D** exhibit the current channel with regular hyperpolarizing current pulses (each -10 pA, lasting 200 ms, every 6 seconds). Dotted horizontal lines denotes FT of each cell, and dosage of CNO was noted right below the traces. Binding of CNO to DREADDs, was expected to depolarize the cells closer to FT thus make cells fire easier compared to their baseline. This effect was observed in PV cells (**C**) yet in VIP cells (**A** & **B**) depolarization was too high and caused cells RMPs to exceed FT. This drove the cells to a constant depolarization block and rather than "activating" the VIP cells, application of CNO "deactivate" them. However, a-non transduced cell (**D**) in a slice from an injected brain, did not show any change in RMP with CNO bath-application.

quantitative difference was crucial because most VIP cells (4 cells with 4 µM dose and 1 cell already with 2 µM dose) were depolarized above the FT (Fig. 22A and B) which induced a constant depolarization block that was not possible to reverse by wash out up to 90 minutes. Also, a paired t-test comparing initial V_M and final V_M (with 4 µM application) confirmed that this difference was significant (t = 5, $M \pm SD_{final\ Vm}$ = -32.24 ± 11.07 mV, p = 0.0008). It is important to note that these cells were still able to fire APs during steady-state depolarization, however, these APs appeared in response to the hyperpolarizing pulses injected regularly. These transient hyperpolarizations allowed a partial de-inactivation of Na^+ conductances.

To test if the depolarizing effect of CNO is specific to transduced cells only, 2 slices from different VIPcre mice were used. Two unlabeled (i.e. non-transduced) cells were recorded from the transduced S1BF area, yet none of these cells responded to CNO and no change was observed in RMP (Fig. 22D). This meant CNO-induced depolarization was specific to transduced cells.

Altogether these results of the patch-clamp experiments showed that, while transduced cells showed their regular characteristics, CNO specifically depolarized these cells but not the non-transduced ones. However, while the depolarization of PV cells was still below FT, VIP cells were driven to a depolarization block with being depolarized above FT. This meant that VIP cells were “deactivated” rather than activated in stark contrast to the expected effect of the chemogenetic manipulation.

DISCUSSION

The current project aimed to discover the roles of S1BF PV and VIP neurons in texture discrimination ability. The major novelty of this project is achieved by the chemogenetic targeting of different IN populations in S1BF to test their contribution to whisker-based texture discrimination in freely behaving mice.

This was a challenging project because of two main reasons. First, there was a lack of non-head-fixed texture discrimination assays in the literature. To overcome this, the textured T-maze was designed and custom-made. The second reason was that the literature lacked reporting on potential troubles/diverse outcomes of the chemogenetics method when applied to different cell types. To observe the effect of chemogenetic manipulation at the cellular level, a new set of "control" experiments (i.e. *in vitro* whole-cell patch-clamp recordings) was needed.

Regardless of the challenges, this project's main findings revealed that S1BF PV and VIP neurons play an integral role in mice's whisker-dependent texture discrimination ability. The activation of DREADDs on both transduced PV and VIP cells caused a significant impairment in texture discrimination, and in both groups animals' performances dropped to the chance level. Therefore, we could show a necessity of proper PV and VIP cell functioning for tactile discrimination in the context of a learning paradigm.

1. Technical considerations

The current project revealed the engagement of S1BF PV and VIP neuronal populations in texture discrimination, yet these cells were not being directly monitored during TT due to the nature of the experiment. This required a set of controls and clarification of some possible confounders to bridge the gap between the observed behavioral change and assumed chemogenetic activation of these cell populations.

I. Textured T-maze (TT) as a novel texture discrimination task

For the behavioral part of the current project, a novel texture discrimination task was designed. TT was a perfect tool to use for the sake of this project for the following reasons. First, it gave the possibility of measuring texture discrimination ability (i.e. success rates in discrimination of textures) reliably in different cre-dependent lines (i.e. VIPcre and

PVcre) and the performance changes resulting from CNO administration. Secondly, it made it possible to eliminate the potential confounding effects such as weight loss, smell, or forepaw touch to the textures as will be discussed below.

There were 2 texture blocks with different grits of SP in TT. To avoid location-based learning, the location of the correct textures in front of the target arms (i.e. either left or right) was decided according to previously designed and tested sequences (Fellows, 1967). This pseudo-randomization of the correct arm/texture was successful in avoiding a biased arm preference or location-based learning of the animals. As these sequences promised, animals were showing on average 50% success in finding the correct arm at the beginning of the training and during CNO conditions in which their texture discrimination ability was disturbed.

In TT, one session mostly consists of 12 trials and ends after a maximum of half an hour. This was quite useful, especially in the testing of multiple animals, and allowed more than 1 session per day when necessary. The general application of 12 trials also ensured that animals were not frustrated by a demanding task like texture discrimination, and kept being cooperative even during CNO conditions, which were rewarding for neither of the animal lines used. The task was indeed so demanding that animals rarely reached hit rates above 75% and they kept performing the task after the CNO sessions in which the application of CNO transiently took away the ability to discriminate textures (i.e. less reward food during that session).

For TT, animals underwent food restriction by receiving a limited amount of food daily. This was a consideration since different levels of hunger/weight loss cause a change in the reinforcing value of the food reward, which means smaller the weight loss the lower the motivation to find food (Raynor & Epstein, 2003). Since animals were weighed every day, and the portion of the food was slightly changed to prevent more than 15% weight loss, it was possible to have control over their weight-loss curves. In the end, both experimental groups showed similar weight-loss patterns which eliminated a potential confounding factor for learning texture discrimination under food-restricted conditions.

The second confounding factor would be the use of other senses or organs to find the correct texture, either in the learning phase or during CNO sessions. The major

candidates for this factor were either potentially different smells of different grits of SP or forepaw touch to the texture blocks. The potentially different smell was eliminated by using freshly alcohol-sprayed texture blocks (Morita et al., 2011). Given that the animals' performance dropped in CNO conditions, the scent did not cue them to find the correct arm. The findings of Pandey et al. (2023) supported this claim by showing that inhibition of S1BF did not disable animals to find scent-related cues. A quite common control for whether the scent of the SP assisted in discriminating texture is testing the animals after clipping/removing all whiskers. For instance, mice were not able to recognize the SP with a different texture (i.e. different grit size) after whisker removal in a novel texture recognition task (Wu et al., 2013). As a recent example of freely behaving animals, Qi et al. (2022) tested mice after clipping all of the whiskers and showed that without whiskers mice could not discriminate different coarseness of SP.

Also, forepaw touch was checked to see whether it contributed to hit rates. According to Wu et al. (2013), touching the textures with paws did not affect the recognition of different textures. The data collected in TT was in line with this finding and analyses showed that the average number of paw contacts with the texture blocks did not change in CNO conditions. In other words, the similar number of contacts in CNO sessions did not help animals to discriminate the textures.

The current project was chosen to be done in freely running animals since it is still debated whether head-fixed setups represent the natural behavior of rodents and thus whether the observed behavior can be generalized (Pacchiarini et al., 2020; Qi et al., 2022). No doubt that these experiments expanded the knowledge in the barrel cortex field, especially since in the study of electrophysiological properties of whisker-to-barrel pathways and microcircuits, there have been no published studies so far to understand the roles of specific GABAergic neuron populations in texture discrimination behavior.

Nowadays the combination of two advances in the field makes the testing of awake and freely behaving mice possible which also benefited this project. The establishment of the chemogenetics method (Armbruster et al., 2007; Alexander et al., 2009) and the generation of cre-driver mouse lines (Taniguchi et al., 2011) made it possible to manipulate different populations of GABAergic neurons in a certain area (e.g. in S1BF). In the making of this project, only one study benefiting from this combination became public, which is not

yet published in a peer-reviewed journal but on bioArxiv (Pandey et al., 2023). So, we can say that the current project is contributing to the literature by the novelty of using this methodological combination.

Also, the establishment of TT was a significant contribution due to the fact that the literature was missing a straightforward texture discrimination test and an adjustable set of discriminanda (e.g. change of contrast between SP to obtain a psychophysical curve). Pretty later than TT was established, one paper with another novel texture discrimination paradigm was published (Qi et al., 2022) because of similar concerns. Although this novel assay was useful for measuring changing performances with changing contrasts between SP, it takes longer than TT for an animal to learn texture discrimination in terms of the number of days with longer durations of sessions per day compared to TT. That is to say, TT was important to establish also for timewise more economical texture discrimination paradigm, other than the high learner rate.

II. Effect of chemogenetic manipulations on the behavioral and cellular level

The initial concern regarding chemogenetic manipulation was the proper target specificity and the spatially correct diffusion of the viral vector in the cre-dependent lines used in this project. The PVcre (Palicz et al., 2024) and VIPcre lines (Prönneke et al., 2015) used in this project were previously tested for cre-specificity and were both validated to be suitable models for studying cortical INs. A cre-dependent AAV was used for the DREADD expression in this project and transduced PV cells in PVcre line, and VIP cells in VIPcre line. With the help of IHC and FISH staining, it was ensured that the virus showed high target specificity and diffused in the target area, covering all layers.

The second question was about the dosage of the designer ligand (i.e. CNO). For the behavioral experiments, 3 mg of CNO per kg body weight was systemically delivered as suggested in the literature to have a peak behavioral effect between 1 and 2 hours after injection and the effect is shown to disappear on average within 10 hours (Rogan et al., 2011; Roth, 2016; Jendryka et al., 2019). This was useful regarding TT, in which animals were tested between 75 and 105 minutes after IP injection, on average.

Another concern was if the expression of DREADDs either changed or even harmed the targeted cells. Krashes et al. (2011) showed that the transduced cells exhibited the same

characteristics as the non-transduced versions of them. Similarly, in the current set of experiments, the electrophysiological characterization of passive and active properties of transduced PV and VIP cells presented characteristics of healthy PV and VIP cells shown in the previous literature (Hu et al., 2014; Prönneke, 2017; Mao & Staiger, 2024). Also, these recordings proved once more that the AAV transduced the correct type of cells.

For sure, the next thing to investigate was the effect of CNO on the cellular level. The DREADDs expressed in the target populations was hM_3D-Gq, a G protein-coupled receptor engineered from the human muscarinic acetylcholine (ACh) receptor M3 (Armbruster et al., 2007). CNO shows high affinity binding to these DREADDs, yet exhibits significantly lower potency at native muscarinic ACh receptors (Armbruster et al., 2007; Atasoy & Sternson, 2018). For depolarization via chemogenetic activation of hM_3D-Gq receptors, there were two potential mechanisms suggested (Atasoy & Sternson, 2018): 1) Similar to native Gq-coupled muscarinic activation, activation of DREADDs might reduce M-current, a K^+ conductance mediated by Kcnq channels (Zhang et al., 2003), 2) CNO binding raises intracellular Ca^{2+}, which might activate the electrogenic Na^+/Ca^{2+} exchanger (with a coupling ratio of 3 Na^+ : 1 Ca^{2+}; Blaustein & Lederer, 1999), and resulting in depolarizing inward current. However, in this review, the authors also warned that this activation might interact with other channels' activation so they suggested especially an electrophysiological control of the assumed activation effect of these DREADDs (Atasoy & Sternson, 2018).

Indeed, the examples in the literature about the diverse neuromodulatory effects of muscarinic ACh receptors support this suggestion. For instance, INs in L4 of the rat barrel cortex respond to ACh mostly with depolarization yet some of them showed hyperpolarization or no response (Qi & Feldmeyer, 2022). The authors also stressed VIP neurons, showing the strongest depolarization among non-fast spiking INs, exhibited occasional AP firing during depolarization (Qi & Feldmeyer, 2022). Another study on the effect of ACh in different INs showed that hippocampal (CA1) VIP and PV neurons respond to optogenetically released ACh differently. ACh induced depolarization in VIP neurons whereas it caused diverse responses in PV cells, like depolarization, hyperpolarization, or biphasic responses (Bell et al., 2015).

Given the variety of muscarinic receptor-mediated responses in different neuron populations, the necessity to control the effect of CNO in transduced cells was obvious. For

the control, CNO was bath applied during the monitoring of RMP of the transduced cells. Bath application of CNO during whole-cell patch-clamp recordings proved the expected activation of PV cells. The RMP slowly increased and then stabilized at a certain point below FT, which was consistent in all recorded PV cells. These cells also exhibited single spikes after depolarization probably due to spontaneous input, which was not observed before CNO application. This meant that after DREADD-induced depolarization, they showed spontaneous AP firing.

However, in VIP cells, CNO induced such a strong depolarization that the cells were finally driven into depolarization block. Once CNO arrived in the recording chamber, it caused a very steep depolarization and transiently elicited irregular AP firing in VIP cells for a few minutes. Later the cells stopped firing and their RMP was stabilized above FT, and no spiking was observed except the ones occasionally elicited by the short hyperpolarizations due to negative current pulses being applied on a regular basis. These short hyperpolarizations might have partially and transiently regenerated the Na^+ conductance and thereby, allowing rebound APs. This meant that in the case of VIP cells expressing hM_3D-Gq receptors, CNO-induced depolarization actually deactivated these cells permanently by depolarization block.

It is important to note that in a few exceptional cases lower doses of CNO did not cause depolarization block. However, the highest dose used in electrophysiological experiments was adjusted with an approximate calculation of the IP injected dose of CNO. CNO was administered on average 75 minutes before TT, which means that the transient AP firing during the initial phase of CNO administration and the start of depolarization block must have happened before the animals started the texture discrimination task, given the fact that the electrophysiological effects in vivo start 5 to 15 minutes later than the IP injection (Rogan et al., 2011).

The differing effects of CNO on PV and VIP cells might be due to many reasons. In principle, it depolarized both cells but depolarization block was observed only in VIP neurons and this effect cannot be caused by an experimental artifact: The surgeries for AAV injection were performed in the same way, as was the bath application, so the difference between these two cell types are very likely to originate from an intrinsic characteristic. The first thing that comes to mind is the high input resistance of VIP cells (Prönneke, 2017)

leading to a larger depolarization. Secondly, while VIP cells show only inward rectification (Prönneke et al., 2020), PV cells show outward rectifying conductances in the case of depolarization (Gorelova et al., 2002). Outward rectification acts against depolarization, which might also be why PV cells showed smaller depolarization compared to VIP cells.

Another aspect to consider is the number of receptors expressed in these cells. Both VIPcre and PVcre animals were stereotactically injected with the same amount of AAV. Still, we do not know, nor is there evidence in the literature yet, that these proportionately (i.e. there are more PV cells than VIP cells) different cell groups express the same number of receptors. In other words, would these neurons still show similar responses to CNO even if they exhibit differing numbers of DREADDs? This is still an unanswered question (Smith et al., 2016). This unexpected finding highlights the need for electrophysiological controls of the activation effect and for caution when interpreting the outcomes of chemogenetic manipulations.

One final issue needs to be taken into account regarding the comparability of in vivo and in vitro experiments. The effects of CNO on the membrane potential were tested in slices, with partially reduced connectivity, whereas during behavioral experiments CNO acted on the intact brain. In slices V_M is relatively hyperpolarized and mostly stable, in vivo however, interneurons are on average more depolarized and show some spontaneous firing (Gentet et al., 2012). How can the depolarizations observed in vitro be translated into the in vivo situation, or in other words, will the CNO-mediated depolarization simply add to the already depolarized membrane potential? If so, PV cells might also be driven into depolarization block in vivo. The persistent depolarization induced by CNO is based on constant manipulations of conductances, most likely potassium conductances as mentioned above, setting a new overall equilibrium potential. This in turn results in depolarized steady-state membrane potentials. The transient depolarizations observed in vivo are largely based on transient barrages of excitatory network activity (Sanchez-Vives & McCormick, 2000; Shu et al., 2003) with decreasing effect when V_M depolarizes. Therefore, they will contribute little to the overall equilibrium potential. As a result, the CNO-mediated depolarizations will most likely be comparable in both situations.

2. S1BF PV and VIP neurons have an integral role in texture discrimination

Although PV and VIP neurons are widely studied, especially on the cellular network level, their behavioral relevance has not yet been fully understood. In recent years, characterizing the roles of these cells on the behavioral level has attracted many scientists (Krabbe et al., 2019; Nahar et al., 2021; Apicella & Marchionni, 2022). This project also aimed to discover the roles of S1BF PV and VIP neurons in tactile perception, specifically in texture discrimination.

There were two main hypotheses for this project. With a quite simplistic view, the first hypothesis was that chemogenetically activating PV cells would cause a decrease in texture discrimination performance, and the second hypothesis of the project was that the chemogenetic activation of VIP cells would increase the performance in texture discrimination due to their involvement in differing connectivity motifs (Staiger & Petersen, 2021). It might be more straightforward to think about the potential results for PV neurons since they preferentially target excitatory cells (Freund & Katona, 2007; Veres et al., 2014) hence regarded as the main players in maintaining the cortical excititation-inhibition balance. Activating the main inhibitors would result in decreased flow of signals through the excitatory network in S1BF and animals would end up with impaired texture discrimination. On the other hand, for VIP cells there were different possibilities. Although it was hypothesized at the beginning of this project that activation of “disinhibitory” VIP neurons would enhance texture discrimination by releasing inhibition on excitatory cells, however, one could also think about a performance drop due to increased noise/signal ratio resulting from non-whisker related network activity not being suppressed by inhibition anymore. These potential opposing effects are hard to test experimentally since the role of these populations in texture discrimination has been remained unresolved so far and we have not obtained mechanistic “neurometric” data in the current project.

However, when it comes to microcircuitries, this simplistic view may underestimate the complexity of network activity. The reason is not only that all GABAergic neurons target excitatory cells, but also that all inhibitory neuron populations are bidirectionally connected with changing strengths (Pfeffer et al., 2013; Jiang et al., 2015; Karnani et al., 2016; Walker et al., 2016; Feldmeyer et al., 2018; Rachel, 2022; Preuß, 2023). Besides, other than the

local connections, both PV and VIP cells receive thalamocortical and corticocortical inputs. For example, PV neurons are known to receive the strongest thalamic input among other cell types (Staiger et al., 1996a; Ji et al., 2016), and also S1 VIP cells are shown to be innervated by VPM and POm, stressing their importance in tactile information processing (Staiger et al., 1996b; Feyerabend, 2020)). Also, S1BF receives inputs from other cortices, in the course of whisker-based detection, especially from the primary vibrissal motor cortex (vM1; Mao et al., 2011; Casas-Torremocha et al., 2017), and there is a bidirectional innervation between two cortices (Helmchen et al., 2018; Okoro et al., 2022). The vM1 excitatory neurons projecting to S1 preferentially target VIP cells (Lee et al., 2013), and also VIP cells are shown to be increasing activity during whisking which is considered as the result of this strong innervation of vM1 excitatory neurons (Lee et al., 2013; Yu et al., 2019). Overall the complexity of the connections of these cells to each other and other thalamic and cortical structures, makes it hard to formulate a biologically plausible hypothesis based on a rather basic inhibition-disinhibition logic in the local circuitry. Thus, the other side of the coin is that chemogenetic manipulation of different inhibitory cell types may significantly disturb the excitation-inhibition balance, potentially causing a collapse of the entire system.

There are few studies though, providing evidence that manipulated activation or inactivation of VIP or PV cells has differing effects and does not disturb the whole sensory system but more specifically changes the performance in sensory tasks. First of all, Pandey et al. (2023) support this claim by showing that animals had performance decreases in finding the textured object when S1(BF) PV neurons were activated. Another good example of a study recruiting chemogenetic manipulation revealed the effect of VIP inactivation on the olfactory system. The authors indicated that both odor detection and discrimination were impaired by the inactivation of VIP cells in the olfactory bulb, due to an increase in Mitral cell firing (Wang et al., 2022). Also, the activation of VIP cells is shown to be effective in increasing perceptual performance. In this study, the authors used the optogenetic method to activate primary visual cortex (V1) VIP cells (although compared to chemogenetics, manipulation is for very short durations) and showed that animals were able to detect differences between lower contrasts during a visual discrimination task (Cone et al., 2019). This pronounced better performance during VIP activation and enhanced

contrast increment detection. The same study also showed that activation of V1 PV cells in the primary visual cortex caused impairment in visual contrast perception (Cone et al., 2019). Overall, these findings provide a basis to claim that activation of PV and VIP neurons would cause a change in texture discrimination behavior and even could have opposing effects on discrimination performance.

As hypothesized, the chemogenetic activation of PV cells led to a significant reduction in texture discrimination performance. Actually, the success rates of the mice dropped on average to the chance level. This meant that these well-trained animals could no longer discriminate between two textures, meaning that texture discrimination ability was impaired. This finding aligns with the well-established role of PV cells as the principal mediators of cortical inhibition, where their activation likely over-suppressed excitatory output in the S1BF and impaired the animals' ability to discriminate textures correctly. Also, the effect of chemogenetic application on the cellular level was in line with this finding. For the activation of VIP cells, the results are more difficult to interpret compared to the effect of PV activation. The mice showed a comparable drop of performance, and were signficantly impaired to discriminate between textures. However, the electrophysiological changes with chemogenetic activation were different on the cellular level. Although VIP cells showed depolarization, as PV cells did, in response to CNO application, the depolarization was comparatively greater, and drove these cells to depolarization block. That is to say, CNO-induced depolarization deactivated VIP cells. These cells were still able to fire when artificially hyperpolarized by current pulses *in vitro*. Such transient hyperpolarizations might occur *in vivo* by inhibitory inputs, which might mean that they were not completely unable to fire during the texture discrimination, yet most probably they were non-responsive to texture-related excitatory input and were only firing in response to the inhibitory input (e.g. from PV cells). However, even in this case, it might end up with delayed disinhibition.

Even though the current knowledge needs to be improved to allow a network-based understanding of sensory processing, the present studies on different sensory modalities point out a consensus on the contrasting roles of VIP and PV neurons in perception (e.g. Cone et al., 2019). This means that the findings of the current project should not be reduced/generalized as a disturbance in the inhibition-excitation balance. The results of this

project confirm the critical importance of PV-mediated inhibition and VIP-mediated disinhibition in shaping sensory processing.

Assuming that the experimental manipulation of PV and VIP neurons in the present study led to rather specific effects, increased inhibition and decreased disinhibition respectively, on texture discrimination, one should consider the possible mechanisms underlying them. In order to do so, the first question would be how these interneurons might possibly act in the non-manipulated animal. As mentioned above, PV and VIP cells are presumably driven by the same inputs as excitatory cells One simple answer would be that inhibition controls the flow of excitatory signals by reducing or even suppressing excitatory inputs to excitatory neurons. In turn, disinhibitory neurons would do the opposite by reducing this inhibition. However, at least PV cells are described to target perisomatic or even axonal compartments of excitatory cells. Therefore, they might control the output of excitatory cells. Regardless of what is actually happening, it does not explain how textures are differently encoded in S1BF to allow texture discrimination. There is consensus in the field, that excitatory cells in S1BF fire sparsely in response to tactile stimulation (Crochet et al., 2011). Which kind of code serves to carry the texture information is unresolved so far (Staiger & Petersen, 2021). Heimendahl et al. (2007) monitored neuronal activity in the barrel cortex as rats used their whiskers to distinguish between different textures. In this study rats had to discriminate between rough SP and a surface without texture. The findings revealed a significantly higher increase in firing rates upon whisker contact with the rough surface. The difference in firing rate, however, disappeared when rats were tested with two different SPs (Jadhav & Feldman, 2010). Therefore, the firing rate code may only apply to large differences between textures. An alternative coding scheme might be the slip-stick theory (Wolfe et al., 2008) proposing that sparse but synchronous firing in neighboring cells may carry texture information. Since firing correlation is stronger in response to rough textures (Garion et al., 2014) it may allow texture discrimination. Whichever theory or mixture of the theories will eventually turn out to be at the base of texture discrimination, the effects of chemogenetic manipulation on the cellular level reported here may explain the observed change in behavioral performance. Increased activation of PV cells may reduce the firing rate of excitatory cells but may also reduce correlated firing. On the one hand side, even proportional reduction

in the different firing rates in response to different textures could decrease the difference between these firing rates and, therefore, decrease the probability of detecting texture differences. On the other hand, correlated firing in a population of excitatory cells is not perfectly synchronous but shows some spike time jitter. An increase of inhibitory input from PV cells may at least slightly delay firing in individual excitatory cells leading to an increase in jitter. As a result, firing correlation will be impaired and again detection of differences between textures will be more difficult. The same line of arguments holds also true for VIP cells. Their inactivation by depolarization block will most likely lead to a reduction of inhibition of other inhibitory neurons, like PV cells, and would, therefore, have the same effect on the texture coding.

The S1BF is considered to be a core node of networks for tactile processing, also taking part in texture discrimination (Stüttgen & Schwarz, 2018; Staiger & Petersen, 2021). In order to understand how S1BF serves this purpose one needs to know if any excitatory cell or population of cells can code for any texture. One study expanded on this by using *in vivo* two-photon calcium imaging to observe L 2/3 neurons in the rat barrel cortex during whisker contact against different grit-sized SP. Their results indicated that neurons within specific barrels columns exhibited differential responses to textures, suggesting a functional organization where neuron populations are tuned to specific tactile features (Garion et al., 2014). Also, it was shown that this texture-selectivity is a result of perceptual learning. Chéreau et al. (2020) proved that the coarseness selectivity of neurons depends on the rewarded texture. With the reversal learning (i.e. changing the rewarded texture), the texture-selectivity of neurons was reshaped to respond to another texture. Authors claimed that the stabilization of the neuronal population to a specific stimulus is for the sake of enhancement of perception, and neuronal selectivity is dynamic and heavily influenced by behavioral contingencies (e.g. detection of a certain texture in discrimination is rewarded), highlighting the adaptability of S1BF in encoding sensory information based on experience and learning (Chéreau et al., 2020).

Moreover, the research on choice-related activity in whisker-based tasks, supports these findings. For instance, S1BF neurons exhibit robust activity correlated with choice during a tactile detection task (Yang et al., 2016). Additionally, a review of the diverse and behavior-dependent neuronal activity patterns in the neocortex during tactile behavioral

tasks, highlighted the intricate dynamics between the S1BF, S2, and vM1, shedding light on the complex interplay of these regions during sensory processing (Helmchen et al., 2018). Recently “decision neurons” have been discovered which might explain the choice-related activity in S1BF. Similar to Chéreau et al., (2020), Buetfering et al. (2022) identified neurons in S1BF that categorically encode the stimulus (e.g. coarseness of the SP) related to decision-making during a texture discrimination task. More importantly, these decision neurons lacked a conclusive decision signal in trials where the subject did not reach a decision, and photostimulation of these neurons increased discrimination performance (Buetfering et al., 2022) emphasizing the potential role of the S1BF in behaviorally relevant decision coding.

Overall, these studies demonstrate the complexity of the contributions of S1BF to tactile information processing. They highlight its pivotal role in texture discrimination, perceptual learning, and decision-making processes, emphasizing the dynamic nature of sensory encoding influenced by behavioral context. Since all these findings are not yet able to explain the sensory processing on the local circuitry level, defining the more general roles of different interneurons in tactile tasks is a crucial contribution to the advancement of the field.

3. Future directions

This project is inspirational for several future studies. First, highlighting the importance of VIP cells, showed that the presence of VIP cells is as crucial as PV cells in tactile perception. This points out the need for further research on the role of VIP neurons on tactile perception. Not only PV and VIP but also effect of the chemogenetic manipulation of SST cells remains an important question to address.

Second, it showed that refining chemogenetic protocols to avoid depolarization blocks is critical for accurate investigation of the roles of VIP cells in sensory processing. This could involve using alternative DREADD variants or especially optimizing ligand doses with the help of electrophysiological experiments. Also the effect of chemogenetic inactivation still needs to be tested for different IN populations.

Another important aspect of the chemogenetic manipulations is to reveal the relevance of the number of expressed DREADDs on the target cells to the effect of CNO

activation. In the state of art, this potential confound makes it a curious question to explain the results of the chemogenetic applications on behavior.

Finally, extending this research to explore the interplay between PV and VIP cells during sensory processing could provide a more comprehensive understanding of how cortical circuits integrate inhibition and disinhibition to shape perception. Such studies would benefit from advanced imaging techniques (e.g. 2-photon guided whole-cell recordings) to visualize real-time activity patterns across cell populations.

CONCLUSION

The precise isomorphic representation of whiskers in the whisker-to-barrel pathways is suggestive of that whisker-based perception being essential for rodents. This organization is absent or reduced in visual mammals (e.g. cats, horses, apes) or those which rely more on other senses (Grant & Goss, 2022). However, it is now important to solve the puzzle of perception by understanding how modifying the cortical excitation-inhibition balance changes the percept of external stimuli.

First of all, this project stressed once more the integral role of S1BF in tactile discrimination. The texture discrimination capacity necessitates a delicate balance of excitation and inhibition in S1BF. Hence, it strengthens the importance of interneurons in perception.

The findings of this study provide valuable insights into the roles of PV and VIP neurons in the primary somatosensory barrel field (S1BF) during whisker-based texture discrimination. Chemogenetic activation of PV cells, as hypothesized, impaired texture discrimination performance, underlining their fundamental role as the main inhibitors within the cortical network. Unexpectedly, chemogenetic activation of VIP cells resulted in a depolarization block, causing reduced rather than enhanced texture discrimination ability yet still pronouncing the importance of disinhibition in sensory shaping.

These results contribute to our understanding of the excitation-inhibition balance and the complex interplay between inhibition and disinhibition in the cortical circuitry. They also underscore the need for methodological refinements in chemogenetic manipulations especially for neuronal activity modulation. The use of freely behaving mice further bridges the gap between naturalistic behavior and electrophysiological properties of interneurons, offering a more comprehensive understanding of sensory processing.

REFERENCES

Adesnik, H., & Naka, A. (2018). Cracking the function of layers in the sensory cortex. *Neuron*, *100*(5), 1028–1043. https://doi.org/10.1016/j.neuron.2018.10.032

Agmon, A., & Connors, B. W. (1991). Thalamocortical responses of mouse somatosensory (barrel) cortex in vitro. *Neuroscience*, *41*(2–3), 365–379. https://doi.org/10.1016/0306-4522(91)90333-j

Ahissar, E., Sosnik, R., & Haidarliu, S. (2000). Transformation from temporal to rate coding in a somatosensory thalamocortical pathway. *Nature*, *406*(6793), 302–306. https://doi.org/10.1038/35018568

Alexander, G. M., Rogan, S. C., Abbas, A. I., Armbruster, B. N., Pei, Y., Allen, J. A., Nonneman, R. J., Hartmann, J., Moy, S. S., Nicolelis, M. A., McNamara, J. O., & Roth, B. L. (2009). Remote control of neuronal activity in transgenic mice expressing evolved G protein-coupled receptors. *Neuron*, *63*(1), 27–39. https://doi.org/10.1016/j.neuron.2009.06.014

Almási, Z., Dávid, C., Witte, M., & Staiger, J. F. (2019). Distribution patterns of three molecularly defined classes of GABAergic neurons across columnar compartments in mouse barrel cortex. *Frontiers in Neuroanatomy*, *13*, 45. https://doi.org/10.3389/fnana.2019.00045

Apicella, A. junior, & Marchionni, I. (2022). VIP-expressing GABAergic neurons: Disinhibitory vs. inhibitory motif and its role in communication across neocortical areas. *Frontiers in Cellular Neuroscience*, *16*, 811484. https://doi.org/10.3389/fncel.2022.811484

Arabzadeh, E., Zorzin, E., & Diamond, M. E. (2005). Neuronal encoding of texture in the whisker sensory pathway. *PLOS Biology*, *3*(1), e17. https://doi.org/10.1371/journal.pbio.0030017

Armbruster, B. N., Li, X., Pausch, M. H., Herlitze, S., & Roth, B. L. (2007). Evolving the lock to fit the key to create a family of G protein-coupled receptors potently activated by an inert ligand. *Proceedings of the National Academy of Sciences*, *104*(12), 5163–5168. https://doi.org/10.1073/pnas.0700293104

Ascoli, G. A., Alonso-Nanclares, L., Anderson, S. A., Barrionuevo, G., Benavides-Piccione, R., Burkhalter, A., Buzsáki, G., Cauli, B., DeFelipe, J., Fairén, A., Feldmeyer, D., Fishell, G., Fregnac, Y., Freund, T. F., Gardner, D., Gardner, E. P., Goldberg, J. H., Helmstaedter, M., Hestrin, S., … The Petilla Interneuron Nomenclature Group (PING). (2008). Petilla terminology: Nomenclature of features of GABAergic interneurons of the cerebral cortex. *Nature Reviews Neuroscience*, *9*(7), 557–568. https://doi.org/10.1038/nrn2402

Atallah, B. V., Bruns, W., Carandini, M., & Scanziani, M. (2012). Parvalbumin-expressing interneurons linearly transform cortical responses to visual stimuli. *Neuron*, *73*(1), 159–170. https://doi.org/10.1016/j.neuron.2011.12.013

Atasoy, D., & Sternson, S. M. (2018). Chemogenetic tools for causal cellular and neuronal biology. *Physiological Reviews*, *98*(1), 391–418. https://doi.org/10.1152/physrev.00009.2017

Bakker, R., Tiesinga, P., & Kötter, R. (2015). The scalable brain atlas: Instant web-based access to public brain atlases and related content. *Neuroinformatics*, *13*(3), 353–366. https://doi.org/10.1007/s12021-014-9258-x

Belford, G. R., & Killackey, H. P. (1979). Vibrissae representation in subcortical trigeminal centers of the neonatal rat. *The Journal of Comparative Neurology*, *183*(2), 305–321. https://doi.org/10.1002/cne.901830207

Bell, L. A., Bell, K. A., & McQuiston, A. R. (2015). Activation of muscarinic receptors by ACh release in hippocampal CA1 depolarizes VIP but has varying effects on parvalbumin-expressing basket cells. *The Journal of Physiology*, *593*(Pt 1), 197–215. https://doi.org/10.1113/jphysiol.2014.277814

Belli, H. M., Yang, A. E. T., Bresee, C. S., & Hartmann, M. J. Z. (2017). Variations in vibrissal geometry across the rat mystacial pad: Base diameter, medulla, and taper. *Journal of Neurophysiology*, *117*(4), 1807–1820. https://doi.org/10.1152/jn.00054.2016

Benjamini, Y., Krieger, A. M., & Yekutieli, D. (2006). Adaptive linear step-up procedures that control the false discovery rate. *Biometrika*, *93*(3), 491–507. https://doi.org/10.1093/biomet/93.3.491

Birrell, J. M., & Brown, V. J. (2000). Medial frontal cortex mediates perceptual attentional set shifting in the rat. *The Journal of Neuroscience*, *20*(11), 4320–4324. https://doi.org/10.1523/JNEUROSCI.20-11-04320.2000

Blanco-Hernández, E., Balsamo, G., Preston-Ferrer, P., & Burgalossi, A. (2024). Sensory and behavioral modulation of thalamic head-direction cells. *Nature Neuroscience*, *27*(1), 28–33. https://doi.org/10.1038/s41593-023-01506-1

Blaustein, M. P., & Lederer, W. J. (1999). Sodium/calcium exchange: Its physiological implications. *Physiological Reviews*, *79*(3), 763–854. https://doi.org/10.1152/physrev.1999.79.3.763

Bourgeon, S., Xerri, C., & Coq, J.-O. (2004). Abilities in tactile discrimination of textures in adult rats exposed to enriched or impoverished environments. *Behavioural Brain Research*, *153*(1), 217–231. https://doi.org/10.1016/j.bbr.2003.12.002

Brecht, M., Preilowski, B., & Merzenich, M. M. (1997). Functional architecture of the mystacial vibrissae. *Behavioural Brain Research*, *84*(1), 81–97. https://doi.org/10.1016/S0166-4328(97)83328-1

Brecht, M., & Sakmann, B. (2002). Dynamic representation of whisker deflection by synaptic potentials in spiny stellate and pyramidal cells in the barrels and septa of layer 4 rat somatosensory cortex. *The Journal of Physiology*, *543*(Pt 1), 49–70. https://doi.org/10.1113/jphysiol.2002.018465

Buetfering, C., Zhang, Z., Pitsiani, M., Smallridge, J., Boven, E., McElligott, S., & Häusser, M. (2022). Behaviorally relevant decision coding in primary somatosensory cortex neurons. *Nature Neuroscience*, *25*(9), 1225–1236. https://doi.org/10.1038/s41593-022-01151-0

Cafaro, J., & Rieke, F. (2010). Noise correlations improve response fidelity and stimulus encoding. *Nature*, *468*(7326), 964–967. https://doi.org/10.1038/nature09570

Carvell, G., & Simons, D. (1990). Biometric analyses of vibrissal tactile discrimination in the rat. *The Journal of Neuroscience*, *10*(8), 2638–2648. https://doi.org/10.1523/JNEUROSCI.10-08-02638.1990

Casas-Torremocha, D., Clascá, F., & Núñez, Á. (2017). Posterior thalamic nucleus modulation of tactile stimuli processing in rat motor and primary somatosensory cortices. *Frontiers in Neural Circuits*, *11*, 69. https://doi.org/10.3389/fncir.2017.00069

Celikel, T., & Sakmann, B. (2007). Sensory integration across space and in time for decision making in the somatosensory system of rodents. *Proceedings of the National Academy of Sciences*, *104*(4), 1395–1400. https://doi.org/10.1073/pnas.0610267104

Chéreau, R., Bawa, T., Fodoulian, L., Carleton, A., Pagès, S., & Holtmaat, A. (2020). Dynamic perceptual feature selectivity in primary somatosensory cortex upon reversal learning. *Nature Communications*, *11*(1), 3245. https://doi.org/10.1038/s41467-020-17005-x

Cone, J. J., Scantlen, M. D., Histed, M. H., & Maunsell, J. H. R. (2019). *Different inhibitory interneuron cell classes make distinct contributions to visual contrast perception. eNeuro, 6*(1). https://doi.org/10.1523/ENEURO.0337-18.2019

Constantinople, C. M., & Bruno, R. M. (2013). Deep cortical layers are activated directly by thalamus. *Science*, *340*(6140), 1591–1594. https://doi.org/10.1126/science.1236425

Crochet, S., Poulet, J. F. A., Kremer, Y., & Petersen, C. C. H. (2011). Synaptic mechanisms underlying sparse coding of active touch. *Neuron*, *69*(6), 1160–1175. https://doi.org/10.1016/j.neuron.2011.02.022

Dávid, C., Schleicher, A., Zuschratter, W., & Staiger, J. F. (2007). The innervation of parvalbumin-containing interneurons by VIP-immunopositive interneurons in the primary somatosensory cortex of the adult rat. *The European Journal of Neuroscience*, *25*(8), 2329–2340. https://doi.org/10.1111/j.1460-9568.2007.05496.x

DeFelipe, J., López-Cruz, P. L., Benavides-Piccione, R., Bielza, C., Larrañaga, P., Anderson, S., Burkhalter, A., Cauli, B., Fairén, A., Feldmeyer, D., Fishell, G., Fitzpatrick, D., Freund, T. F., González-Burgos, G., Hestrin, S., Hill, S., Hof, P. R., Huang, J., Jones, E. G., … Ascoli, G. A. (2013). New insights into the classification and nomenclature of cortical GABAergic interneurons. *Nature Reviews Neuroscience*, *14*(3), 202–216. https://doi.org/10.1038/nrn3444

Deschenes, M., & Urbain, N. (2009). Vibrissal afferents from trigeminus to cortices. *Scholarpedia*, *4*(5), 7454. https://doi.org/10.4249/scholarpedia.7454

Diamond, M. E., Armstrong-James, M., & Ebner, F. F. (1992). Somatic sensory responses in the rostral sector of the posterior group (POm) and in the ventral posterior medial nucleus (VPM) of the rat thalamus. *The Journal of Comparative Neurology*, *318*(4), 462–476. https://doi.org/10.1002/cne.903180410

Diamond, M. E., Von Heimendahl, M., Knutsen, P. M., Kleinfeld, D., & Ahissar, E. (2008). 'Where'and'what'in the whisker sensorimotor system. *Nature Reviews Neuroscience, 9*(8), 601-612. https://doi.org/10.1038/nrn2411

Douglas, R. J., & Martin, K. A. (1991). A functional microcircuit for cat visual cortex. *The Journal of Physiology*, *440*, 735–769. https://doi.org/10.1113/jphysiol.1991.sp018733

Douglas, R. J., & Martin, K. A. C. (2004). Neuronal circuits of the neocortex. *Annual Review of Neuroscience*, *27*, 419–451. https://doi.org/10.1146/annurev.neuro.27.070203.144152

Douglas, R. J., & Martin, K. A. C. (2007). Mapping the matrix: The ways of neocortex. *Neuron*, *56*(2), 226–238. https://doi.org/10.1016/j.neuron.2007.10.017

Druga, R., Salaj, M., & Al-Redouan, A. (2023). Parvalbumin - positive neurons in the neocortex: A review. *Physiological Research*, *72*(Suppl 2), S173–S191. https://doi.org/10.33549/physiolres.935005

Ebara, S., Kumamoto, K., Matsuura, T., Mazurkiewicz, J. E., & Rice, F. L. (2002). Similarities and differences in the innervation of mystacial vibrissal follicle-sinus complexes in the rat and cat: A confocal microscopic study. *The Journal of Comparative Neurology*, *449*(2), 103–119. https://doi.org/10.1002/cne.10277

El-Boustani, S., Sermet, B. S., Foustoukos, G., Oram, T. B., Yizhar, O., & Petersen, C. C. H. (2020). Anatomically and functionally distinct thalamocortical inputs to primary and secondary mouse whisker somatosensory cortices. *Nature Communications*, *11*(1), 3342. https://doi.org/10.1038/s41467-020-17087-7

Erzurumlu, R. S., & Gaspar, P. (2020). How the barrel cortex became a working model for developmental plasticity: A historical perspective. *Journal of Neuroscience*, *40*(34), 6460–6473. https://doi.org/10.1523/JNEUROSCI.0582-20.2020

Feldmeyer, D. (2012). Excitatory neuronal connectivity in the barrel cortex. *Frontiers in Neuroanatomy*, *6*, 24. https://doi.org/10.3389/fnana.2012.00024

Feldmeyer, D., Brecht, M., Helmchen, F., Petersen, C. C. H., Poulet, J. F. A., Staiger, J. F., Luhmann, H. J., & Schwarz, C. (2013). Barrel cortex function. *Progress in Neurobiology*, *103*, 3–27. https://doi.org/10.1016/j.pneurobio.2012.11.002

Feldmeyer, D., Qi, G., Emmenegger, V., & Staiger, J. F. (2018). Inhibitory interneurons and their circuit motifs in the many layers of the barrel cortex. *Neuroscience*, *368*, 132–151. https://doi.org/10.1016/j.neuroscience.2017.05.027

Fellows, B. J. (1967). Chance stimulus sequences for discrimination. *Psychological Bulletin*, *67*(2). https://doi.org/10.1037/h0024098

Feyerabend, M. (2020). *Thalamocortical innervation of GABAergic iInterneurons in mouse primary vibrissal somatosensory cortex* [Doctoral Dissertation, Georg-August-University Göttingen]. https://doi.org/10.53846/goediss-8331

Fishell, G., & Rudy, B. (2011). Mechanisms of inhibition within the telencephalon: “Where the wild things are.” *Annual Review of Neuroscience*, *34*, 535–567. https://doi.org/10.1146/annurev-neuro-061010-113717

Forkmann, G., & Dangelmayr, B. (1980). Genetic control of chalcone isomerase activity in flowers of Dianthus caryophyllus. *Biochemical Genetics*, *18*(5–6), 519–527. https://doi.org/10.1007/BF00484399

Freund, T. F., & Katona, I. (2007). Perisomatic inhibition. *Neuron*, *56*(1), 33–42. https://doi.org/10.1016/j.neuron.2007.09.012

Garion, L., Dubin, U., Rubin, Y., Khateb, M., Schiller, Y., Azouz, R., & Schiller, J. (2014). Texture coarseness responsive neurons and their mapping in layer 2–3 of the rat barrel cortex in vivo. *eLife*, *3*, e03405. https://doi.org/10.7554/eLife.03405

Gentet, L. J., Kremer, Y., Taniguchi, H., Huang, Z. J., Staiger, J. F., & Petersen, C. C. H. (2012). Unique functional properties of somatostatin-expressing GABAergic neurons in mouse barrel cortex. *Nature Neuroscience*, *15*(4), 607–612. https://doi.org/10.1038/nn.3051

Gorelova, N., Seamans, J. K., & Yang, C. R. (2002). Mechanisms of dopamine activation of fast-spiking interneurons that exert inhibition in rat prefrontal cortex. *Journal of Neurophysiology*, *88*(6), 3150–3166. https://doi.org/10.1152/jn.00335.2002

Grant, R. A., & Goss, V. G. A. (2022). What can whiskers tell us about mammalian evolution, behaviour, and ecology? *Mammal Review*, *52*(1), 148–163. https://doi.org/10.1111/mam.12253

Grant, R. A., Ryan, H., & Breakell, V. (2023). Demonstrating a measurement protocol for studying comparative whisker movements with implications for the evolution of behaviour. *Journal of Neuroscience Methods*, *384*, 109752. https://doi.org/10.1016/j.jneumeth.2022.109752

Graupner, M., & Reyes, A. D. (2013). Synaptic input correlations leading to membrane potential decorrelation of spontaneous activity in cortex. *The Journal of Neuroscience*, *33*(38), 15075–15085. https://doi.org/10.1523/JNEUROSCI.0347-13.2013

Guy, J., Möck, M., & Staiger, J. F. (2023). Direction selectivity of inhibitory interneurons in mouse barrel cortex differs between interneuron subtypes. *Cell Reports*, *42*(1). https://doi.org/10.1016/j.celrep.2022.111936

Guy, J., & Staiger, J. F. (2017). The functioning of a cortex without layers. *Frontiers in Neuroanatomy, 11*, 54. https://www.frontiersin.org/articles/10.3389/fnana.2017.00054

Haidarliu, S., Yu, C., Rubin, N., & Ahissar, E. (2008). Lemniscal and extralemniscal compartments in the VPM of the rat. *Frontiers in Neuroanatomy*, *2*, 304. https://doi.org/10.3389/neuro.05.004.2008

Harris, J. A., Petersen, R. S., & Diamond, M. E. (1999). Distribution of tactile learning and its neural basis. *Proceedings of the National Academy of Sciences*, *96*(13), 7587–7591. https://doi.org/10.1073/pnas.96.13.7587

Harris, K. D., & Mrsic-Flogel, T. D. (2013). Cortical connectivity and sensory coding. *Nature*, *503*(7474), 51–58. https://doi.org/10.1038/nature12654

Harris, K. D., & Shepherd, G. M. G. (2015). The neocortical circuit: Themes and variations. *Nature Neuroscience*, *18*(2), 170–181. https://doi.org/10.1038/nn.3917

Heimendahl, M. von, Itskov, P. M., Arabzadeh, E., & Diamond, M. E. (2007). Neuronal activity in rat barrel cortex underlying texture discrimination. *PLOS Biology*, *5*(11), e305. https://doi.org/10.1371/journal.pbio.0050305

Helmchen, F., Gilad, A., & Chen, J. L. (2018). Neocortical dynamics during whisker-based sensory discrimination in head-restrained mice. *Neuroscience*, *368*, 57–69. https://doi.org/10.1016/j.neuroscience.2017.09.003

Herrnstein, R. J., & Loveland, D. H. (1974). Hunger and contrast in a multiple schedule. *Journal of the Experimental Analysis of Behavior*, *21*(3), 511–517. https://doi.org/10.1901/jeab.1974.21-511

Hioki, H., Okamoto, S., Konno, M., Kameda, H., Sohn, J., Kuramoto, E., Fujiyama, F., & Kaneko, T. (2013). Cell type-specific inhibitory inputs to dendritic and somatic compartments of parvalbumin-expressing neocortical interneuron. *Journal of Neuroscience*, *33*(2), 544–555. https://doi.org/10.1523/JNEUROSCI.2255-12.2013

Hippenmeyer, S., Vrieseling, E., Sigrist, M., Portmann, T., Laengle, C., Ladle, D. R., & Arber, S. (2005). A developmental switch in the response of DRG neurons to ETS transcription factor signaling. *PLoS Biology*, *3*(5), e159. https://doi.org/10.1371/journal.pbio.0030159

Hires, S. A., Pammer, L., Svoboda, K., & Golomb, D. (2013). Tapered whiskers are required for active tactile sensation. *eLife*, *2*, e01350. https://doi.org/10.7554/eLife.01350

Hu, H., Gan, J., & Jonas, P. (2014). Fast-spiking, parvalbumin+ GABAergic interneurons: From cellular design to microcircuit function. *Science*, *345*(6196), 1255263. https://doi.org/10.1126/science.1255263

Isaacson, J. S., & Scanziani, M. (2011). How inhibition shapes cortical activity. *Neuron*, *72*(2), 231–243. https://doi.org/10.1016/j.neuron.2011.09.027

Jadhav, S. P., & Feldman, D. E. (2010). Texture coding in the whisker system. *Current Opinion in Neurobiology*, *20*(3), 313–318. https://doi.org/10.1016/j.conb.2010.02.014

Jendryka, M., Palchaudhuri, M., Ursu, D., van der Veen, B., Liss, B., Kätzel, D., Nissen, W., & Pekcec, A. (2019). Pharmacokinetic and pharmacodynamic actions of clozapine-N-oxide, clozapine, and compound 21 in DREADD-based chemogenetics in mice. *Scientific Reports*, *9*(1). https://doi.org/10.1038/s41598-019-41088-2

Jenkinson, E. W., & Glickstein, M. (2000). Whiskers, barrels, and cortical efferent pathways in gap crossing by rats. *Journal of Neurophysiology*, *84*(4), 1781–1789. https://doi.org/10.1152/jn.2000.84.4.1781

Ji, X.-Y., Zingg, B., Mesik, L., Xiao, Z., Zhang, L. I., & Tao, H. W. (2016). Thalamocortical innervation pattern in mouse auditory and visual cortex: Laminar and cell-type specificity. *Cerebral Cortex*, *26*(6), 2612–2625. https://doi.org/10.1093/cercor/bhv099

Jiang, X., Shen, S., Cadwell, C. R., Berens, P., Sinz, F., Ecker, A. S., Patel, S., & Tolias, A. S. (2015). Principles of connectivity among morphologically defined cell types in adult neocortex. *Science*, *350*(6264), aac9462. https://doi.org/10.1126/science.aac9462

Jouhanneau, J.-S., Ferrarese, L., Estebanez, L., Audette, N. J., Brecht, M., Barth, A. L., & Poulet, J. F. A. (2014). Cortical fosGFP expression reveals broad receptive field excitatory neurons targeted by POm. *Neuron*, *84*(5), 1065–1078. https://doi.org/10.1016/j.neuron.2014.10.014

Kameda, H., Hioki, H., Tanaka, Y. H., Tanaka, T., Sohn, J., Sonomura, T., Furuta, T., Fujiyama, F., & Kaneko, T. (2012). Parvalbumin-producing cortical interneurons receive inhibitory inputs on proximal portions and cortical excitatory inputs on distal dendrites. *European Journal of Neuroscience*, *35*(6), 838–854. https://doi.org/10.1111/j.1460-9568.2012.08027.x

Karnani, M. M., Jackson, J., Ayzenshtat, I., Sichani, A. H., Manoocheri, K., Kim, S., & Yuste, R. (2016). Opening holes in the blanket of inhibition: Localized lateral disinhibition by VIP interneurons. *Journal of Neuroscience*, *36*(12), 3471–3480. https://doi.org/10.1523/JNEUROSCI.3646-15.2016

Krabbe, S., Paradiso, E., d'Aquin, S., Bitterman, Y., Courtin, J., Xu, C., Yonehara, K., Markovic, M., Müller, C., Eichlisberger, T., Gründemann, J., Ferraguti, F., & Lüthi, A. (2019). Adaptive disinhibitory gating by VIP interneurons permits associative learning. *Nature Neuroscience*, *22*(11), 1834–1843. https://doi.org/10.1038/s41593-019-0508-y

Krashes, M. J., Koda, S., Ye, C., Rogan, S. C., Adams, A. C., Cusher, D. S., Maratos-Flier, E., Roth, B. L., & Lowell, B. B. (2011). Rapid, reversible activation of AgRP neurons drives feeding behavior in mice. *The Journal of Clinical Investigation*, *121*(4), 1424–1428. https://doi.org/10.1172/JCI46229

Krupa, D. J., Matell, M. S., Brisben, A. J., Oliveira, L. M., & Nicolelis, M. A. L. (2001). Behavioral properties of the trigeminal somatosensory system in rats performing whisker-dependent tactile discriminations. *Journal of Neuroscience*, *21*(15), 5752–5763. https://doi.org/10.1523/JNEUROSCI.21-15-05752.2001

Lee, K. J., & Woolsey, T. A. (1975). A proportional relationship between peripheral innervation density and cortical neuron number in the somatosensory system of the mouse. *Brain Research*, *99*(2), 349–353. https://doi.org/10.1016/0006-8993(75)90035-9

Lee, S., Kruglikov, I., Huang, Z. J., Fishell, G., & Rudy, B. (2013). A disinhibitory circuit mediates motor integration in the somatosensory cortex. *Nature Neuroscience*, *16*(11), 1662–1670. https://doi.org/10.1038/nn.3544

Lefort, S., Tomm, C., Floyd Sarria, J.-C., & Petersen, C. C. H. (2009). The excitatory neuronal network of the C2 barrel column in mouse primary somatosensory cortex. *Neuron*, *61*(2), 301–316. https://doi.org/10.1016/j.neuron.2008.12.020

Lein, E. S., Hawrylycz, M. J., Ao, N., Ayres, M., Bensinger, A., Bernard, A., Boe, A. F., Boguski, M. S., Brockway, K. S., Byrnes, E. J., Chen, L., Chen, L., Chen, T.-M., Chin, M. C., Chong, J., Crook, B. E., Czaplinska, A., Dang, C. N., Datta, S., … Jones, A. R. (2007). Genome-wide atlas of gene expression in the adult mouse brain. *Nature*, *445*(7124), 168–176. https://doi.org/10.1038/nature05453

Lenschow, C., & Brecht, M. (2015). Barrel cortex membrane potential dynamics in social touch. *Neuron*, *85*(4), 718–725. https://doi.org/10.1016/j.neuron.2014.12.059

Lerchner, W., Corgiat, B., Der Minassian, V., Saunders, R. C., & Richmond, B. J. (2014). Injection parameters and virus dependent choice of promoters to improve neuron targeting in the nonhuman primate brain. *Gene Therapy*, *21*(3), 233–241. https://doi.org/10.1038/gt.2013.75

Letzkus, J. J., Wolff, S. B. E., Meyer, E. M. M., Tovote, P., Courtin, J., Herry, C., & Lüthi, A. (2011). A disinhibitory microcircuit for associative fear learning in the auditory cortex. *Nature*, *480*(7377), 331–335. https://doi.org/10.1038/nature10674

Lipp, H.-P., & Van der Loos, H. (1991). A computer-controlled Y-maze for the analysis of vibrissotactile discrimination learning in mice. *Behavioural Brain Research*, *45*(2), 135–145. https://doi.org/10.1016/S0166-4328(05)80079-8

Lübke, J., & Feldmeyer, D. (2007). Excitatory signal flow and connectivity in a cortical column: Focus on barrel cortex. *Brain Structure and Function*, *212*(1), 3–17. https://doi.org/10.1007/s00429-007-0144-2

Ma, P. M., & Woolsey, T. A. (1984). Cytoarchitectonic correlates of the vibrissae in the medullary trigeminal complex of the mouse. *Brain Research*, *306*(1), 374–379. https://doi.org/10.1016/0006-8993(84)90390-1

Mao, T., Kusefoglu, D., Hooks, B. M., Huber, D., Petreanu, L., & Svoboda, K. (2011). Long-range neuronal circuits underlying the interaction between sensory and motor cortex. *Neuron*, *72*(1), 111–123. https://doi.org/10.1016/j.neuron.2011.07.029

Mao, X., & Staiger, J. F. (2024). Multimodal cortical neuronal cell type classification. *Pflugers Archiv: European Journal of Physiology*, *476*(5), 721–733. https://doi.org/10.1007/s00424-024-02923-2

Meyer, H. S., Schwarz, D., Wimmer, V. C., Schmitt, A. C., Kerr, J. N. D., Sakmann, B., & Helmstaedter, M. (2011). Inhibitory interneurons in a cortical column form hot zones of inhibition in layers 2 and 5A. *Proceedings of the National Academy of Sciences*, *108*(40), 16807–16812. https://doi.org/10.1073/pnas.1113648108

Milani, H., Steiner, H., & Huston, J. P. (1989). Analysis of recovery from behavioral asymmetries induced by unilateral removal of vibrissae in the rat. *Behavioral Neuroscience*, *103*(5), 1067–1074. https://doi.org/10.1037/0735-7044.103.5.1067

Montuori, L. M., & Honey, R. C. (2016). Perceptual learning with tactile stimuli in rats: Changes in the processing of a dimension. *Journal of Experimental Psychology: Animal Learning and Cognition*, *42*(3), 281–289. https://doi.org/10.1037/xan0000104

Morita, T., Kang, H., Wolfe, J., Jadhav, S. P., & Feldman, D. E. (2011). Psychometric curve and behavioral strategies for whisker-based texture discrimination in rats. *PLoS One*, *6*(6), e20437. https://doi.org/10.1371/journal.pone.0020437

Nahar, L., Delacroix, B. M., & Nam, H. W. (2021). The role of parvalbumin interneurons in neurotransmitter balance and neurological disease. *Frontiers in Psychiatry*, *12*. https://doi.org/10.3389/fpsyt.2021.679960

Naka, A., Veit, J., Shababo, B., Chance, R. K., Risso, D., Stafford, D., Snyder, B., Egladyous, A., Chu, D., Sridharan, S., Mossing, D. P., Paninski, L., Ngai, J., & Adesnik, H. (2019). Complementary networks of cortical somatostatin interneurons enforce layer specific control. *eLife*, *8*, e43696. https://doi.org/10.7554/eLife.43696

Okoro, S. U., Goz, R. U., Njeri, B. W., Harish, M., Ruff, C. F., Ross, S. E., Gerfen, C., & Hooks, B. M. (2022). Organization of cortical and thalamic input to inhibitory neurons in mouse motor cortex. *Journal of Neuroscience*, *42*(43), 8095–8112. https://doi.org/10.1523/JNEUROSCI.0950-22.2022

Pacchiarini, N., Berkeley, R., Fox, K., & Honey, R. C. (2020). Whisker-mediated texture discrimination learning in freely moving mice. *Journal of Experimental Psychology. Animal Learning and Cognition*, *46*(1), 40–46. https://doi.org/10.1037/xan0000212

Packer, A. M., & Yuste, R. (2011). Dense, unspecific connectivity of neocortical parvalbumin-positive interneurons: A canonical microcircuit for inhibition? *Journal of Neuroscience*, *31*(37), 13260–13271. https://doi.org/10.1523/JNEUROSCI.3131-11.2011

Palicz, R., Pater, B., Truschow, P., Witte, M., & Staiger, J. F. (2024). Intersectional strategy to study cortical inhibitory parvalbumin-expressing interneurons. *Scientific Reports*, *14*(1), 2829. https://doi.org/10.1038/s41598-024-52901-y

Pandey, A., Kang, S., Pacchiarini, N., Wyszynska, H., Grewal, A., Griffiths, A., Healy-Millett, I., Masseri, Z., Hardingham, N., O'Neill, J., Honey, R. C., & Fox, K. (2023). *Interdependence of primary and secondary somatosensory cortices for plasticity and texture discrimination learning* (p. 2023.04.25.538217). bioRxiv. https://doi.org/10.1101/2023.04.25.538217

Paxinos, G., & Franklin, K. B. J. (2019). *Paxinos and Franklin's the Mouse Brain in Stereotaxic Coordinates* (5th ed.). Academic Press. San Diego, USA.

Pfeffer, C. K., Xue, M., He, M., Huang, Z. J., & Scanziani, M. (2013). Inhibition of inhibition in visual cortex: The logic of connections between molecularly distinct interneurons. *Nature Neuroscience*, *16*(8), 1068–1076. https://doi.org/10.1038/nn.3446

Pi, H.-J., Hangya, B., Kvitsiani, D., Sanders, J. I., Huang, Z. J., & Kepecs, A. (2013). Cortical interneurons that specialize in disinhibitory control. *Nature*, *503*(7477). https://doi.org/10.1038/nature12676

Piccolino, M., & Wade, N. J. (2008). Galileo's eye: A new vision of the senses in the work of Galileo Galilei. *Perception*, *37*(9), 1312–1340. https://doi.org/10.1068/p6011

Porter, J. T., Johnson, C. K., & Agmon, A. (2001). Diverse types of interneurons generate thalamus-evoked feedforward inhibition in the mouse barrel cortex. *Journal of Neuroscience*, *21*(8), 2699–2710. https://doi.org/10.1523/JNEUROSCI.21-08-02699.2001

Preuß, F. (2023). *Disinhibitory circuit motifs in mouse primary somatasensory (barrel) cortex* [Doctoral Dissertation, Georg-August-University Göttingen].

Prönneke, A. (2017). *Untangling neuronal diversity: A quantitative electrophysiological and morphological characterization of VIP expressing interneurons* [Doctoral Dissertation, Georg-August-University Göttingen]. https://doi.org/10.53846/goediss-6200

Prönneke, A., Scheuer, B., Wagener, R. J., Möck, M., Witte, M., & Staiger, J. F. (2015). Characterizing VIP neurons in the barrel cortex of VIPcre/tdTomato mice reveals layer-specific differences. *Cerebral Cortex, 25*(12), 4854–4868. https://doi.org/10.1093/cercor/bhv202

Prönneke, A., Witte, M., Möck, M., & Staiger, J. F. (2020). Neuromodulation leads to a burst-tonic switch in a subset of VIP neurons in mouse primary somatosensory (barrel) cortex. *Cerebral Cortex*, *30*(2), 488–504. https://doi.org/10.1093/cercor/bhz102

Qi, G., & Feldmeyer, D. (2022). Cell-type specific neuromodulation of excitatory and inhibitory neurons via muscarinic acetylcholine receptors in layer 4 of rat barrel cortex. *Frontiers in Neural Circuits*, *16*, 843025. https://doi.org/10.3389/fncir.2022.843025

Qi, J., Ye, C., Naskar, S., Inácio, A. R., & Lee, S. (2022). Posteromedial thalamic nucleus activity significantly contributes to perceptual discrimination. *PLOS Biology*, *20*(11), e3001896. https://doi.org/10.1371/journal.pbio.3001896

Rachel, J. (2022). *Functional connectivity of the L2/3 VIP-to-L4 SST cell circuit motif in the primary somatosensory and visual cortices of mouse* [Doctoral Dissertation, Georg-August-University Göttingen]. https://doi.org/10.53846/goediss-10361

Ramamurthy, D. L., Chen, A., Zhou, J., Park, C., Huang, P. C., Bharghavan, P., Krishna, G., Liu, J., Casale, K., & Feldman, D. E. (2023). VIP interneurons in sensory cortex encode sensory and action signals but not direct reward signals. *Current Biology*, *33*(16), 3398-3408.e7. https://doi.org/10.1016/j.cub.2023.06.086

Raynor, H. A., & Epstein, L. H. (2003). The relative-reinforcing value of food under differing levels of food deprivation and restriction. *Appetite*, *40*(1), 15–24. https://doi.org/10.1016/S0195-6663(02)00161-7

Rice, F. L., Mance, A., & Munger, B. L. (1986). A comparative light microscopic analysis of the sensory innervation of the mystacial pad. I. Innervation of vibrissal follicle-sinus complexes. *The Journal of Comparative Neurology*, *252*(2), 154–174. https://doi.org/10.1002/cne.902520203

Rodgers, C. C., Nogueira, R., Pil, B. C., Greeman, E. A., Park, J. M., Hong, Y. K., Fusi, S., & Bruno, R. M. (2021). Sensorimotor strategies and neuronal representations for shape discrimination. *Neuron*, *109*(14), 2308-2325. https://doi.org/10.1016/j.neuron.2021.05.019

Rogan, S. C., Roth, B. L., & Morrow, A. L. (2011). Remote control of neuronal signaling. *Pharmacological Reviews*, *63*(2), 291–315. https://doi.org/10.1124/pr.110.003020

Roth, B. L. (2016). DREADDs for neuroscientists. *Neuron*, *89*(4), 683–694. https://doi.org/10.1016/j.neuron.2016.01.040

Rudy, B., Fishell, G., Lee, S., & Hjerling-Leffler, J. (2011). Three groups of interneurons account for nearly 100% of neocortical GABAergic neurons. *Developmental Neurobiology*, *71*(1), 45–61. https://doi.org/10.1002/dneu.20853

Rupert, D. D., & Shea, S. D. (2022). Parvalbumin-positive interneurons regulate cortical sensory plasticity in adulthood and development through shared mechanisms. *Frontiers in Neural Circuits*, *16*, 886629. https://doi.org/10.3389/fncir.2022.886629

Sanchez-Vives, M. V., & McCormick, D. A. (2000). Cellular and network mechanisms of rhythmic recurrent activity in neocortex. *Nature Neuroscience*, *3*(10), 1027–1034. https://doi.org/10.1038/79848

Schubert, D., Kötter, R., & Staiger, J. F. (2007). Mapping functional connectivity in barrel-related columns reveals layer- and cell type-specific microcircuits. *Brain Structure and Function*, *212*(2), 107–119. https://doi.org/10.1007/s00429-007-0147-z

Schwarz, C., Hentschke, H., Butovas, S., Haiss, F., Stüttgen, M. C., Gerdjikov, T. V., Bergner, C. G., & Waiblinger, C. (2010). The head-fixed behaving rat—Procedures and pitfalls. *Somatosensory & Motor Research*, *27*(4), 131–148. https://doi.org/10.3109/08990220.2010.513111

Shu, Y., Hasenstaub, A., & McCormick, D. A. (2003). Turning on and off recurrent balanced cortical activity. *Nature*, *423*(6937), 288–293. https://doi.org/10.1038/nature01616

Silberberg, G., & Markram, H. (2007). Disynaptic Inhibition between neocortical pyramidal cells mediated by Martinotti cells. *Neuron*, *53*(5), 735–746. https://doi.org/10.1016/j.neuron.2007.02.012

Smith, K. S., Bucci, D. J., Luikart, B. W., & Mahler, S. V. (2016). DREADDS: Use and application in behavioral neuroscience. *Behavioral Neuroscience*, *130*(2), 137–155. https://doi.org/10.1037/bne0000135

Staiger, J. F., Bojak, I., Miceli, S., & Schubert, D. (2015). A gradual depth-dependent change in connectivity features of supragranular pyramidal cells in rat barrel cortex. *Brain Structure and Function*, *220*(3), 1317–1337. https://doi.org/10.1007/s00429-014-0726-8

Staiger, J. F., Masanneck, C., Schleicher, A., & Zuschratter, W. (2004). Calbindin-containing interneurons are a target for VIP-immunoreactive synapses in rat primary somatosensory cortex. *The Journal of Comparative Neurology*, *468*(2), 179–189. https://doi.org/10.1002/cne.10953

Staiger, J. F., Möck, M., Proenneke, A., & Witte, M. (2015). What types of neocortical GABAergic neurons do really exist? *E-Neuroforum*, *6*(2), 49–56. https://doi.org/10.1007/s13295-015-0006-y

Staiger, J. F., & Petersen, C. C. H. (2021). Neuronal circuits in barrel cortex for whisker sensory perception. *Physiological Reviews*, *101*(1), 353–415. https://doi.org/10.1152/physrev.00019.2019

Staiger, J. F., Zilles, K., & Freund, T. F. (1996a). Distribution of GABAergic elements postsynaptic to ventroposteromedial thalamic projections in layer IV of rat barrel cortex. *European Journal of Neuroscience*, *8*(11), 2273–2285. https://doi.org/10.1111/j.1460-9568.1996.tb01191.x

Staiger, J. F., Zilles, K., & Freund, T. F. (1996b). Innervation of VIP-immunoreactive neurons by the ventroposteromedial thalamic nucleus in the barrel cortex of the rat. *The Journal of Comparative Neurology*, *367*(2), 194–204. https://doi.org/10.1002/(SICI)1096-9861(19960401)367:2<194::AID-CNE3>3.0.CO;2-0

Stüttgen, M. C., & Schwarz, C. (2018). Barrel cortex: What is it good for? *Neuroscience*, *368*, 3–16. https://doi.org/10.1016/j.neuroscience.2017.05.009

Taniguchi, H., He, M., Wu, P., Kim, S., Paik, R., Sugino, K., Kvitsiani, D., Fu, Y., Lu, J., Lin, Y., Miyoshi, G., Shima, Y., Fishell, G., Nelson, S. B., & Huang, Z. J. (2011). A resource of Cre driver lines for genetic targeting of GABAergic neurons in cerebral cortex. *Neuron*, *71*(6), 995–1013. https://doi.org/10.1016/j.neuron.2011.07.026

Tremblay, R., Lee, S., & Rudy, B. (2016). GABAergic Interneurons in the neocortex: From cellular properties to circuits. *Neuron*, *91*(2), 260–292. https://doi.org/10.1016/j.neuron.2016.06.033

Urban, D. J., & Roth, B. L. (2015). DREADDs (Designer Receptors Exclusively Activated by Designer Drugs): Chemogenetic tools with therapeutic utility. *Annual Review of Pharmacology and Toxicology*, *55*, 399–417. https://doi.org/10.1146/annurev-pharmtox-010814-124803

Van Der Loos, H. (1976). Barreloids in mouse somatosensory thalamus. *Neuroscience Letters*, *2*(1), 1–6. https://doi.org/10.1016/0304-3940(76)90036-7

Varani, S., Vecchia, D., Zucca, S., Forli, A., & Fellin, T. (2022). Stimulus feature-specific control of layer 2/3 subthreshold whisker responses by layer 4 in the mouse primary somatosensory cortex. *Cerebral Cortex*, *32*(7), 1419–1436. https://doi.org/10.1093/cercor/bhab297

Veres, J. M., Nagy, G. A., Vereczki, V. K., Andrási, T., & Hájos, N. (2014). Strategically positioned inhibitory synapses of axo-axonic cells potently control principal neuron spiking in the basolateral amygdala. *Journal of Neuroscience*, *34*(49), 16194–16206. https://doi.org/10.1523/JNEUROSCI.2232-14.2014

Vincent, S. B. (1912). The function of the vibrissae in the behavior of the white rat. *Animal Behavior Monographs*, *1, 5*, 84–84.

Voigts, J., Herman, D. H., & Celikel, T. (2015). Tactile object localization by anticipatory whisker motion. *Journal of Neurophysiology*, *113*(2), 620–632. https://doi.org/10.1152/jn.00241.2014

Walker, F., Möck, M., Feyerabend, M., Guy, J., Wagener, R. J., Schubert, D., Staiger, J. F., & Witte, M. (2016). Parvalbumin- and vasoactive intestinal polypeptide-expressing neocortical interneurons impose differential inhibition on Martinotti cells. *Nature Communications*, *7*(1), 13664. https://doi.org/10.1038/ncomms13664

Wang, D., Wu, J., Liu, P., Li, X., Li, J., He, M., & Li, A. (2022). VIP interneurons regulate olfactory bulb output and contribute to odor detection and discrimination. *Cell Reports*, *38*(7), 110383. https://doi.org/10.1016/j.celrep.2022.110383

Williams, C. M., & Kramer, E. M. (2010). The advantages of a tapered whisker. *PloS One*, *5*(1), e8806. https://doi.org/10.1371/journal.pone.0008806

Wimmer, V. C., Bruno, R. M., de Kock, C. P. J., Kuner, T., & Sakmann, B. (2010). Dimensions of a projection column and architecture of VPM and POm axons in rat vibrissal cortex. *Cerebral Cortex*, *20*(10), 2265–2276. https://doi.org/10.1093/cercor/bhq068

Wolfe, J., Hill, D. N., Pahlavan, S., Drew, P. J., Kleinfeld, D., & Feldman, D. E. (2008). Texture coding in the rat whisker system: Slip-stick versus differential resonance. *PLoS Biology*, *6*(8), e215. https://doi.org/10.1371/journal.pbio.0060215

Woolsey, T. A. (1967). Somatosensory, auditory and visual cortical areas of the mouse. *The Johns Hopkins Medical Journal*, *121*(2), 91–112.

Woolsey, T. A., & Van der Loos, H. (1970). The structural organization of layer IV in the somatosensory region (SI) of mouse cerebral cortex. The description of a cortical field composed of discrete cytoarchitectonic units. *Brain Research*, *17*(2), 205–242. https://doi.org/10.1016/0006-8993(70)90079-x

Woolsey, T. A., Welker, C., & Schwartz, R. H. (1975). Comparative anatomical studies of the Sml face cortex with special reference to the occurrence of “barrels” in layer IV. *Journal of Comparative Neurology*, *164*(1), 79–94. https://doi.org/10.1002/cne.901640107

Wu, H.-P. P., Ioffe, J. C., Iverson, M. M., Boon, J. M., & Dyck, R. H. (2013). Novel, whisker-dependent texture discrimination task for mice. *Behavioural Brain Research*, *237*, 238–242. https://doi.org/10.1016/j.bbr.2012.09.044

Xu, H., Jeong, H.-Y., Tremblay, R., & Rudy, B. (2013). Neocortical somatostatin-expressing GABAergic interneurons disinhibit the thalamorecipient layer 4. *Neuron*, *77*(1), 155–167. https://doi.org/10.1016/j.neuron.2012.11.004

Yang, H., Kwon, S. E., Severson, K. S., & O’Connor, D. H. (2016). Origins of choice-related activity in mouse somatosensory cortex. *Nature Neuroscience*, *19*(1), 127–134. https://doi.org/10.1038/nn.4183

Yu, J., Hu, H., Agmon, A., & Svoboda, K. (2019). Recruitment of GABAergic interneurons in the barrel cortex during active tactile behavior. *Neuron*, *104*(2), 412-427.e4. https://doi.org/10.1016/j.neuron.2019.07.027

Zhang, H., Craciun, L. C., Mirshahi, T., Rohács, T., Lopes, C. M. B., Jin, T., & Logothetis, D. E. (2003). PIP2 activates KCNQ channels, and its hydrolysis underlies receptor-mediated inhibition of M currents. *Neuron*, *37*(6), 963–975. https://doi.org/10.1016/S0896-6273(03)00125-9

Zhou, X., Rickmann, M., Hafner, G., & Staiger, J. F. (2017). Subcellular targeting of VIP boutons in mouse barrel cortex is layer-dependent and not restricted to interneurons. *Cerebral Cortex*, *27*(11), 5353–5368. https://doi.org/10.1093/cercor/bhx220

Zhu, J. J., & Connors, B. W. (1999). Intrinsic firing patterns and whisker-evoked synaptic responses of neurons in the rat barrel cortex. *Journal of Neurophysiology*, *81*(3), 1171–1183. https://doi.org/10.1152/jn.1999.81.3.1171

LIST OF FIGURES

LIST OF TABLES

ABBREVIATIONS

AAV	adeno-associated viral vector
2AFC	2-alternative forced-choice
ACh	acetylcholine
ACSF	artificial cerecrospinal fluid
AP	action potential
AP-A	action potential amplitude
AP-FT	action potential firing threshold
AP-S	action potential slope
AP-W	action potential width
CNO	clozapine-N-oxide
CNO-S	average score in CNO sessions
DREADD	designer receptors exclusively activated by designer drugs
FISH	fluorescent in situ hybridization
FT	firing threshold
GABA	gamma(γ)-aminobutyric acid
hM_3D-Gq	modified human muscarinic acetylcholine receptor 3 which couples to Gq-type G proteins
IHC	immunohistochemistry
IN	inhibitory neuron/interneuron
IP	intraperitoneal
L	layer
LAVES	Das Niedersächsische Landesamt für Verbraucherschutz und Lebensmittelsicherheit
LS	learner score
POm	the posterior medial thalamic nucleus
PrV	the principal sensory nuclei
PV	parvalbumin
$R_{i(hd)}$	input resistance in highest voltage deflection
$R_{i(ss)}$	input resistance in steady state
RMP	resting membrane potential

RT	room temperature
S1	the primary somatosensory cortex
S1BF	the primary somatosensory cortex barrel field
S2	the secondary somatosensory cortex
SI	saline injection
SP	sandpaper
SpV	the spinal nuclei
SS	stereotactic surgery
SST	somatostatin
TT	Textured T-maze
VIP	vasoactive intestinal polypeptide
vM1	the vibrissal primary motor cortex
VPM	the ventral posteromedial nucleus
τ	membrane time constant

ACKNOWLEDGEMENTS

Completing a PhD is an incredibly challenging yet rewarding journey. There are moments of doubt, frustration, and exhaustion, but with perseverance and the support of those around you, it is possible to push through. This project would not have been possible without the guidance, encouragement, and kindness of many individuals, to whom I am deeply grateful.

I would like to express my gratitude to my main advisor, Prof. Dr. Jochen Staiger, who gave me the opportunity for this project. Our journey did not start smoothly, and there were challenges in the beginning, but over the years, we built a strong and trusting relationship. I deeply appreciate how Jochen trusted my instincts and allowed me to expand my research in new directions. His support was especially crucial during the most difficult phases of this project—when everything seemed stuck and progress felt impossible. I will never forget his encouragement during those moments, which made all the difference.

A very special thank you goes to Dr. Martin Möck, my direct supervisor, who played the most crucial role in making this project a reality. He not only guided me through the process of writing this thesis but also taught me electrophysiology with incredible enthusiasm and patience. His patience, dedication, and scientific insight were invaluable, and our discussions—whether over coffee, during long experiments, or with a bottle of really good wine—made this journey so much more enjoyable. Beyond being a brilliant scientist, Martin has been a great mentor and a true friend, and I will always be grateful for his support.

I would also like to thank Dr. Julien Guy, my former supervisor, who welcomed me into the lab and supported me in the early stages of my PhD. Although he left in the middle of my project, his guidance in the initial phases of my PhD helped shaping my work. More importantly, I am grateful that our connection did not end there—we remained friends, which is something I deeply value.

I am also grateful to my committee members, Prof. Dr. Hansjörg Scherberger and Prof. Dr. Hannelore Ehrenreich, for their support and suggestions throughout the PhD years, which have greatly encouraged me to finish this project.

I want to give special thanks to Dr. Mirko Witte for handling the bureaucratic processes and providing insight into stainings and cell counting procedures. I am also thankful for his cooperation with Dr. Monique Silter and the animal caretaker team at the ENI animal facility. Their cooperation and support throughout the experiments were essential.

I am grateful to Dr. Sahab Arinrad, who generously took the time to discuss and provide valuable input during the development of the behavioral part of this project. I would also like to thank Vahid Khatibi for his help with whole-cell patch-clamp experiments. His willingness to assist was invaluable in the data collection process within a short period.

I would like to thank Sandra Heinzl, Patricia Sprysch, and Antonia Latona for their technical assistance for stainings. Also, thanks to Pavel Truschow, I managed to obtain best images out of these stainings. Thank you all for your support and contributions to complete this project with nice representations of my data.

I am also grateful for the student assistants Josi Dittmann and Lea Pappe, who assisted me patiently for the video analyses of the behavioral task.

I want to thank Torsten Nägel from Central Scientific Workshop of UMG, who built the behavioral maze for me and was always ready to solve any kind of mechanical problem I have with it.

I want to thank all past and present members of Neuroanatomie, for being welcoming and their feedback on various presentations and findings.

Very special thanks goes to Anouk Meeuwissen, Jenifer Rachel, Felix Preuß, and Ima Mansori. I was so lucky to find you in this lab, you always made me feel comfortable and supported with delicious cakes, dinners, cups of coffee, or glasses of beer.

And Oğuzhan. Thank you for being always there for me. Without you I cannot even imagine how the journey of PhD would end up good. Words are not enough to express my gratitude.

Final thanks goes to my big beloved family, and friends in Göttingen and beyond, thank you all for never letting me down.